Scattering of an X-Ray beam on a Surface Acoustic Wave

zur Erlangung des

DOKTORGRADES DER NATURWISSENSCHAFTEN (Dr. rer. nat.)

im Fachbereich Physik

der Freien Universität Berlin

eingereichte Dissertation

Simone Vadilonga

Berlin

2018

Datum der Disputation:	16 Juli 2018
Vorsitzender der Promotionskommission:	Prof. Dr. Martin Weinelt
Erstgutachter der Promotion:	Prof. Dr. Alexei Erko
Zweitgutachter der Promotion:	Prof. Dr. Wolfgang Kuch
Promoviertes Mitglied der Kommission:	Dr. Evangelos Golias
Promovierendes Mitglied der Kommission:	Herr Alexander Humeniuk

"It's funny. All you have to do is say something nobody understands and they'll do practically anything you want them to."

D. Salinger

Abstract

In this work surface acoustic waves (SAWs) are studied as a tool to manipulate spatially and temporally an X-ray beam. SAWs have been intensively studied in the last decades, and X-ray diffraction proved to be a useful tool to investigate the propagation of a SAW in different materials. A SAW induces a sinusoidal deformation on the substrate surface, which acts as a grating when illuminated by X-rays producing diffraction satellites. Their intensity and angular separation depend on the amplitude and wavelength of the ultrasonic superlattice. The first two experiment presented in this work studied the spacial manipulation of an X-ray beam. In this case a SAW was excited continuously on the sample. The third and fourth experiment used a pulsed SAW to temporally manipulate an X-ray beam.

The first experiment studied sagittal diffraction in Bragg condition. It demonstrates that it is possible to achieve an effective diffraction of an X-ray beam in sagittal geometry. The proper theoretical model has been applied for calculation of the SAW amplitude and wavelength. The experimental results and the theoretical predictions show a good agreement.

The second experiment investigated for the first time the diffraction of X-rays by a SAW in the soft X-ray region. The results of X-ray Bragg diffraction and total external reflection in meridional geometry are analyzed. The possibility to achieve an effective diffraction is demonstrated.

The third experiment explored the possibility to electronically manipulate the SAW amplitude, obtaining different scattering conditions for different X-ray pulses. It was performed in quasi-sagittal geometry in Bragg condition. The result of this experiment indicates that pulsed SAW can be used to select which X-ray pulse reaches the detector, as long as the X-ray pulses are separated by at least 120 ns.

The fourth experiment aimed to study the propagation of pulsed SAW on the substrate surface. Individual SAW pulse were localized on the surface. The structure of SAW pulses was investigated and revealed inhomogeneity in the structure.

Finally an application is proposed. SAW could be used to develop a pulse picker driven by a SAW, able to pick individual X-ray pulses separated by at least 120 ns.

Kurzzusammenfassung

In dieser Arbeit wurden akustische Oberflächenwellen (Surface Acoustic Waves, SAW) als Werkzeug zur räumlichen und zeitlichen Manipulation eines Röntgen-Strahls untersucht. Akustische Oberflächenwellen wurden bereits in den letzten Jahrzehnten intensiv untersucht. Dabei erwies sich die Methode der Röntgen-Beugung als ein nützliches Werkzeug, um die Ausbreitung der akustischen Oberflächenwellen in verschiedenen Materialien zu untersuchen. Eine akustische Oberflächenwelle induziert eine sinusförmige Verformung auf der Substratoberfläche, die als ein Gitter arbeitet, wenn diese mit Röntgen-Strahlen beleuchtet wird. Dadurch werden Beugungssatelliten erzeugt, bei denen die Intensität und Winkeltrennung von der Amplitude und der Wellenlänge der akustischen Oberflächenwelle abhängt. Die ersten zwei Experimente, die in dieser Arbeit vorgestellten werden, untersuchten, wie dieser Effekt für die räumliche Manipulation eines Röntgen-Strahls genutzt werden kann. In diesen beiden Fällen wurde die akustische Oberflächenwelle kontinuierlich an der Probe angeregt. In den beiden folgenden Experimenten wurde eine akustische Oberflächenwelle gepulst angeregt, um den Röntgen-Strahl zeitlich manipulieren zu können.

Das erste Experiment untersuchte die Sagittal-Beugung unter Bragg-Bedingungen. Es zeigt, dass es möglich ist, eine effektive Beugung eines Röntgen-Strahls in sagittaler Geometrie zu erreichen. Zur Berechnung der Amplituden und Wellenlängen der akustischen Oberflächenwellen wurde ein theoretisches Modell verwendet. Die experimentellen Ergebnisse zeigten eine gute Übereinstimmung mit den theoretischen Vorhersagen. Im zweiten Experiment wurde zum ersten Mal die Beugung von Röntgenstrahlen durch eine akustische Oberflächenwelle für weiche Röntgen-Strahlen gezeigt. Die Ergebnisse für die Röntgen-Bragg-Streuung und die totalen externen Reflektion wurden hierbei in der meridionalen Geometrie aufgenommen. Dabei wurde eine effektive Beugung demonstriert. Das dritte Experiment untersuchte die Möglichkeit, die akustische Oberflächenwellen-Amplitude elektronisch zu manipulieren, um unterschiedliche Streubedingungen für verschiedene Röntgen-Lichtpulse zu erhalten. Es wurde in einer quasi-sagittalen Geometrie unter Bragg-Bedingungen durchgeführt. Das Ergebnis dieses Experiments zeigt, dass mit gepulsten akustische Oberflächenwellen ausgewählt werden kann, welcher Röntgen-Lichtpuls aus einem Pulszug, den Detektor erreicht. Dies funktioniert mit der vorgestellten Methode, solange die Röntgen-Lichtpulse um mindestens 120 ns getrennt sind. Das vierte Experiment zielte darauf ab, die Ausbreitung von gepulsten akustischen Oberflächenwellen auf der Substrat-Oberfläche zu untersuchen. Einzelne, gepulst angeregte, akustische Oberflächenwellen wurden auf der Oberfläche lokalisiert. Dabei wurde die Struktur der akustischen Oberflächenwellen untersucht, wobei sich Inhomogenitäten in der Struktur zeigten.

Abschließend wird in dieser Arbeit eine mögliche Anwendung vorgeschlagen: Akustische Oberflächenwellen könnten dafür verwendet werden, um einen sogenannten „Puls-Picker“ zu entwickeln, der von einer akustischen Oberflächenwelle angesteuert wird und in der Lage ist, einzelne Röntgen-Lichtpulse für ein nachfolgendes Experiment zu selektieren, sofern diese um mindestens 120 ns getrennt sind.

Contents

Dedicated to my parents,
and to Núria.

Introduction

X-ray time resolved experiments allow the investigation of the dynamics of chemical reactions or physical phenomena [1, 2, 3]. Hard X-rays, with energies above 5 keV are particularly suitable for structural research since their wavelength matches the atomic distances in crystals and they can penetrate deep in solid samples. Soft X-rays, with photon energies below 2000 eV, are mainly used for surface analysis and molecular structure investigation. Synchrotron radiation (SR) facilities and X-ray Free electron laser (FEL) facilities are the most advanced X-ray sources available nowadays to perform this kind of experiments. They provide high brilliance, optimal excitation energy and polarized light. However they need appropriate optical elements to transport the radiation from the source to the experimental chamber, and this is achieved exploiting physical processes as reflection, diffraction and refraction. In addition SR and FEL sources naturally have a fine time structure of the emitted radiation, and they produce a continuous series of short X-ray pulses with a duration down to several pico-seconds. In the last decade this remarkable property found very challenging applications, opening a new era in material science, biology, etc. The necessity of ultra-fast time modulation of an X-ray beam lead to the development of different kind of mechanical and piezo-mechanical choppers with operational frequencies up to 1 MHz. Further improvement in time resolution of mechanical systems is not on the horizon. The scope of this thesis is to study the interaction between a surface acoustic wave (SAW) and a X-ray beam, exploiting diffraction process to manipulate spatially and temporally the beam itself.

In 1885 Lord Rayleigh described an acoustic wave motion with sub Herz frequencies that plays an important part in seismology [4], and its existence was confirmed by their appearance in seismic records. For some decades the acoustic wave remained an elegant description of a natural phenomena without any direct application. In 1965 the advent of the interdigital transducers (IDT) introduced a mean to generate and detect the SAW on piezoelectric crystals [5]. The IDTs are suitably shaped metallic thin film deposited on the surface of a piezoelectric crystal, enabling to generate SAW. Such devices can be easily fabricated by litographic techniques, developed by the semiconductor manufacture industry. While the excitation frequencies of SAW in seismology are in the sub Hertz region, the excitation frequencies in piezoelectric crystals are six to nine orders of magnitude higher. Thanks to this fact the SAW devices started to be used for the realization of bandpass filters, which is still their dominant use [6, 7]. SAW became of great interest because they are confined to the surface of a crystal, they have a short wavelength for a given frequency, and luckily there are many substrate materials on which the wave propagation is sufficiently well behaved (high piezoelectric constants, low diffraction effects, low attenuation, low dispersion...) [8].

In 1984 *Kikuta et al.* foresaw the possibility of using the SAW to manipulate an X-ray beam[9]. SAW propagate on the surface of solids, parallel to it, and their amplitude shows an exponential decay in the bulk. SAW modulate the surface of a crystal or a multilayer and can be used as diffraction grating for X-ray radiation. SAW phase velocity is 3000-5000 m/s [10], which is five orders of magnitude slower than the velocity of light. So, the SAW can be described as a static grating, neglecting the Doppler effect influence on the light frequency. It has been shown that SAW penetrate in the bulk up to the order of one SAW wavelength [11].

The diffraction of X-ray radiation on crystals modulated by a SAW has been investigated in a number of publications. Different materials, such as $LiNbO_3$ or quartz, were used as a carrier of the SAW in different crystallographic geometries[12, 13, 14, 15, 16].

Recently new materials such as langasite (LGS) crystal ($La_3Ga_5SiO_{14}$) [11, 14, 17], langatate crystal ($La_3Ga_{5.5}Ta_{0.5}O_{14}$) [18], $Ca_3TaGa_3Si_2O_14$ (CNGS) [19, 20] and $Ca_3NbGa_3Si_2O_14$ (CTGS) [21], developed for the use in microelectronic industry, were studied using SAW / X-ray methods. The measurements were carried on in meridional geometry, with the SAW wavefront perpendicular to the direction of the incoming X-ray beam. This new class of materials are of great interest because of the high values of the piezoelectric constants, and because they maintain piezoelectric properties at high temperatures.

Additionally it has been shown that the SAW can propagate to multilayer structures [22, 23, 24, 25], and that can be excited on non piezoelectric crystals, like Silicon [26, 27], and diamond carbon like thin films can increase the speed of the SAW [28]. It has been shown that graphene can be used to increase the amplitude of the SAW [29], and that changing the SAW amplitude enables controlling the magnitude and direction of current in graphene film on the surface of piezoelectric crystals [30]. The proper theoretical models were developed for the explanation of diffraction properties, especially the dependence of the diffracted intensity on the amplitude of high-frequency signal applied to the device for the SAW excitation [31, 32, 16].

This thesis exploits two different approaches, either based on meridional geometry in Bragg or total external reflection conditions, or on sagittal diffraction geometry in Bragg conditions, demonstrated for the first time in [33]. In sagittal diffraction the SAW wavefront is parallel to the direction of the incoming beam. Such a geometry is of great interest because it opens new possibilities regarding the applications of SAWs in the X-ray optics field. Moreover the interaction of the X-rays and SAW is studied for the first time in the soft X-ray region.

The first chapter of this thesis provides to the reader a theoretical framework relevant for the understanding of the experimental part. A description of the SAW and their excitation on crystalline structures taking advantage of the piezoelectric effect is given. The interaction of the SAW with X-rays is described, and this lays the basics to understand the experimental choices and the data analysis.

The first part of the second chapter reviews and explains the material chosen for the investigation, provides the guidelines for the fabrication of SAW devices and supplies a handful diagnostic system for SAW devices. The second part reviews the methods of investigation used in this thesis.

The third chapter describes the experiments that investigate the X-ray/SAW interaction.

The first experiment is X-ray Bragg diffraction in sagittal geometry on the Y-cut of langasite crystal modulated by SAW, studied at the BESSY II synchrotron radiation facility. Due to the crystal lattice modulation by the SAW diffraction the satellites appear. Their intensity and angular separation depends on the amplitude and wavelength of the ultrasonic super-lattice. Experimental results are compared with the corresponding theoretical model that exploits the kinematical diffraction theory.
The second experiment is X-ray Bragg diffraction and total external reflection on a SI/W multilayer modulated by SAW at energies below 1000 eV, performed at the Optics beamline at BESSY II. For the first time the interaction of X-ray with SAW is studied in the soft X-ray region.
The third experiment is a time resolved experiment that exploits almost-sagittal geometry, performed at the B16 beamline at Diamond Light Source. The fourth and last experiment is a time resolved experiment in Bragg diffraction in meridional geometry, performed at the mySpot beamline at BESSY II. These two experiments take advantage of short SAW pulses to proof the time structure of the synchrotron in use.
The four experiments presented in this work show that the propagation of the SAW creates a dynamical diffraction grating on the crystal surface, and this can be used for space-time modulation of an X-ray beam. SAW may represent a useful tool to make a new generation of X-ray optics, and a possible application is presented in fourth chapter. If a SAW is pulsed, it produces a SAW pulse which is limited in time and space and that travels on the surface of the substrate, whether it is a crystal or a multilayer. If the X-ray source has a periodic time structure, the SAW pulses can be synchronized with the incoming X-ray pulses, and diffraction effect can be used to select which pulse reaches the experimental chamber. Preliminary tests show that such a device would be able to select X-ray pulses separated by at least 120 ns.

Chapter 1

Fundamentals

This chapter provides the fundamentals of SAW and their interaction with X-rays.

1.1 Surface acoustic waves

A SAW can be generated at the free surface of an elastic solid. In the devices considered in this text the generation of the waves is obtained applying an oscillating voltage to a metal film interdigital transducer deposited on the surface of a piezoelectric crystal. In this section the basic properties of the SAW are described, as well as their generation. A short mathematical outline of stress and strain relations in piezoelectric material is given.

1.1.1 Piezoelectric materials

The piezoelectric phenomenon was first discovered in 1880 by Pierre and Jacques Curie. A determinate class of materials, the piezoelectrics, shows a measurable surface charge when subject to a mechanical stress. In addition, the same materials show a strain when an electric field is applied to them. The two effects are called direct and converse piezoelectric effect.

Dielectric permittivity

If an electric field, $\boldsymbol{E}$ [V/m], is applied to a homogeneous, linear, and isotropic dielectric medium, a polarization $\boldsymbol{P}_i$ [C/m^2], is induced in the material, and is given by

$$P_i = \varepsilon_0 \chi_{ij} E_j, \tag{1.1}$$

where the ϵ_0 is the permittivity in the vacuum and χ_{ij} is a dimensionless second rank tensor known as *susceptibility*. The total surface charge density, that is induced in the medium by the applied electric field, is given by the dielectric displacement vector

$$D_i = \varepsilon_0 E_i + P_i. \tag{1.2}$$

It easily follows from equations (1.1) and (1.2) that

$$D_i = \varepsilon_0 E_i + \varepsilon_0 \chi_{ij} E_j = \varepsilon_0 \delta_{ij} E_j + \varepsilon_0 \chi_{ij} E_j = (\varepsilon_0 \delta_{ij} + \varepsilon_0 \chi_{ij}) E_j = \varepsilon_{ij} E_j, \tag{1.3}$$

where $\varepsilon_{ij} = \varepsilon_0(\delta_{ij} + \chi_{ij})$ is the dielectrical permittivity of the material and δ_{ij} is the Kronecker's delta. In the case of an anisotropic material, the dielectric permittivity is a second rank tensor. Using free energy arguments it can be shown that χ_{ij}, as well of ε_{ij}, must be a simmetrical tensor, $\chi_{ij} = \chi_{ji}$, with six independent components [34]. The electric field above is the electric field averaged over the volume of the piezoelectric material and defines the macroscopic electric field $\boldsymbol{E}$ as in Maxwell equations [35].

Stress and Strain

The *stress* tensor is a second order tensor with nine components. It defines the state of stress at a point inside a material. The tensor relates a unit vector $\hat{\boldsymbol{n}}$ to the stress vector $T^{(n)}$ [N m^{-2}] across an imaginary surface perpendicular to $\hat{\boldsymbol{n}}$, and is defined as follows

$$T_j^n = \sigma_{ij} n_i. \tag{1.4}$$

In a similar way the *strain* tensor, S_{ij} [N m^{-2}], that describes the deformation in terms of relative displacement of the material in the body, is defined. In the linear approximation the relation between stress and strain is given by Hooke's law:

$$S_{ij} = s_{ijkl} T_{kl}, \tag{1.5}$$

where s_{ijkl} [m^2 N^{-1}] is the *elastic compliance* and it is a fourth rank tensor. Strain and stress tensors are by definition symmetric second rank tensors.

Piezoelectric coupling coefficient

The piezoelectric coupling coefficient represents the effectiveness of a piezoelectric material in converting the mechanical energy in electrical energy, and is denoted as k_{ij}. Since the values are usually small, it is expressed in percentage. The subscript i indicates the direction along which the electric energy is applied, while j denotes the direction along which the mechanical energy is developed. For instance $k_{zx} = 9\%$ tells us that the electric field is applied along the z-axis, parallel to the polarization direction of the piezoelectric material, and that along the x-axis mechanical strain is observed.

Piezoelectric effect

Piezoelectric materials are a class of materials that can be polarized, in addition to an electric field, by the application of a mechanical stress. A linear relationship is assumed between the mechanical stress applied to a piezoelectric material and the change of polarization in the material. Such a change of polarization results in a different charge density. This is known as the *direct piezoelectric effect*

$$D_i = d_{ijk} S_{jk}, \tag{1.6}$$

where d_{ijk} [C N^{-1}] is a third rank tensor of piezoelectric coefficients. Moreover, when an electric field is applied to a piezoelectric material, a change in the dimensions of the piezoelectric material such as a contraction or an expansion is observed. The *converse piezoelectric effect* describes and quantify the strain that is developed in a piezoelectric material due to the applied electric field:

$$S_{ij} = d_{kij} E_k = d^t_{ijk} E_k, \tag{1.7}$$

where d^t_{ijk} [m V^{-1}] is a third rank tensor and t denotes the transposed matrix. The sign of the piezoelectric charge D_i, as well as the one of the strain S_{ij}, depends on the direction of the mechanical and electric field respectively.

Piezoelectric constitutive equations

The behavior of piezoelectric materials is assumed to be linear at low electric field and at low mechanical stress applied. Of course, at high electric field or stress level the piezoelectric materials show a non linear response to the external input. The constitutive equations are based on the assumption that the total strain in the transducer is the sum of the mechanical strain induced by the mechanical stress and the one induced by the applied electric voltage. The consitutive equations are [36]:

$$S_i = C_{ji}^E T_j + d_{mi} E_m, \tag{1.8}$$

$$D_i = d_{mi}^t T_m + \epsilon_{ki}^\sigma E_k, \tag{1.9}$$

where the indexes $i, j = 1, 2, \ldots, 6$ and $m, k = x, y, z$ are the reference axis. The equations can be rewritten in the following form:

$$S_i = C_{ji}^D T_j + g_{mi} D_m, \tag{1.10}$$

$$E_i = g_{mi}^t T_m + \beta_{ki}^\sigma E_k, \tag{1.11}$$

where the superscripts D, E and σ represent measurements taken at constant electric displacement, constant electric field and constant stress.

Equations (1.8) and (1.10) hold for the *converse piezoelectric effect*, while equations (1.9) and (1.11) express the *direct piezoelectric effect*.

1.1.2 Surface acoustic wave

A SAW is generated on the surface of an elastic solid, and it travels parallel to it. The phase velocity is in the range of 2000 - 5000 m/s. Their amplitude shows an exponential decay in the bulk, and is confined within one SAW wavelength [10, 7]. The propagation of a SAW is associated mechanically with a time dependent elliptical displacement of the surface structure. To describe the acousto-wave propagation in an arbitrary anisotropic piezoelectric medium one needs a set of linear equation [37]. The equation of motion is given by

$$\frac{\partial T_{ij}}{\partial x_i} = \rho \frac{\partial^2 u_j}{\partial t^2}, \tag{1.12}$$

where T is the stress tensor, ρ the mass density and u the mechanical displacement. The linear strain mechanical displacement relation reads:

$$S_{kl} = \frac{1}{2}\left(\frac{\partial u_k}{\partial x_l}\frac{\partial u_l}{\partial x_k}\right), \tag{1.13}$$

where S is the strain tensor. The two following equations are derived from Maxwell's equation under the quasi-static assumption:

$$\begin{aligned} \frac{\partial D_i}{\partial x_i} &= 0, \\ E_i &= -\frac{\partial \varphi}{\partial x_i}, \end{aligned} \tag{1.14}$$

where D is the electric displacement, E is the electric field and φ is the electric potential. Finally the linear piezoelectric constitutive equations are

$$\begin{aligned} T_{ij} &= c'^{E}_{ijkl} S_{kl} - e'_{nij} E_n, \\ D_m &= e'_{mkl} S_{kl} + \epsilon'^{S1}_{mn} E_n, \end{aligned} \tag{1.15}$$

where c'_{ijkl} are the elastic constants, e'_{nij} are the piezoelectric constants, and ϵ'^{S1}_{mn} are the dielectric constants. They all refer to a rotated coordinate system through the Euler transformation matrix in which the propagation will always be in the 1 direction [38]. The previous set of equations, valid only within the crystalline substrate, can be reduced by substitution into

$$c'_{ijkl} u_{k,li} + e'_{kij} \varphi_{,ki} = \rho \frac{\partial u_j}{\partial t}, \quad j = 1, 2, 3 \tag{1.16}$$

$$e'_{ikl} u_{k,li} - \epsilon'_{ik} \varphi_{,ki} = 0. \tag{1.17}$$

where an index preceded by a comma denotes the differentiation with respect to a space coordinate. The eq. (1.16) and (1.17) have a solution in the standard complex traveling wave form

$$u_i = \beta_i e^{-\alpha \omega x_3 / v_{SAW}} e^{j\omega(t - x_1/v_{SAW})}, \quad i = 1, 2, 3 \tag{1.18}$$

$$\varphi = \beta_4 e^{-\alpha \omega x_3 / v_{SAW}} e^{j\omega(t - x_1/v_{SAW})}, \quad i = 1, 2, 3 \tag{1.19}$$

where α denotes the exponential decay into the crystal, ω is the excitation frequency related to the SAW wavenumber K through the relation $\omega = k v_{SAW}$ Reasonable values of α can be obtained assuming that the determinant of the coefficients of the unknown in these equations must be zero in order to have a non-trivial solution [39]. Finally the general solution for the displacements vector component is a linear combination of four simple waves, propagating with the same velocity

$$u_i = \sum_{l=1}^{4} B^l \beta_i^l e^{-\alpha^l \omega x_3 / v_{SAW}} e^{j\omega(t - x_1/v_{SAW})}, \quad i = 1, 2, 3 \tag{1.20}$$

and

$$\varphi = \sum_{l=1}^{4} B^l \beta_4^l e^{-\alpha^l \omega x_3 / v_{SAW}} e^{j\omega(t - x_1/v_{SAW})}. \tag{1.21}$$

1.1.3 Interdigital Transducers

To excite a SAW on the surface of a crystal an electrical radio frequency (RF) signal must be converted into an acoustic wave. The conversion is achieved using a periodic metallic structure called interdigital transducer (IDT). Such a structure is also able to convert an incoming SAW into an electric RF signal. The simplest form of an IDT is shown in Fig. 1.1a. This consist of two thin film electrodes deposited on the surface of a piezoelectric substrate. The two electrodes are called fingers. When an AC voltage is applied to the them, an oscillating strain wave is excited on the surface of the substrate. This wave is periodic in both time and space, and it radiates away from each single pair. Normally a variable number of finger pairs N_p per IDT is used, with $10 \leq N_p \leq 10^4$. Such an IDT is called *single* IDT. For the purpose of this thesis only IDTs with uniform finger spacing and constant finger overlap will be considered. Referring to Fig. 1.2, the period of the IDT corresponds to four times

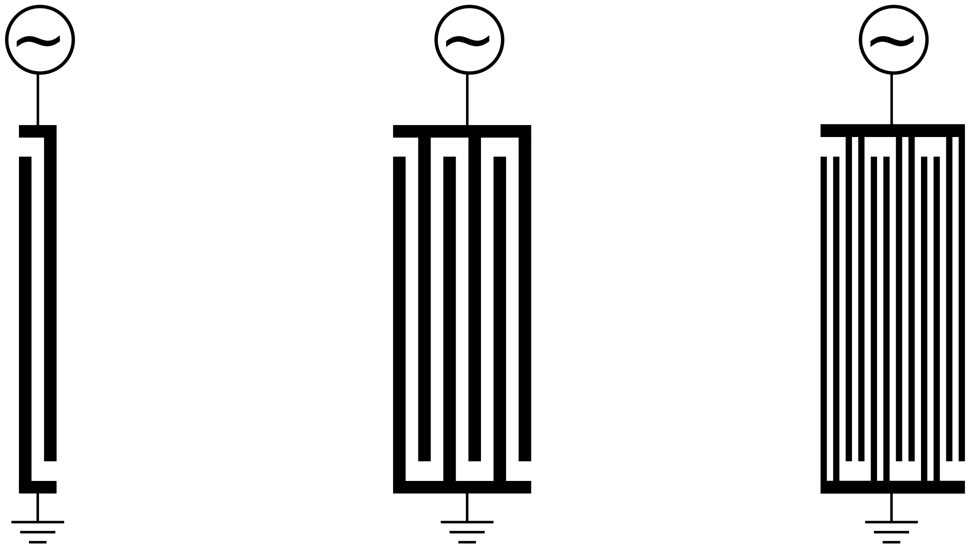

(A) (B) (C)

FIGURE 1.1: **A**: the simplest possible configuration for an IDT, **B** the *single* IDT configuration, and **C** the *double* or *split* IDT configuration.

the width of a single finger $d = 4p$. The wavelength of the SAW excited by such an IDT is approximately $\Lambda = d$. The approximation rely in the fact that the speed of the SAW in the portion of sample where there is the IDT is slightly lower than the speed of the IDT in the free piezoelectric crystal. The frequency at which the SAW are excited can be estimated through the relation

$$f_0 = v_{SAW}/\Lambda \tag{1.22}$$

The bandwidth of the IDT can be estimated via $f_B = f_0/N_p$. Until now ideal op-

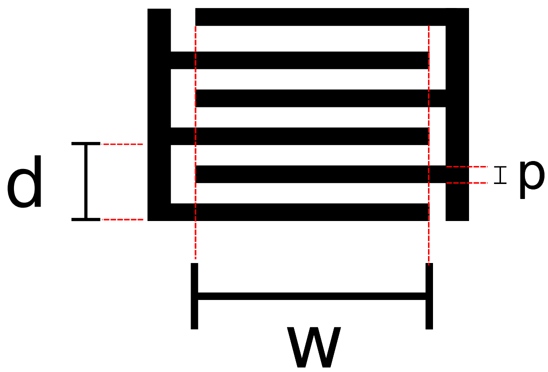

FIGURE 1.2: Single IDT scheme

erating conditions were assumed. Even though those are usually good working approximation, an IDT is not an ideal device. Various second order effects perturb the ideal environment to some degree and degrade the IDT response. Luckily most of these second order effects do really matter only if the main interest is building a SAW filter or sensor, which is not the case. It follows a short list of the principal second order effects:

- **Electromagnetic feedthrough (crosstalk)**: essentially if two IDTs are deposited on the crystal surface at a distance of a few acoustic wavelength Λ, they act as capacitors plates. The amount of electromagnetic feedthrough increases with the frequency as the capacitive reactance decreases. This gave rise to periodic ripples of amplitude and phase at ripple frequency $f_{rem} = 1/\tau$, where τ is the propagation time needed by SAW to travel from one IDT to the other. This is not of great concern for the purposes of the thesis, due to the large separation between two IDT in the SAW devices under study.

- **Triple transit interference**: this effect is due to multiple SAW reflections between bidirectional IDTs. This results in amplitude and phase ripples at the frequency $f_{rtti} = 1/2\tau$. Again, due to the large distance between the IDTs in the SAW devices under study, this effect is neglectable.

- **Electrode finger reflection**: the IDT fingers introduce impedance and mass loading discontinuity such that a portion of the wave is reflected. This effect plays an important role for our purposes. It can be solved by using IDTs with *split electrode* geometry, see Fig. 1.1c.

- **Bulk wave interference**: SAW are not the only kind of acoustic waves that can be excited by the IDT. Bulk waves may corrupt the passband amplitude and phase response. However this effect does not interfere significantly with the devices under study.

- **Circuit factor loading**: it results from the finite source and load impedances that are external to the SAW device. Input and output impedences of a SAW device are frequency dependent. The input voltage is divided then between source impedance and IDT impedance in a frequency dependent way. This second order effect does not matter for our SAW devices because they are used only at the resonant frequency.

- **Impedance mismatches**: the maximum power transmission by the SAW occurs when the resistance of the IDT matches the generator resistance. This is the case for our SAW devices. However when designing the IDT other parameters are favored during the design (i.e. the acoustic aperture)

- **Diffraction**: ideally the SAW wavefront should be flat, so that the wavefront of SAW launched by one IDT finger reaches the next finger in phase. However the wavefront is spherical to a degree which is dependent on the aperture of the radiating source. It can be done a parallel with optical diffraction from a slit, see Fig. 1.3. The smaller is the acoustic aperture of the IDT, the more relevant is the effect. The optimal aperture for an IDT is approximately 100Λ [6, 7]. One way of compensating this effect is to increase the acoustic aperture. In addition, due to the fact that piezoelectric crystals are anisotropic regarding the SAW propagation, this can increase or decrease the SAW beam spreading. For instance, for certain orientation lithium niobate shows a decrease in beam spreading. This phenomenon is known as *autocollimation*.

Split electrode geometry The split electrode geometry, see Fig. 1.1c, has the advantage to reduce the finger reflection effects. In this case each single finger in the single IDT geometry is replaced by two fingers with electrode width $\Lambda/8$. The differential path is such that the SAW reflection from each split electrode pair cancels out at the

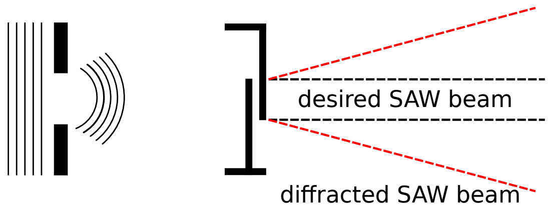

FIGURE 1.3: Comparison between optical diffraction (Left), and SAW diffraction by an IDT finger pair (right)

resonant frequency. The drawback is that to produce an IDT with the same period of the corresponding single IDT geometry the width of the fingers has to be reduced by half. The typical period of the SAW devices employed is approximately 4 μm, and to produce single electrode with 0.5 μm width is possible from the technological point of view.

Network Scattering Parameter Matrix The scattering matrix describes the input-output relationship between ports in an electrical system. A port can be loosely defined as any place where voltage and current can be delivered. In this case the ports are two IDTs. Understanding this matrix allows for direct measurements of the S-parameters of the IDT. Let's consider the case depicted in Fig.1.4, where two identical IDTs are facing each other at the distance D. We can then write the network scattering matrix that describes the system.

$$\begin{pmatrix} V_a & V_b \end{pmatrix} = \begin{pmatrix} S_{11} & S_{12} \\ S_{21} & S_{22} \end{pmatrix} \begin{pmatrix} V_a \\ V_b \end{pmatrix}. \tag{1.23}$$

The S_{12} parameter represents the power transferred from the IDT 2 to the IDT 1. S_{21} represents the power transferred from the IDT 1 to the IDT 2. S_{11} is the reflected power from the IDT 1, and S_{22} is the reflected power from IDT 2. The S-parameters are a function of frequency, and are usually expressed in dB. For instance, $S_{21} = 0$ dB implies that all the power delivered to the IDT 1 ends up at the IDT 2. If $S_{21} = -10$ dB, then if 1 W (or 0 dB) is delivered to IDT 1, then -10 dB (0.1 Watts) of power is received at IDT 2. The S-parameters can be easily measured using a Vector Network Analyzer, commercially available off the shelf.

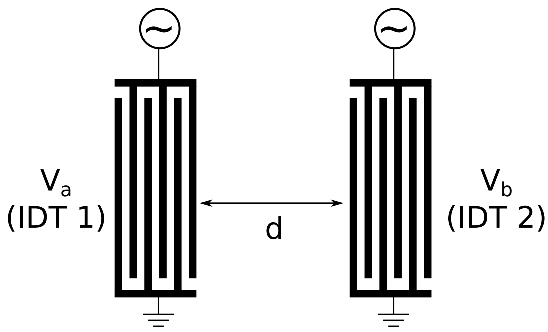

FIGURE 1.4: Double IDT scheme

P-Matrix It is well known that the IDTs can be represented by a three port admittance matrix [40], which describes an equivalent circuit representation. This circuit has one electrical port and two acoustic ports for each finger. To describe the whole transducer the three ports have to be cascaded acoustically, and the electrical ports have to be connected in parallel [41]. However the coefficients of the admittance matrix can not be measured directly nor calculated because a shortcut of the acoustical port is not feasible. For this reason it was introduced the P-matrix for non reflective transducers, a mixed matrix related to the transducers physics. This matrix is a combination of the scattering S-matrix and of the admittance matrix. Considering the situation depicted in Fig. 1.5, the IDT is considered a three port electric device. The acoustic variables are the amplitude A of the incoming and outgoing waves Φ, while the electrical variables are the voltage and the current. This matrix and the following considerations are valid only in the case of a non reflective transducer, which is the case in the split finger configuration with four fingers per period [42]:

$$\begin{pmatrix} A_{out}^- \\ A_{out}^+ \\ I \end{pmatrix} = \begin{pmatrix} P_{11} & P_{12} & P_{13} \\ P_{21} & P_{22} & P_{23} \\ P_{31} & P_{32} & P_{33} \end{pmatrix} \begin{pmatrix} A_{in}^+ \\ A_{in}^- \\ V \end{pmatrix}. \tag{1.24}$$

To better understand the entries of this matrix the three equations can be explicitly written:

$$\begin{aligned} A_{out}^- &= P_{11}A_{in}^+ + P_{12}A_{in}^- + P_{13}V, \\ A_{out}^+ &= P_{21}A_{in}^+ + P_{22}A_{in}^- + P_{23}V, \\ I &= P_{31}A_{in}^+ + P_{32}A_{in}^- + P_{33}V. \end{aligned} \tag{1.25}$$

The coefficients P_{11} and P_{22} are the reflection coefficient, as can be noticed setting $V = 0$ and $A_{in}^- = 0$ or $A_{in}^+ = 0$ respectively. Supposing to have a non reflective transducers, one can set $P_{11} = P_{22} = 0$. The first two equations can be then rewritten as $A_{out}^- = +P_{12}A_{in}^-$ and $A_{out}^+ = P_{21}A_{in}^+$. The coefficients $P_{12} = P_{21} = \exp(-jKL)$ are the ratio between two waves, the transfer coefficients. K is the SAW wavenumber and L is the distance traveled by the wave. Considering the case where there are no waves at all, from the third equation we obtain $P_{33} = I/V$, which is, by definition, the admittance of the transducer. A reciprocal three port P-matrix obey the reciprocity relations, and expressing the scattering matrix in terms of the P-matrix lead to the following relations [42]:

$$P_{12} = P_{21}, \quad 4P_{13} = -P_{31}, \quad 4P_{23} = P_{32}. \tag{1.26}$$

The last coefficient can be calculated with an equivalent circuit [42]:

$$P_{13} = -P_{31}/4 = j\vec{\rho_e}(k)\sqrt{\omega W \Gamma_s/2}\exp(-jKL/2) \tag{1.27}$$

where $\Gamma_s = (\Delta v/v)/\epsilon_{\text{inf}}$, $\epsilon_{\text{inf}} = 5.6\epsilon_0$ and $\vec{\rho_e}$ is the Fourier transform of the electrostatic charge density ρ_e [43] :

$$\vec{\rho_e}(k) = \epsilon_{\text{inf}}\frac{2\sin(\pi s)}{P_{-s}(-\cos\Delta)}P_m(\cos\Delta), m \le \frac{Kp}{2\pi} \le m+1 \tag{1.28}$$

where $s = Kp/(2\pi) - m$ so that $0 \le s \le 1$ and $\Delta = \pi a/p$. $P_{-s}(-\cos\Delta)$ is a Legendre function and $P_m(\cos\Delta)$ is a Legendre polynomial.

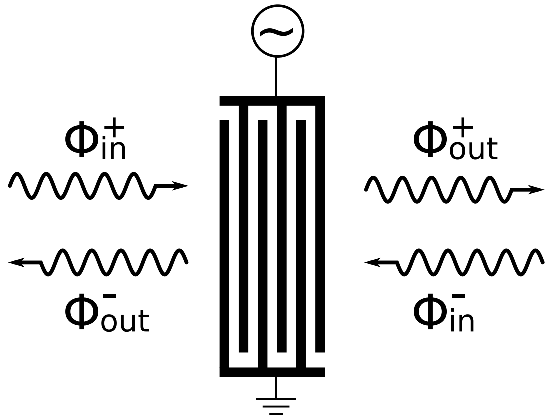

FIGURE 1.5: The three port model for an IDT

1.2 X-rays/SAW interaction

When a SAW is excited on a crystal surface, the excitation frequency (f) depends on the velocity (v_{SAW}) of the SAW on the exploited crystal, and on the period (Λ) of the SAW via the simple expression $f = v_{SAW}/\Lambda$. The deformation induced in the crystal in first approximation can be written as

$$h = h_0 \sin(Kx), \tag{1.29}$$

where $K = 2\pi/\Lambda$ is the SAW wave vector, h_0 is the SAW amplitude on the crystal surface, and $\hat{u}_1$ is the unit vector perpendicular to the crystal surface [10].
The samples described in this thesis have been tested mainly in Bragg geometry. The first diffraction process to take into account is Bragg diffraction, which is valid in a perfect and non deformed crystal

$$m\lambda = 2d \sin(\theta_B), \tag{1.30}$$

where m is the diffraction order, λ is the wavelength of the incident radiation, d is the interplanar distance of the crystal under study, and θ is the incident angle of the radiation on the crystal. When a SAW is excited on the crystal surface, a second diffraction process must be taken into account, due to the interaction of the radiation with the SAW. Since the phase velocity of a SAW is much lower than the speed of of light, $v_{SAW}/c \sim 10^{-5}$, the acoustic deformation can be considered static and characterized only by its wavelength and amplitude. If an X-ray plane wave diffracts on a SAW, it results in a splitting of the Bragg peak into diffraction satellites.

Meridional diffraction geometry In meridional diffraction geometry at the Bragg angle, the SAW wavefront is perpendicular to the scattering plane, as defined by the incoming and outgoing X-ray beam, Fig. 1.6. The diffraction takes place in the scattering plane, therefore the SAW diffracted satellites appear only when the sample is rotated by $\delta\theta$, see eq. (1.37). The angular position of the satellites can be calculated from the grating equation

$$k \cos(\theta_m) = k \cos(\theta_{inc}) + mK, \tag{1.31}$$

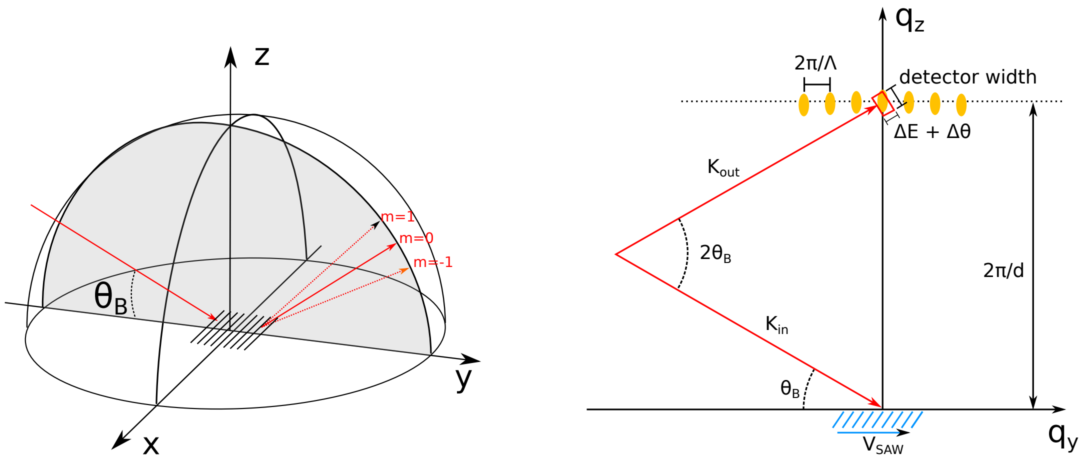

FIGURE 1.6: **Meridional diffraction (left)**: The grating created by a SAW lies in the xy plane, and the grooves of the grating are perpendicular to the incoming beam. The diffraction takes place in the optical plane. For simplicity in the picture are represented only the $m = 0, \pm 1$ orders. **Meridional diffraction in reciprocal space (right)**: The blue lines represent the sample with a SAW. $\mathbf{k_{in}}$ and $\mathbf{k_{out}}$ are the incoming and outgoing beam. The angle between the incoming beam and the sample, θ, and the angle between the incoming and outgoing beam, 2θ, are here represented for the particular case of the Bragg angle. The distance between the maxima in reciprocal space is $2\pi/\Lambda$. The length of the scattering vector is $\mathbf{k_{in}} - \mathbf{k_{out}} = 2\pi/d$, where d is the interplanar spacing. The red rectangle is the scanned area in reciprocal space. Its length and width are given respectively by the length of the detector in reciprocal space, the vertical divergence of the beam $\Delta\theta$ and the energy spread ΔE.

where $k = 2\pi/\lambda$ is the wavenumber of the incident radiation, $K = 2\pi/\Lambda$ is the wavenumber of the SAW, m is the diffraction order and θ_{inc} is the Bragg angle. Consider the situation depicted in Fig. 1.7, where the X-rays interact with a crys-

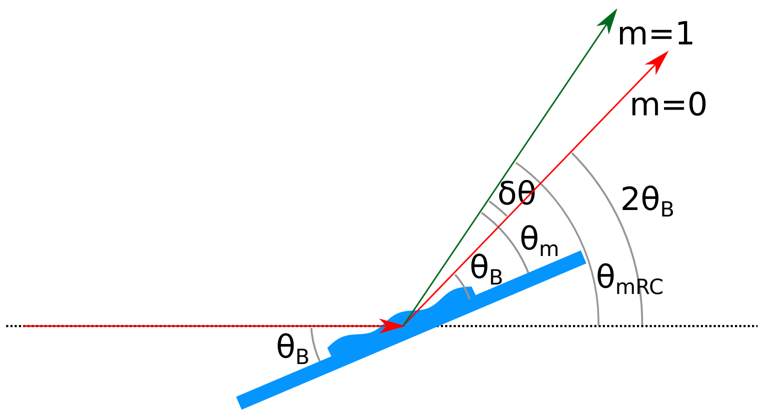

FIGURE 1.7: X-rays interacting with a crystalline sample distorted by a SAW at Bragg angle θ_B. The interaction with SAW give rise to diffraction satellites.

talline sample with interplanar spacing d at the incident Bragg angle θ_B, and they are diffracted by the crystal and by the SAW, giving rise to diffraction satellites. The following equation can be written

$$\theta_{mRC} = \theta_B + \delta\theta, \tag{1.32}$$

$$\theta_m = 2\theta_B - \theta_{mRC}. \tag{1.33}$$

From the two last equations the value of θ_m can be derived, $\theta_m = \theta_B - \delta\theta$. Additionally, the incident angle can be written as $\theta_{inc} = \theta_B + \delta\theta$, where the first order of diffraction has a maximum. Using the prosthaphaeresis formula

$$\cos p - \cos q = -2\sin\left(\frac{p+q}{2}\right)\sin\left(\frac{p-q}{2}\right), \tag{1.34}$$

and setting p=θ_m and q=θ_{inc}, eq. (1.31) can be rewritten as

$$-2\sin\left(\frac{\theta_m+\theta_{inc}}{2}\right)\sin\left(\frac{\theta_m-\theta_{inc}}{2}\right) = m\frac{\lambda}{\Lambda}. \tag{1.35}$$

Substituting the expression for θ_m and θ_{inc} into the last equation lead to the following result

$$-2\sin(\theta_B - \delta\theta)\sin(-\delta\theta) = m\frac{\lambda}{\Lambda}. \tag{1.36}$$

Since $\delta\theta$ is in the order of the millidegree, and θ_B varies in between 1 to 40 degrees

$$\delta\theta = \frac{m\lambda}{2\Lambda\sin\theta_B} = \frac{md}{\Lambda} \tag{1.37}$$

Finally, the relation $\Lambda = v_{SAW}/f$, we obtain a tool to measure the SAW speed

$$v_{SAW} = \frac{mdf}{\delta\theta}. \tag{1.38}$$

Sagittal diffraction In sagittal diffraction geometry at the Bragg angle, the SAW wavefront is parallel to the scattering plane, as defined by the incoming and outgoing X-ray beam, Fig. 1.8. The diffraction takes place perpendicularly to the scattering plane, therefore the Bragg diffracted and the SAW diffracted satellites appear simultaneously, and the diffraction satellites lie on the surface of a cone. The diffraction pattern are neither equally spaced nor positioned on a straight line. To calculate the distance between two diffraction satellites in sagittal geometry, consider Fig. 1.8. In reciprocal space, the distance between two satellites is given by $q_m = 2\pi/\Lambda$, and $k_{out} = 2\pi/\lambda$ depends on the wavelength λ of the incident radiation. The angular separation of two diffraction satellites, in the small angle approximation is

$$\delta\theta = \frac{q_m}{k_{out}} = \frac{\lambda}{\Lambda}. \tag{1.39}$$

1.2.1 Kinematical model for satellites intensity

This model is valid only when the penetration depth of X-rays is minor that the SAW penetration depth, usually estimated as one acoustic wavelength Λ, see Fig. 1.9. Following the work of *Tucoulou et al.* [15], the amplitude of the SAW is assumed to be exponentially dumped in the bulk. The vertical displacements of the atoms at

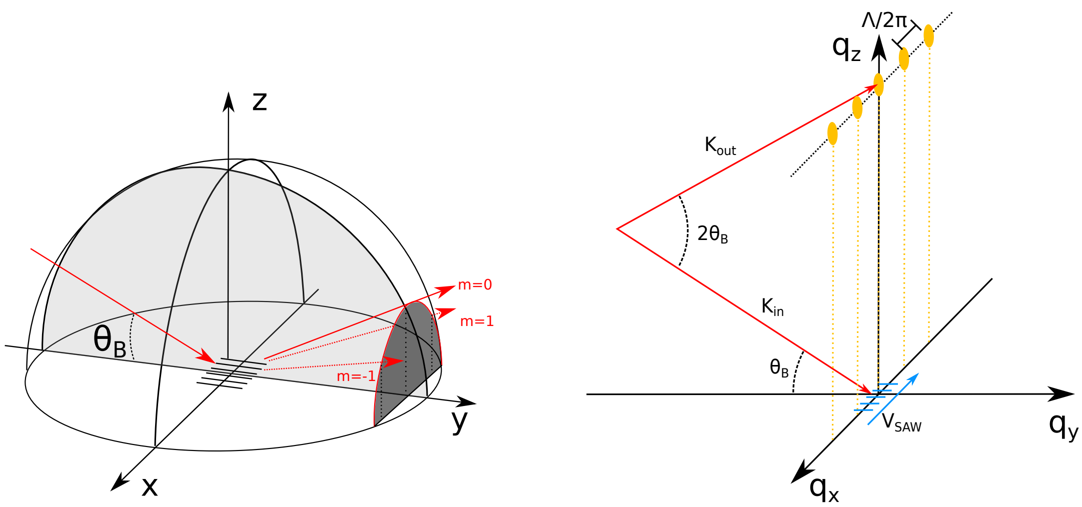

FIGURE 1.8: **Sagittal diffraction (left)**: The grating created by SAWs lies in the xy plane, and the grooves of the grating are parallel to the scattering plane (light grey). The diffraction satellites propagate on the surface of a cone (dark grey). For simplicity in the picture are represented only the $m = 0, \pm 1$ orders. **Sagittal diffraction in reciprocal space (right)**: The blue lines represent the sample with SAW. $\mathbf{k_{in}}$ and $\mathbf{k_{out}}$ are the incoming and outgoing beam. The angle between the incoming beam and the sample, θ, and the angle between the incoming and outgoing beam, 2θ, are here represented for the particular case of the Bragg angle. The distance between the maxima in reciprocal space is given by $2\pi/\Lambda$. The length of the scattering vector is $\mathbf{k_{in}} - \mathbf{k_{out}} = 2\pi/d$, where d is the interplanar spacing.

coordinate (x, y, z) can be approximated with

$$H(x, z) = H_0 e^{-\mu_{SAW}} e^{iKx}, \tag{1.40}$$

where μ_{SAW}^{-1} is the penetration depth of SAW, and K the SAW wavevector. The

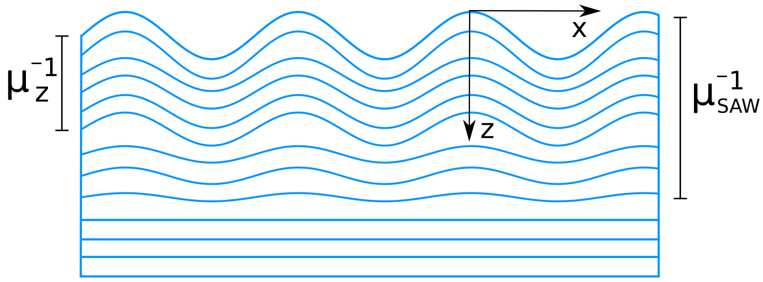

FIGURE 1.9: Scheme of the atomic planes in a crystal distorted by a SAW. The Z and X axis are not to scale and only a few planes are represented.

amplitude of a wave diffracted by a crystal is proportional to

$$A(\boldsymbol{Q}) \propto \sum_{i=1}^{N} F_{hkl} e^{i\boldsymbol{Q}\cdot\boldsymbol{r}_i}, \tag{1.41}$$

where N is the number of unit cells, $\boldsymbol{r}_i$ is the coordinate from the surface of the crystal, $\boldsymbol{Q}$ is the momentum transfer vector, and F_{hkl} is the structure factor. Since the unit cells are distorted by $\Delta d/d \sim 10^{-4}$, the variation of the structure factor can be neglected with respect to the lattice distortion due to a SAW. The position of the *i-th* unit cell in respect to the position of that same cell when a SAW is not present can be written as

$$\boldsymbol{r}_i = \boldsymbol{r}_{i0} + \boldsymbol{u}(\boldsymbol{r}_{i0}). \tag{1.42}$$

Inserting eq. (1.42) in eq. (1.41), and neglecting the structure factor, the amplitude of a diffracted wave can be written as

$$A(\boldsymbol{Q}) \propto \sum_{i=1}^{N} e^{i\boldsymbol{Q}\cdot(\boldsymbol{r}_{i0}+\boldsymbol{h}(\boldsymbol{r}_{i0}))}. \tag{1.43}$$

One can now introduce the X-ray absorption coefficient μ_x, and insert the expression for the deformation induced by a SAW as in eq. (1.29) explicitly written for the direction $(q_x, 0, q_z)$

$$A(\boldsymbol{Q}) \propto \sum_{x=1}^{N_x}\sum_{z=1}^{N_z} e^{-\mu_x zd} e^{i[q_x xa + q_z zd + q_z H(xa,zd)]}, \tag{1.44}$$

where N_x and N_z are the number of unit cell in the x,z direction, respectively, and a is the unit cell size in the x direction. Using the relation

$$e^{ic\sin\phi} = \sum_{m=-\infty}^{m=\infty} J_m(c) e^{im\phi}, \tag{1.45}$$

where J_m is the *m-th* Bessel function of the first kind, one can rewrite the previous equation as

$$A(\boldsymbol{Q}) \propto \sum_m \sum_{x=1}^{N_x} e^{i(q_x+mK)xa} \sum_{z=1}^{N_z} e^{-\mu_x zd} e^{iq_z zd} \cdot J_m(h_0 q_z e^{-\mu_{SAW} zd}). \tag{1.46}$$

For $N_x \gg 1$ the sum over N_x averages to zero, unless $q_x + mK = 0$. This condition is set by the grating equation. Finally to obtain the intensity of the m-th satellite, one must integrate over z and take the squared module

$$I_m \propto \left| \int_0^\infty e^{-\mu_z z} \cdot J_m(h_0 q_z e^{-\mu_{SAW} z}) dz \right|^2. \tag{1.47}$$

If the X-rays interact only with areas of the crystal modulated by SAW, as in Fig. 1.9, the intensities of the diffraction satellites can be calculated in the frame of the kinematical diffraction theory. The integral in eq. (1.47) can be solved assuming that the modulation of the crystal lattice is constant in the portion of the sample in which the X-rays penetrate ($e^{-\mu_{SAW} z} = constant$)

$$I_m \sim C \cdot |J_m(h_0 \cdot q_z)|^2. \tag{1.48}$$

1.2.2 Dynamical theory

The dynamical theory of diffraction, unlike the Kinematical theory, takes into account multiple scattering effects. Dynamical theory has been shown to be a powerful method to calculate the interaction of X-rays with a perfect crystal [44]. When approaching the interaction with a distorted lattice the Takagi-Taupin equations are a formalism that results particularly effective. They generalize the dynamical diffraction and allow to simulate rocking curves for an arbitrary deformation [45, 46, 47]. In the case of a crystal modulated by SAW, the atomic planes can be assumed to be shifted relatively to a perfect crystal, and their scattering capabilities not to be affected. Thus the electronic density distribution is not modified but only shifted, and the polarizability of the distorted crystal can be written as [16]

$$\chi(\boldsymbol{r}) = \chi^{id}\left[\boldsymbol{r} - \boldsymbol{u}(\boldsymbol{r})\right] = \sum_g \chi_g^{id} e^{ig[\boldsymbol{r}-\boldsymbol{u}(\boldsymbol{r})]}, \tag{1.49}$$

where $\sum_g$ is the sum over all the reciprocal lattice vectors. Equation (1.49) holds only when the deformation is smaller than the wavelength [48, 49]

$$\left|\frac{\delta u_i}{\delta x_k}\right| \ll 1. \tag{1.50}$$

Once the polarizability is defined, the Takagi-Taupin equations simplified for the case of Bragg symmetric reflection read [50]

$$\begin{cases} \dfrac{\delta D_0}{\delta s_0} = -i\pi q_{in}\chi_{-h} D_h(\boldsymbol{r}), \\ \dfrac{\delta D_h}{\delta s_h} = -i\pi q_{in}\chi_h D_0(\boldsymbol{r}) + iq_{in}\beta'(\boldsymbol{r}) D_h(\boldsymbol{r}), \end{cases} \tag{1.51}$$

where β' is

$$\beta'(\boldsymbol{r}) = -(\theta - \theta_B)\sin(2\theta_B) - \frac{2\pi}{q_{in}}\frac{\delta(\boldsymbol{q}_{out}\boldsymbol{u})}{\delta s_h}, \tag{1.52}$$

where s_0 and s_h are the coordinates along the forward and diffracted directions, χ_h and χ_{-h} are the components of the Fourier expansion of the dielectric susceptibility, $q_{in} = 2\pi/\lambda$, $\boldsymbol{h}$ is the diffraction vector and $\boldsymbol{u}$ is the displacement vector. D_0 and D_h are the forward and diffracted wave fields. The difference $\theta - \theta_B$ is the deviation from the Bragg angle due to the distorted surface and finally $\boldsymbol{r} = (s_0, s_h)$ is the position coordinate in the diffraction plane. The equations (1.51) are then numerically solved by inserting the displacement $\boldsymbol{u}$ produced by the SAW calculated for each value of the angle θ [32] [51].

1.2.3 RCWA method

Over the past 30 years the rigorous coupled wave analysis (RCWA) method have been widely used to analyze the results of the diffraction of electromagnetic waves by periodic structures. RCWA is technique that delivers an exact solution of Maxwell equations for the above mentioned case. The general approach for solving the exact electromagnetic-boundary-value problem associated with the diffraction grating is to find solutions that satisfy Maxwell's equations in each of the three (input, grating, and output) regions and then match the tangential electric and magnetic field components at the two boundaries. RCWA is a semi-analytical technique, meaning that it solves analytically one direction (longitudinal), and numerical the other two (transversal). It uses discrete Fourier transformation to discretize the fields in the transversal direction. A formulation for one dimensional binary grating in the conical-diffraction case is presented, following Moharam et al. [52]. The conical

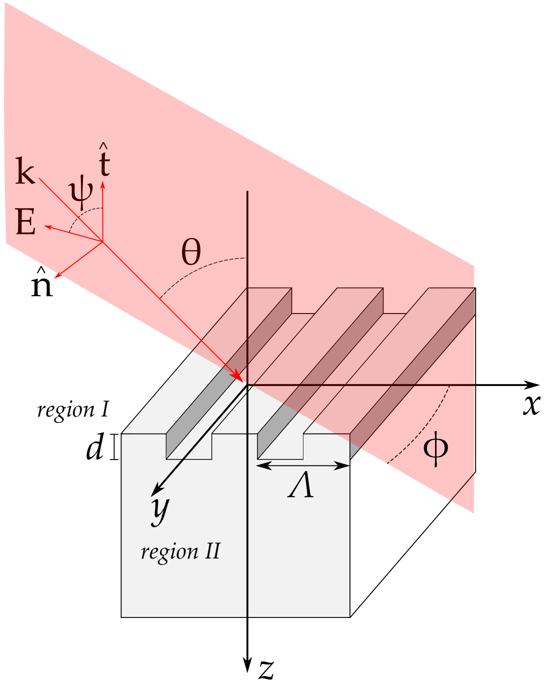

FIGURE 1.10: Geometry for the binary rectangular groove grating diffraction problem. Without any loss of generality the normal to the boundary is in the z direction, and the grating vector is in the x direction

diffraction is obtained when the grooves of the grating are not parallel to the incident beam. In Fig. 1.10 the general three dimensional binary grating is depicted. A linearly polarized electromagnetic wave is incident upon arbitrary angle θ and azimuthal angle ϕ. ψ is the angle between the incident electric field vector and the plane of incidence. The grating, with period Λ, lies in the region $0 < z < d$, bound to two different media with refractive index n_I and n_{II}. The grating consists of several regions with different refractive index. Consider Maxwell's equation inside a medium that is uniform in the z direction

$$\begin{aligned} \nabla \times \boldsymbol{E} &= -j\omega\mu_0 \boldsymbol{H}, \\ \nabla \times \boldsymbol{H} &= -j\omega\varepsilon_0\epsilon_0(x)\boldsymbol{E}, \end{aligned} \tag{1.53}$$

with the magnetic field normalized according to $\boldsymbol{H_g} = -j\sqrt{\frac{\mu_0}{\epsilon_0}}\boldsymbol{H}$. In the grating region the periodic relative permittivity can be expanded in Fourier series

$$\epsilon(x) = \sum_h \epsilon_h \exp\left(j\frac{2\pi h}{\Lambda}\right), \tag{1.54}$$

where ϵ_h is the *h-th* Fourier component of the relative permittivity in the grating region. The incident electric field vector is written as

$$\boldsymbol{E}_{inc} = \boldsymbol{u}\exp\left[-jk_0 n_I\left(\sin\theta\cos\phi x + \sin\theta\sin\phi y + \cos\theta z\right)\right], \tag{1.55}$$

where

$$\begin{aligned}\boldsymbol{u} = &(\cos\psi\cos\theta\cos\phi - \sin\psi\sin\phi)\,\hat{x}\\ &(\cos\psi\cos\theta\cos\phi - \sin\psi\sin\phi)\,\hat{y}\\ &(-cos\psi\sin\theta)\,\hat{z}.\end{aligned} \tag{1.56}$$

The normalized solution for $0 < z$ reads

$$\boldsymbol{E}_I = \boldsymbol{E}_{inc} + \sum_i \boldsymbol{R}_i \exp\left[-j\left(k_{xi}x + k_y y - k_{I,zi}z\right)\right], \tag{1.57}$$

while for the region $z > d$

$$\boldsymbol{E}_{II} = \sum_i \boldsymbol{T}_i \exp\left\{-j\left[k_{xi}x + k_y y + k_{II,zi}\left(z - d\right)\right]\right\}. \tag{1.58}$$

$\boldsymbol{R}_i$ and $\boldsymbol{T}_i$ are the normalized electric field vector amplitude of the reflected and transmitted wave in region II. The three component of the wavevector $\boldsymbol{k}$ are given as

$$\begin{aligned} k_{xi} &= k_0\left\{n_I\sin\theta\cos\phi - i(\lambda_0/\Lambda)\right\}\\ k_y &= k_0 n_I \sin\theta\sin\phi\\ k_{l,zi} &= \begin{cases}\left[(k_0n_l)^2 - k_{xi}^2 - k_y^2\right]^{1/2} & (k_{xi}^2 + k_y^2) < k_0 n_l\\ -j\left[k_{xi}^2 + k_y^2 - (k_0n_l)^2\right]^{1/2} & (k_{xi}^2 + k_y^2)11/2\end{cases} \qquad l = I, II.\end{aligned} \tag{1.59}$$

In the grating region, where $0 < z < d$, the electric and magnetic field vector are Fourier expanded in terms of the space harmonics fields

$$\boldsymbol{E}_g = \sum_i \left\{S_{xi}(z)\boldsymbol{x} + S_{yi}(y)\boldsymbol{x} + S_{zi}(z)\boldsymbol{z}\right\}\exp\left\{-j\left(k_{xi}x + k - yy\right)\right\}, \tag{1.60}$$

$$\boldsymbol{H}_g = -j\left(\frac{\varepsilon_0}{\mu_0}\right)^{1/2}\sum_i \left\{U_{xi}(z)\boldsymbol{x} + U_{yi}(y)\boldsymbol{x} + U_{zi}(z)\boldsymbol{z}\right\}\exp\left\{-j\left(k_{xi}x + k - yy\right)\right\}. \tag{1.61}$$

where $S_i(z)$ and $U_i(z)$ are the amplitude of the normalized vector of the *i-th* space harmonic fields such that satisfy Maxwell equations (1.53) in the grating region. Substituting eq. (1.61) and (1.61) in the Maxwell equations (1.53), and taking into account that the z components of the fields are constant one can obtain the expression for the diffraction efficiencies

$$DE_{ri} = |R_{s,i}|\, Re\left(\frac{k_{I,zi}}{k_0 n_i\cos\theta}\right) + |R_{p,i}|^2\, Re\left(\frac{k_{I,zi}/n_I^2}{k_0 n_I\cos\theta}\right), \tag{1.62}$$

$$DE_{ri} = |T_{s,i}|\, Re\left(\frac{k_{II,zi}}{k_0 n_i\cos\theta}\right) + |T_{p,i}|^2\, Re\left(\frac{k_{II,zi}/n_I I^2}{k_0 n_I\cos\theta}\right). \tag{1.63}$$

1.3 Summary

In this chapter a short description of SAW is given. A SAW is excited taking advantage of the converse piezoelectric effect via an IDT. The IDTs can be produced in different configurations. Within this work the IDTs in single and split configurations were chosen due to their simple and effective design. Three different models that describe the interaction of X-rays with SAW are presented. The kinematical theory of diffraction describes scattering of spherical waves by scattering density at fixed phase and it does not take into account multiple scattering. The results of the kinematical theory of diffraction are used to describe the interaction of X-rays first with the substrate via the Bragg law, and then with the SAW in either meridional or sagittal geometry. Within this framework the angular distance of the diffraction satellites can be calculated. The dynamical theory takes into account the phase of the waves and multiple scattering, correcting for refraction shape and width of the peaks. The results are used to calculate the penetration depth of the X-rays in different materials. The intensity of the diffraction satellites can be simulated using the kinematical theory of diffraction, the dynamical theory of diffraction, or the RCWA method. The latter is rigorous method able to solve Maxwell's equations without approximation, and it takes into account only the refractive index and permittivity of the materials involved. The latter method is preferred for its simplicity and used to calculate the intensity of the diffraction satellites within this work.

Chapter 2

Materials and Methods

In this chapter the materials used in this thesis are reviewed. The SAW devices under study in this thesis have been fabricated on Lithium Niobate, $LiNbO_3$, and Lanthanum gallium silicate, $La_3Ga_5SiO_{14}$, two piezoelectric crystals. To design the layout of the IDT was used Python, and in particular the Gdspy module, a module for creating, importing and merging GDS stream files. The functions defined to design the IDTs are available in Appendix B. It follows a short and non exhaustive protocol about the production of the samples. A method for testing the functionality of the samples with a Vector Network Analyzer is described. Finally a short review of the experimental methods is given.

2.1 Material Choice

The technical characteristics of SAW devices are susceptible to the materials used in their design. However there is no universal list of materials intended for different SAW devices. A brief summary of the criteria used to search and individuate the optimal material is discussed. SAW characteristics such as their speed, amplitude and frequency depend both on the physical response of the surface and on external influences. At the present time none of the known SAW material satisfies all the requirement simultaneously, thus the material choice is the result of a trade-off. The external influences consist of temperature, pressure or surface contamination. The SAW devices under study in this work have been used in air or in vacuum, where no contamination is assumed, at room temperature, 300 K. The physical response of the material consists of parameters as the rigidity, the conductivity, the density and dielectric constants. In the SAW devices considered in this work, the generation of waves is achieved by application of a voltage to the IDT deposited on a piezoelectric crystal. A piezoelectric material, which is necessarily anisotropic, can be classified as a ceramic or a crystal. Ceramic materials are limited by the attenuation of SAW, that is generally too high for frequencies above 50 MHz. A great number of publication studied SAW propagation in piezoelectric crystals, since it depends not only on the material but also on its orientation: the surface normal direction and the wave propagation direction, relative to the crystal lattice, influence both the speed and amplitude of the SAW. In table 2.1 a comparison of the piezoelectrics used as substrate for SAW device in this work with Quartz is shown. For the purpose of this work, the most important parameter is k^2, the piezoelectric coupling coefficient.

Additionally to the substrate also the appropriate material for the IDT should be selected. The three most common metals and their properties are shown in table 2.2. It is preferable to choose a material with low electrical resistance. Since the devices under study are operated at room temperature, Aluminum is the optimal choice.

Material	Formula	Cut	V [m/s]	Att. rate [dB/μs]*	k^2 [%]	Source
Quartz	$Si0_2$	ST,X	3158	0.75/18.6	0.11	[7]
Quartz	$Si0_2$	YX	3159	0.38/14	0.19	[53]
Lithium Niobate	$LiNbO_3$	YZ	3488	0.25/5.8	4.5	[7, 53]
Lithium Niobate	$LiNbO_3$	128°Y	3992	0.27/5.2	5.54	[53]
Lithium Tantalate	$LiTaO_3$	YZ	3230	0.26/6.13	0.66	[53]
Langasite	$La_3Ga_5SiO_{14}$	Y	2343	–/17.0	0.44	[54]

TABLE 2.1: Physical properties of materials commonly used as SAW substrates. * On frequency 433/2450 MHz

Material	Electrical resistance [$\mu\Omega \times cm$]	Melting Point [°]	Cost
Aluminum	2.65	660	low
Titanium	50	1668	medium
Platinum	20-25	1768.3	high

TABLE 2.2: Characteristics of the metal commonly used for the production of IDT, from [53]

Quartz Quartz is a piezoelectric crystal with chemical formula SiO_2. This material belongs to the point group 32, but exhibit the phase transition at 573°C. Quartz is one of the first material used as SAW substrate, and it is therefore included in the table. Due to the low value of the k^2 constant it was not chosen as a substrate for the SAW devices.

Lanthanum Gallium Silicate Often shortened in Langasite or LGS, is a piezoelectric crystal with chemical formula $La_3Ga_5SiO_{14}$. This crystal belongs to the same point group as quartz, 32, but exhibit the phase transition at much higher temperature, 1475°C. LGS is interesting for application at synchrotron facilities because of strong scattering, and small penetration depth for X-rays, due to the high concentration of heavy element atoms.

Lithium Niobate Often shorted in LNB, it is a piezoelectric crystal with chemical formula $LiNbO_3$. It belongs to the point group 3m, and it exhibits a phase transition at 1257°C. LNB is interesting for application at synchrotron facilities because of strong scattering, and small penetration depth for X-rays, due to the high concentration of heavy element atoms. Moreover, the SAW speed on the 128° cut of LNB is relatively high, and the piezoelectric coupling coefficient is 50 times higher than in quartz.

2.2 IDT design

When it comes to designing the IDT, it is a matter of trade-off. It follows a short list of the parameters taken into account.

- **Period**: the IDT period influences the SAW wavelength. The smaller the SAW wavelength, the higher the angles at which the diffraction satellites appear, the easier will be to resolve the diffraction satellites on a detector. At the same time, the smaller is the period, the more complicated is to obtain the structures. A good trade off is to make an IDT that excites SAW with $\Lambda = 4\ \mu$m.

- **Acoustic aperture**: the larger the acoustic aperture, see Fig. 1.2, the easier it will be to overlap the SAW path with the X-ray beam. The optimal aperture is in the order of 100 Λ. It can be stretched to values that are two or three times higher, but not ten times higher.

- **SAW amplitude**: for practical application, see chapter 4 for an example, it is important that the first order of diffraction reaches its maximum intensity. Choosing an IDT in *split electrode geometry*, Fig. 1.1c, rather than in *simple geometry*, Fig. 1.1a, guarantees higher SAW amplitude for the same voltage.

- **Simplicity**: The IDT designs described in this thesis, are some of the simplest designs that can be realized. This guarantees that the behavior of the IDT is easily understandable and predictable. Many other designs, much more complicated, can be produced, see [6, 7].

2.3 Sample Fabrication

Two standard techniques have been used for the fabrication of SAW devices, photolithography and e-beam lithography. The first one is more suited for mass production of the samples, while the second one, more time consuming, is indicated to produce single samples that require greater precision. Even though the chemicals used for fabricating SAW devices differ depending on the used technique, the procedure itself, apart from two steps, is really similar. Once selected the desired substrate, polished to a roughness of 5 Å, the procedure is as follows, see Fig. 2.2.

Step 1 – Substrate preparation The substrate is mounted on a spinner and accelerated to approximately 6000 rev/min, while pouring on the substrate acetone, followed by methanol and then distilled water.

Step 2 – Coating Once the appropriate kind of resist is selected, the substrate is spin-coated with it. The dilution of the resist, and the final thickness depends both on the design of the IDT, and on the thickness that should be achieved. The sample is usually baked for a better adhesion of the resist on the substrate.

Step 3 – Conductive Layer application (Only for e-beam lithography) To prevent charge accumulation on the surface, that would deviate the electron beam, a low resistance path from the sample to ground must be provided. This can be realized depositing a thin Aluminum layer on top of the resist layer.

Step 4 – Pattern exposure The substrate are exposed either to the electron beam or to UV light.

Step 5 – Development The substrates is then submerged in a developing agent. To remove all the resist residual from the IDT pattern, the samples undergo an air plasma etching. This ensure better adhesion during the IDT deposition.

Step 6 – Metallization For the samples used in this work, approximately 100 nm of Aluminum have been deposited. The excess of Al and resist is then removed during the lift-off process, where the substrate are submerged in an appropriate acid solution.

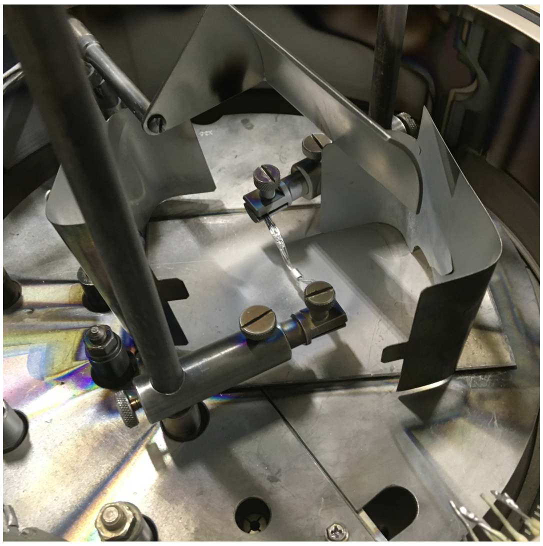

FIGURE 2.1: Experimental setup of the evaporator. It is visible in the middle the filament with some Al on it, and the shutter.

Step 7 – Wiring The substrate are glued on a breadboard. Contact wires are glued with a conductive silver based glue on the contact pads and soldered on the side on the breadboard, see Fig. 2.3 for an example.

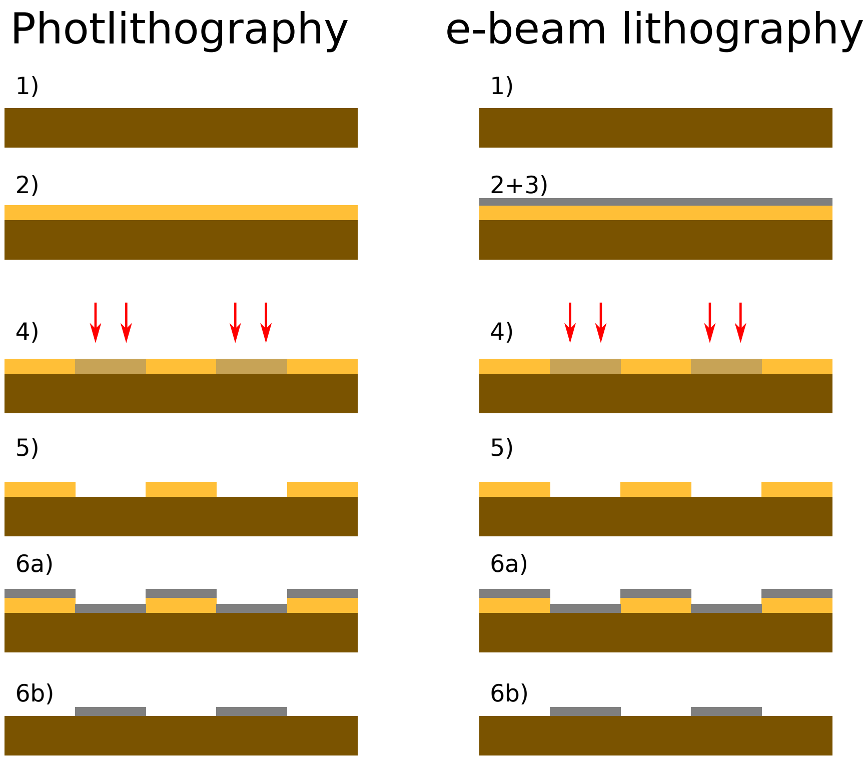

FIGURE 2.2: Schematic of the IDT production process with photolithography and e-beam lithography. The numbers refer to the steps described in text.

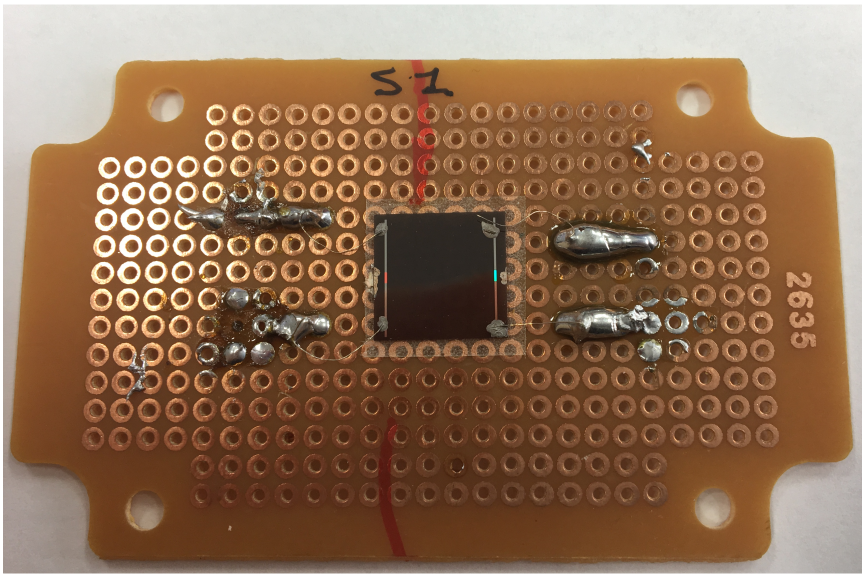

FIGURE 2.3: Example of a sample mounted on a breadboard.

2.4 Vector Network Analyzer measurements

The S-parameters describe the input-output relationship between ports (or terminals) in an electrical system, see section 1.1.3. A port can be loosely defined as any place where voltage and current can be delivered. When measuring SAW devices the ports are the IDTs. Having a SAW device with two identical IDTs facing each other, two different measurements are possible. One can measure either the S_{11} parameter, the reflected power delivered to the connected IDT, or the S_{21}, the power that is delivered from IDT 1 to IDT 2. Note that S-parameters are a function of frequency.

The measurements performed with a Vector Network Analyzer (VNA) are particularly useful. Once a new sample is delivered and connected, the functionality of the IDT can be tested, and the working frequency can be easily found. Theoretically, knowing the speed of SAW on a certain substrate, and knowing the period of the IDT, the frequency can be estimated via the simple relation $f_0 = v_{SAW}/\Lambda$. The activation frequency can differ from the theoretical frequency for several reasons. The speed of the SAW is influenced by the rigidity of the body, in fact SAW speed measurements are often used to estimate material properties of the substrate, as the Young's modulus. The purity of the material is another factor that could modify the speed of the SAW. In Fig. 2.4a and 2.4b are shown the plot for the measured S_{11} and S_{21} parameters for three different samples, S1, M1 and L1, which have the same IDT period on a 128° $LiNbO_3$ substrate, but with a different number of fingers. Given the tabulated SAW speed of v_{SAW} =3992 m/s and the SAW period of Λ =4 μm, the resulting activation frequency should be 998 MHz. The activation frequency measured by the VNA is approximately 985 MHz.

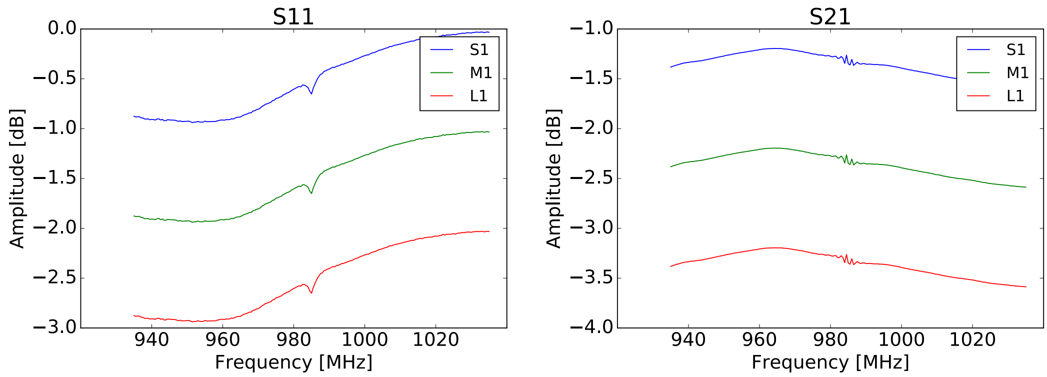

(A) (B)

FIGURE 2.4: S_{11} (**A**) and the S_{21} (**B**) parameter measured for the S1, M1 and L1 sample.

Moreover, having a portable VNA device, is practical to check all the cables and the connections. For example, the 50 Ω radio frequency cables used to connect the sample with a high frequency generator, do not optically differ much from the 75 Ω cables, but they are not able to transmit the RF signal. If the measurements have to be performed in vacuum, as it is the case for measurements with soft X-rays, all the connection and feedthroughs must be checked to ensure that a SAW is actually excited on the substrate surface. In Fig. 2.5 six different S_{11} measurements of the same sample, on the same IDT, with three different cables and a feed-through for a vacuum chamber are shown. The measured activation frequency, does not depend on the cables nor on the feedthrough, and it is stable around the value 285 MHz. This measurements ensure that the IDT is working and a SAW is excited on the crystal surface. For different combination of cable and feedthrough the VNA measures different loss. This is not connected with the amplitude of the SAW, which can not be deduced from such a plot. Different passive electrical components along the connection between the VNA and the sample have different reflection coefficients, which in turn depend on the frequency. This explains the different loss and the different electrical behavior.

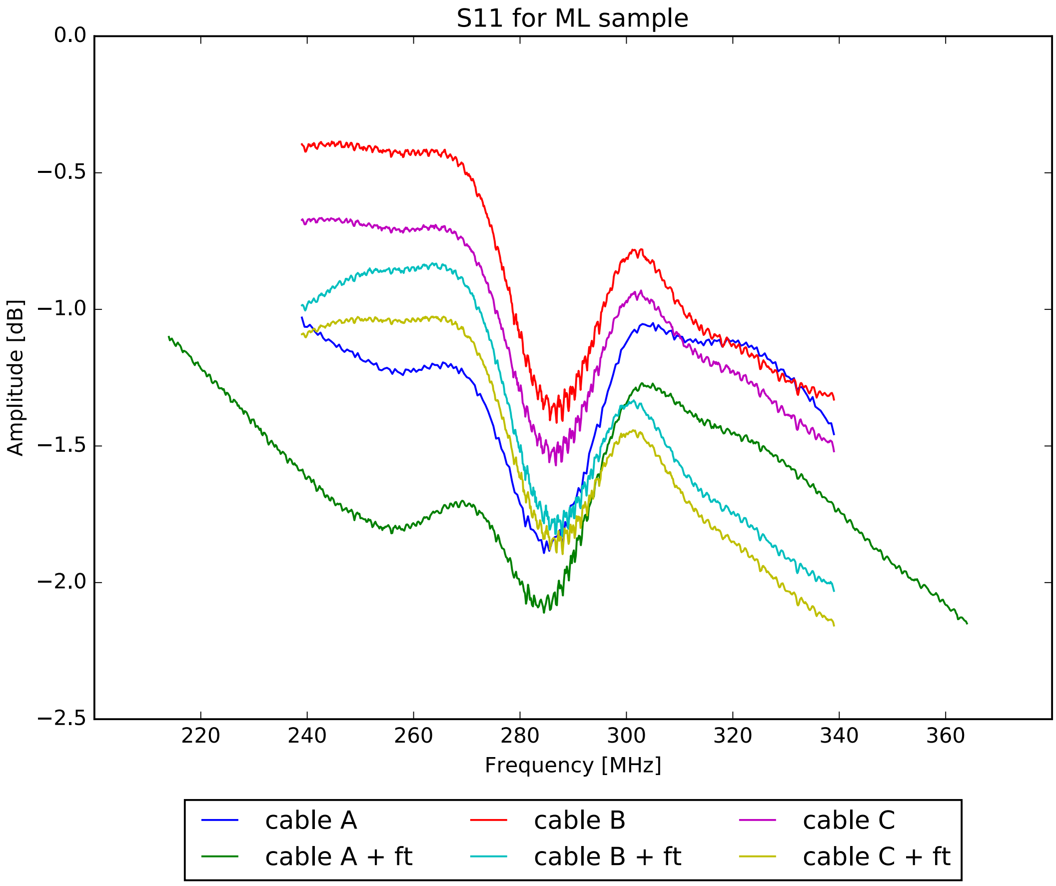

FIGURE 2.5: S_{11} measurements performed with a VNA. Three different cables are tested, and one feedthrough (abbreviated in "ft" in the legend.)

2.5 Diffraction measurements – short review

A short review of the methods used in the experimental part of the thesis is provided.

Meridional geometry – Rocking Curve The detector is fixed at the center of the expected Bragg reflection, the sample is tilted step wise (*rock it*) and for every angular step the diffracted intensity is recorded. The result is a distribution of intensities over tilting angles. To resolve the diffraction satellites, one must make sure that the divergency of the beam is smaller than the angular distance of the diffraction satellites, and that the detector slits, or the pixels of a CCD camera, are small enough to not be hit by X-rays coming from different diffraction satellites.

Sagittal geometry – Diffraction pattern The detector is fixed at the center of the expected Bragg reflection. If an area detector is used, the diffraction pattern can be recorded in one shot, since the diffraction satellites appear all at once. If a point detector is used, this must scan perpendicularly to the scattering plane. To resolve the diffraction satellites, one must make sure that the divergency of the beam is smaller than the angular distance of the diffraction satellites. Additionally, considering a CCD camera, one must be sure that two diffraction satellites do not hit the same pixel. If this is the case there are two trivial solutions. Move the detector further away from the sample, or use a detector with smaller pixel size.

Bragg topography It is an imaging technique, and it represents a two dimensional spatial intensity mapping of the diffracted X-rays. It reflects the irregularities of the sample. An area detector is fixed at the center of the expected Bragg reflection, the sample is illuminated with wide beam and an image is recorded. When a SAW is excited it is possible to see the trace of the waves on the sample, a line less intense compared to the neighboring areas. Note that if the beam is manipulated with some optics, Bragg topography will be the result of the convolution of the signal due to the optic elements and the sample.

Heat map or Bragg diffraction map The detector is placed at the center of the first diffraction satellite. Normally is used a point detector with slits or an area detector selecting only the region of interest corresponding to the pixel(s) where the first diffraction satellite is diffracted. While a SAW is excited on the surface of the sample, the surface is scanned. When the beam overlap with the SAW trace on the sample higher intensity is expected. If the sample is not plane, or it not possible to align it perfectly, at every point (x,y) a rocking curve is recorded. The result can be plotted as a heat map.

$\Theta - 2\Theta$ map For a selected range of 2Θ values, the detector is fixed at a certain 2Θ angle, and a rocking curve centered at $\theta = 2\theta/2$ is measured. Such a map can be transformed in a **reciprocal space map** by a simple change of coordinates:

$$q_x = \frac{2\pi}{\lambda}(\sin(2\Theta)\sin(\Theta - \frac{2\Theta}{2}))) \tag{2.1}$$

$$q_z = \frac{2\pi}{\lambda}(\sin(2\Theta)\cos(\Theta - \frac{2\Theta}{2}))) \tag{2.2}$$

Y scan The emission of a SAW is electronically pulsed and synchronized with the arrival of the X-ray pulse. The SAW pulse duration and delay are set to fix values. The sample is set to the Bragg peak and scanned along the y direction, parallel to the incoming beam direction. Since it would not be possible to align perfectly the sample for its complete length, every few step in y position the sample must be re-aligned.

Voltage Scan While the angular position of the diffraction satellites depends on the wavelength of the incoming beam, the SAW wavelength, and the incident angle, the intensity of the diffraction satellites depends on the amplitude of the SAW, as in eq. 1.47. A voltage scan is a series of diffraction patterns measured with increasing SAW amplitude. This is done increasing the voltage delivered to the IDT, hence the name voltage scan. This can be performed both in meridional or sagittal geometry. For a given experimental setup, the amplitude of the SAW depends on the voltage applied to the IDT, and the proportionality factor C of equation 1.48 can be estimated by comparison with the simulated rocking curves.

2.6 Sample Alignment Procedure – Tip and Tricks

When operating a beamline and performing diffraction experiments, the alignment procedure is not always straightforward. The alignment procedure of the complete beamline is beyond the scope of this work, and it will not be described. Consider the angle and the axis shown in Fig. 2.6. Let us assume that the center of the detector

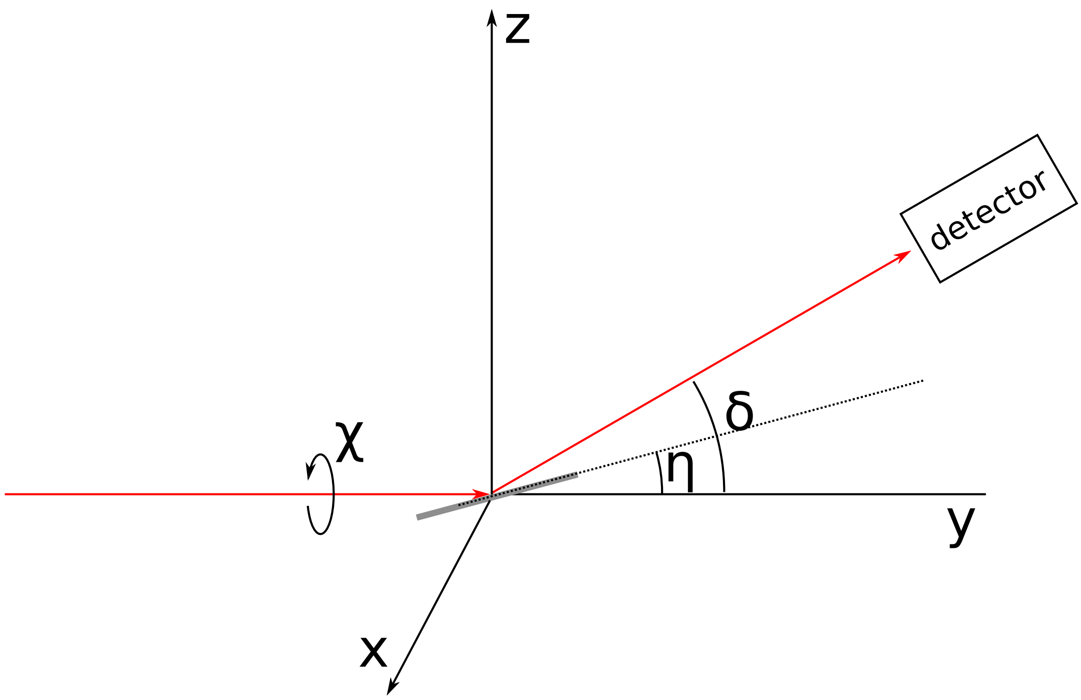

FIGURE 2.6: The X-ray beam is represented by the red arrows. The sample is represented by the grey bar, rotated by an angle η. The detector is rotated by an angle δ.

is aligned to the X-ray beam, as in Fig. 2.7a. The first step is to align the sample to be parallel to the incoming beam, acting on z, η and χ, until reaching the situation in Fig. 2.7b. Once the sample is perfectly aligned it can be rotated to the theoretical value of the Bragg angle, $\eta = \Theta_B$. The detector is rotated to $\delta = 2\Theta_B$. The higher

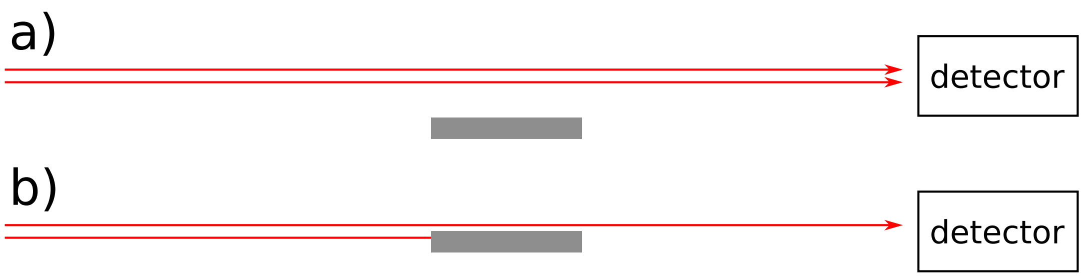

FIGURE 2.7: The X-ray beam is represented by the red arrows. The sample is represented by the grey bar. In a) the detector is aligned to the beam and the sample is out of the X-ray beam. In b) the sample have been aligned and it is shadowing half of the X-ray beam.

the distance between the sample and the detector, the more complicated can be to find the Bragg peak. This because even small error in the alignment of the sample might cause the beam to not hit the detector. If this is the case, the simplest solution is to mount a second detector close to the sample to individuate the Bragg angle. If a second detector is not available the detector can be moved close to sample, but all the information about the absolute value of the δ angle will not be reliable. Once the Bragg angle has been found, it is easier to find the Bragg peak with the detector far away, since the c of the problem have been reduced from three (η, χ, δ) to two ($\eta = \Theta_B$, χ, δ).

Once the Bragg peak has been found, the X-ray beam footprint must overlap with the SAW path on the sample. There are three different paths that can be followed.

Finding SAW using fluorescence or burn paper Fluorescence paper is a special paper that emits visible light when hit by X-rays. Burn paper is a special paper that changes permanently its color when hit by X-rays. A little strip of one of this two papers can be mounted next to the crystal, possibly approximately at the same height. If it is possible to look at the sample with a camera sensible to visible light, once the X-rays will hit a fluorescence dot will appear. The position of the beam can be noted, and then it is easy to overlap the X-ray beam with the SAW path, which run straight in front of the IDT.

Finding SAW using lead wing This method is especially useful if the beamline is not equipped with a camera pointing at the sample. Lead wings are simply stripes of adhesive lead that can be mounted perpendicularly to the sample surface. Lead strongly absorb X-rays, and even only one millimeter of lead might completely shield the X-ray beam. The wings can be placed in strategic positions on the sample, and their position in x and y direction can be easily found if the sample and the detector are set to $\eta, \delta = 0$.

Finding SAW using Bragg reflection It is possible, even though more complicated, to overlap the X-ray beam footprint with the SAW path even without any fluorescence/burn paper nor lead wings. Once the sample is set to the Bragg angle, it is enough to scan the x and y directions for the complete range of the motors. If the motors can move far enough, the Bragg peak will drastically disappear when the X-ray beam footprint reaches the the edge of the sample and it overlaps with non-reflective material. Once found the two edges in x direction, and the two edges in y direction, and knowing the topology of the sample, it is easy to move the beam to the coordinates where the SAW path is. The drawbacks of this method are at least two. First, sometimes it is difficult to follow the Bragg reflection because the sample might be not flat, for example due to polishing. Second, it is possible that the motor can not move enough, and the X-rays never fall off the sample.

What might seem a trivial problem, it can turn into several hours wasted to align the sample. One should consider that the indications we have on the activation frequency of the sample, obtained either via the theoretical formula $f = v_{SAW}/\Lambda$ or with the Vector Network Analyzer, for a number of reason might differ from the frequency that activates the SAW when connected to a high frequency generator.

2.7 Summary

Choosing the proper materials for a SAW device could be a long and difficult process. Especially because most of the publications and books are not aiming to study the interaction of X-rays with SAW. In this chapter the guidelines to choose the proper materials and the most effective IDT design are defined. It is explained how to use a Vector Network Analyzer for SAW devices diagnostic. A short review of the X-ray methods used to study the interaction of X-rays and SAW is provided in the last section.

Chapter 3

Experimental Results

In this chapter four experiments are presented. The first one is Bragg diffraction in sagittal geometry on a Langasite crystal modulated by $\Lambda = 3$ μm SAW at E = 8 keV. The second one comprises measurements in Bragg diffraction and total external reflection conditions in meridional geometry on a Si/W multilayer modulated by $\Lambda = 4$ μ, at E = 1000 eV and E = 600 eV. The third one and the fourth one are time resolved measurements in meridional and sagittal geometry respectively, aimed to prove the time structure of a Synchrotron using the interaction of X-rays with SAW.

3.1 Synchrotron radiation sources

Synchrotron radiation (SR) takes its name from a specific type of particle accelerator, the synchrotron. SR is generated when a light charged particle traveling at relativistic speed is subject to a transverse acceleration. This last condition is usually realized when a particle travels in a strong magnetic field, and is forced to travel along curved paths. In synchrotrons, electrons travel on a path comprised of short straight segments, deflected by bending magnets. Bending magnets generate a continuous spectrum from infrared radiation up to soft or hard X-rays, depending on the energy of the electrons. In between the bending magnets, electrons may pass through other kind of insertion devices, like wigglers and undulators. In this case the spectrum of emitted radiation is not continuous, but rather strongly peaked, depending on the strength of the magnetic field of the insertion device. The energy of an electron with mass m_e traveling at speed v is

$$E_e = \frac{m_e c^2}{\sqrt{1 - \left(\frac{v}{c}\right)^2}}. \tag{3.1}$$

This is usually conveniently expressed in units of its rest mass energy $\gamma = E_e/mc^2$, and of the speed of the electron measured in units of the speed of light $\beta_e \equiv v/c$

$$\gamma = \frac{1}{\sqrt{1 - \beta_e^2}}. \tag{3.2}$$

From eq. (3.2) the expression for the speed of the electron can be obtained, and since for synchrotron radiation $1/\gamma^2 \simeq 10^{-8}$ one can expand the equation and obtain

$$\beta_e = \left[1 - \frac{1}{\gamma^2}\right]^{1/2} \simeq 1 - \frac{1}{2\gamma^2}. \tag{3.3}$$

At relativistic speed, the radiation emitted by an electron is no longer shaped in a dipole pattern, but it is emitted in a narrow cone

$$d\vartheta \simeq \frac{1}{\gamma}. \tag{3.4}$$

In the case of BESSY II, where $\gamma = 3332$ and $\beta \simeq 1$, the angle is approximately $\vartheta = 0.3$ milliradians. The concentration of emitted photons into such a small cone is the reason why synchrotron radiation is such a powerful X-ray source.

BESSY II is made up of three main parts, a linear accelerator (linac), a booster and a storage ring. The linac and the booster are subsequently used to generate electrons and accelerate them up to 1.7 GeV. The electron are then injected in the storage ring, where are forced to travel in a circle (polygonal approximated), and where they stay up to ten hours. Several bending magnets are used to keep the electrons running in a closed loop. BESSY II operates in the so called Top-Up injection mode, that guarantees an almost continuous refill of the storage ring with electrons, that leads not only to a higher and more constant flux, but also to a better thermal stability of the storage ring components. In the straight sections between the bending magnets there are two more kind of insertion devices, wigglers and undulators. Those consists of arrays of magnets with alternating field directions. The electron beam passes through such a periodic arrays in nearly sinusoidal trajectories. At each turn the electrons radiate with a critical wavelength given by

$$\lambda_c = 5.59R[m]/E^3[GeV]. \tag{3.5}$$

An important quantity characterizes wigglers and undulators, the K parameter

$$K = 0.934\lambda_0[cm]B_0[T], \tag{3.6}$$

where λ_0 is the periodicity of the alternating magnetic field, and B_0 is the peak magnetic field. The distinction between wigglers and undulators is based on the K parameter.
If $K >> 1$ the insertion device is called a wiggler. When the electrons pass through the poles of a wiggler they emit radiation which is incoherently superimposed. The wiggler spectrum is similar to the one produced by a bending magnet, but with a critical energy determined by the peak magnetic field in the wiggler. Given a wiggler with N periods, which emit radiation with an horizontal opening angle of $2\delta = 2K/\gamma$, then the intensity of the emitted radiation is $2N$ times higher than the one emitted by a bending magnet within the same 2δ angle, see Fig. 3.1.
If $K < 1$ the insertion device is called undulator. The radiation emitted by the electrons passing in the alternated magnetic field of a undulator superimpose coherently. The spectrum, emitted within an horizontal angle $\delta = k/\gamma$, see Fig. 3.1, is thus characterized by interference effects, which lead to a spectrum consisting of sharp peaks at

$$\lambda = \frac{\lambda_0}{2\gamma i}\left(1 + \frac{1}{2}K^2 + \gamma^2\Theta^2\right), \quad i = 1, 2, 3, ... \tag{3.7}$$

where λ_0 is the undulator period.

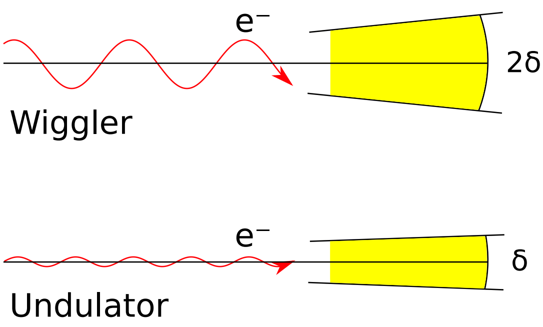

FIGURE 3.1: SR from a wiggler and an undulator

3.1.1 The time structure of synchrotron radiation

When the electrons pass through an insertion device they emit radiation and loose energy. In order to restore this energy the electrons pass through radio frequency cavities, and they are kept stored in their orbit. In the radio frequency cavity a time dependent sinusoidal field is present, and only the electrons with the right phase can surf the RF wave and be accelerated, see Fig. 3.2. As a consequence, it exists a defined number of positions for which electrons can be in phase with the cavity voltage, the so called *buckets*. Thus electrons are not homogeneously distributed along the orbit, but are grouped in buckets. The electrons in a bucket constitute a *bunch*. The maximum number of buckets that can be stored in the ring is limited by

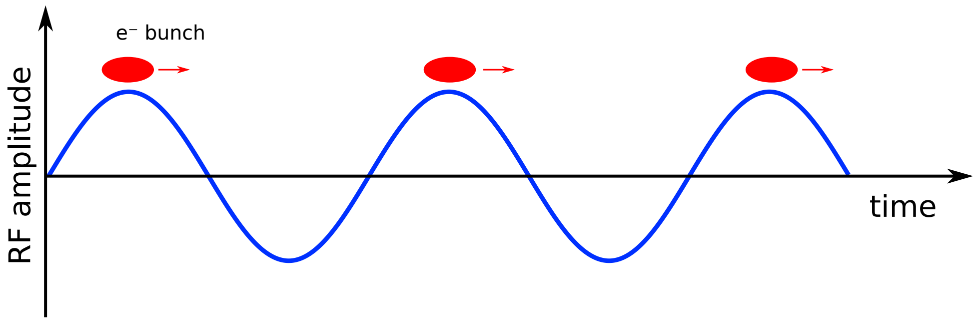

FIGURE 3.2: Schematic of the interaction of the electrons with the RF wave. The electron in phase with the wave are accelerated, while the others are scattered by the out of phase excitation and lost.

$$N_{max}^{buckets} = f_{RF} \cdot \frac{L}{c}, \tag{3.8}$$

where f_{RF} is the radio frequency, L is the circumference of the storage ring and c is the speed of light. The time between two consecutive bunches is

$$\Delta t = \frac{L}{c} \cdot \frac{1}{N_{max}^{buckets}}. \tag{3.9}$$

For instance at BESSY II $\Delta t = 2$ ns. Naturally, the radiation produced by the electron bunches is not continuous, but it has a time structure. Since time resolved measurements gained more and more importance, short flashes of light became really important. Unluckily the short flashes of light produced by the electron bunches have a too high repetition rate to be useful in the majority of those experiments. The easiest solution is to fill only one bucket with electrons. This operation mode is usually called *single bunch mode* or *single bunch fill pattern*, see Fig. 3.3. In such a case the time between two bunches is

$$\Delta t_{sb} = \frac{L}{c}. \tag{3.10}$$

However, the single bunch operation mode has several disadvantages. It reduces the overall flux emitted by the synchrotron, making impossible or extremely slow experiments that do not strictly require the single bunch operation mode. It is not particularly flexible, because the repetition rate is fixed and can not be modified. As a consequence, during the year only a few weeks are dedicated to this mode in a synchrotron radiation facility. Nowadays synchrotron run most of year in the so

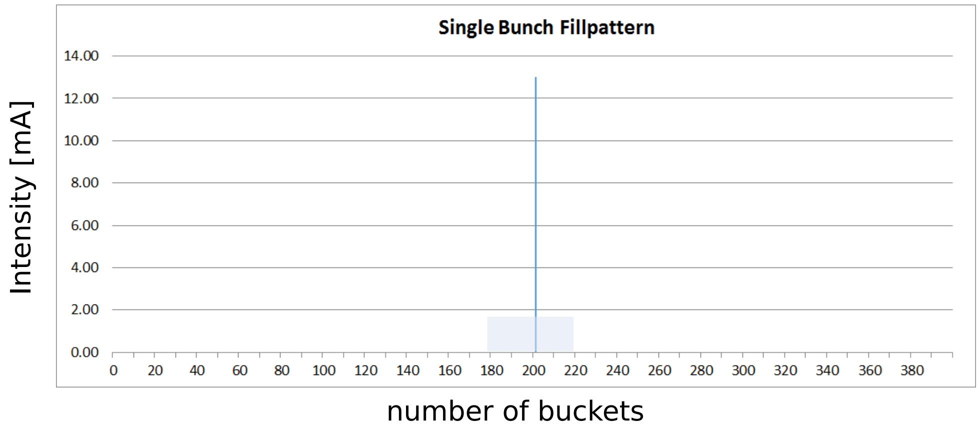

FIGURE 3.3: The single bunch operation mode at BESSY II. Only one bucket (number 201) is populated with electrons. The photon pulse derived from this bunch returns every 800 ns (1.25 MHz) according to the ring energy and the circumference. The purity of this single bunch, i.e. the ratio of electrons in the bunch to the number of electrons in other bunches, is 10^4.

called *hybrid mode*, see Fig. 3.4, which consist of a multibunch, several contiguous buckets filled with electron bunches, followed by a gap in the middle of which there is a single bunch. With such an operation mode, the simplest way to perform time resolved experiments is to switch on the detector only when the single bunch is coming, and keep it closed during the multibunch. This is said to *gate* the detector. This smart approach has, nevertheless, some disadvantages. First one, the detector has to be gated, and not all the detector can be gated, and not all the detector that can be gated are fast enough to open and close in a few hundreds nanoseconds. Second, the level of the noise can be quite high. Finally, even though the detector is gated, the sample is exposed also to the radiation coming from the multibunch. In this case the ideal approach is to use some optics in the beamline that rejects the radiation of the multibunch, and let pass the radiation generated by the single bunch. Such a device is called a *bunch selection chopper*, or more correctly a *pulse picker*.

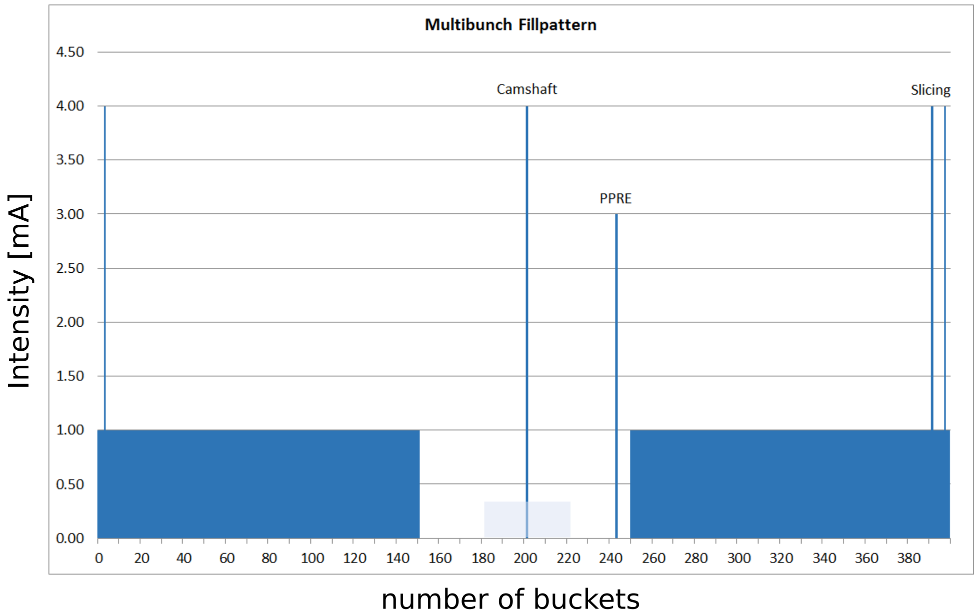

FIGURE 3.4: Consists of a Hybrid (or Camshaft) bunch at 4 mA (Chopper) in the center of the 200 ns wide ion clearing gap followed by the so-called PPRE-bunch of variable transverse excitation at 3 mA and 84 ns later. Together with the usual multibunch filling and the 3 slicing bunches on top of the multibunch train, now 302 out of 400 possible buckets in the storage ring are filled and topped up.

3.2 Bragg diffraction in sagittal geometry

Diffraction of X-ray radiation on an acoustically modulated LGS crystal was studied at the XPP-KMC 3 beamline [55] at the BESSY II synchrotron radiation facility.

3.2.1 SAW setup

The experimental setup presented in Fig. 3.5 is used to excite SAW continuously on the sample. SAW are excited using a high frequency (HF) generator (Hameg, HM8134/5), and a wideband RF amplifier with 5 W power (AR, KAW1020). The amplifier is needed because the signal generated by the HF generator has a maximal voltage of 1 V. The HF generator is controlled by PC via a Python script, and frequency and voltage can be changed remotely. The same PC can control also the area detector, if needed. The pc is then connected to the beamline control and acquisition system. To characterize a SAW device the SAW are excited continuously on the sample, and diffraction pattern are recorded.

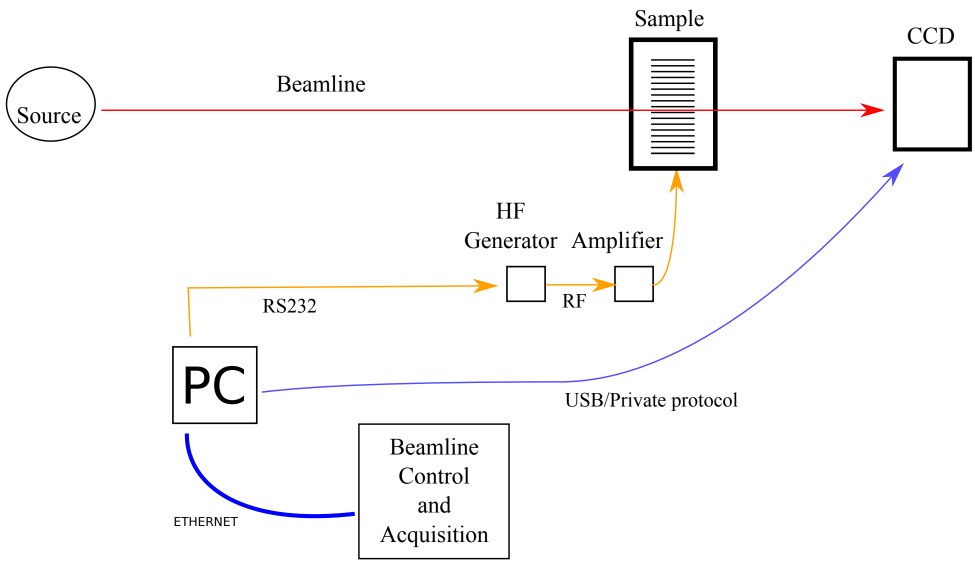

FIGURE 3.5: Experimental setup for SAW static experiment

3.2.2 XPP-KMC-3 beamline at BESSYII

The XPP-KMC3 beamline has a dipole as a source. In Fig. 3.6 is shown the beamline schematic. M1 is a parabolic mirror that makes the beam parallel. The desired X-ray energy, E = 8 keV, was selected with a double crystal Si (111) monochromator, with an energy resolution $\Delta E/E = 1/4000$. The beam is focused on the sample with the second mirror, M2. The sample was mounted on a goniometer that could translate and rotate the sample around the three axis. The intensity of diffracted X-ray radiation was recorded with a CCD camera with pixel size of 6.5 μm (Proscan), enough to see the order separation with a CCD sample distance of 1.1 m. The beam size at the sample position can be varied using the second pair of slits and it was cut down to 0.1×0.05 (h$\times$v) mm^2. The slits were closed vertically to 0.05 mm to increase the angular resolution.

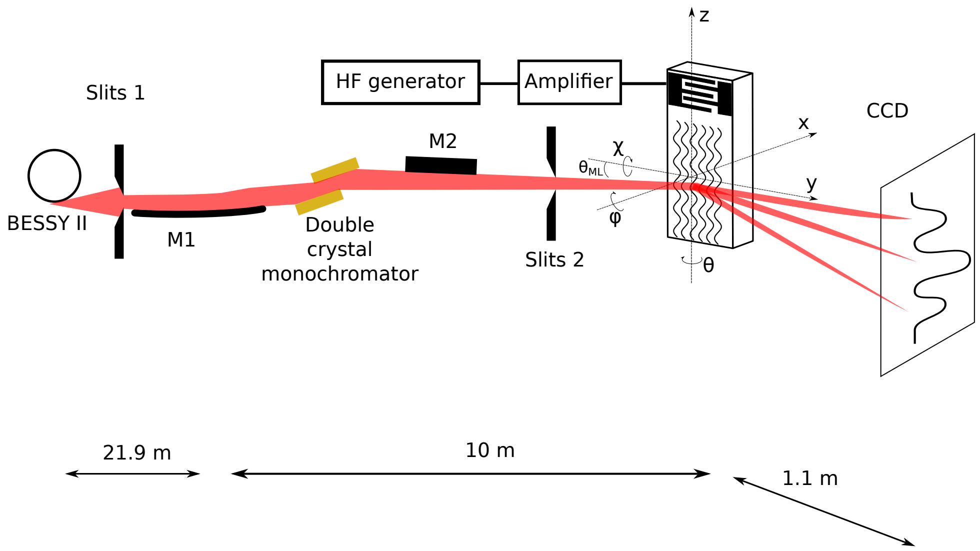

FIGURE 3.6: XPP-KMC3 beamline outline picture not to scale.

3.2.3 Sample – SAW device

For an overview of the sample and its properties see table A.1, at the voice LGS_1. The SAW device was made on a Y-cut of a LGS crystal, of point group symmetry 32. The crystal lattice parameters are $a = 8.170$ Å and $c = 5.095$ Å. The interplanar spacing was $d = 3.54$Å. The crystal was polished with roughness of approximately 5 Å. The crystal was grown along [210] axis by the Czochralski technique at *Fomos-Materials*. To excite a SAW, an interdigital transducer(IDT) made of Aluminum was deposited on the surface of the LGS crystal. The structure of an IDT was written on the LGS substrate coated with PMMA resist by e-beam lithography. The IDT was in single configuration, see section 1.1.3, the SAW wavelength was $\Lambda = 3$ μm, the propagation velocity was $v_{SAW} = 2343$ m/s. The resonance frequency was estimated with eq. (1.1.3) to be 781 MHz, and it coincided with the experimental value. The acoustic aperture, see Fig. 1.2, was w = 0.3 mm.

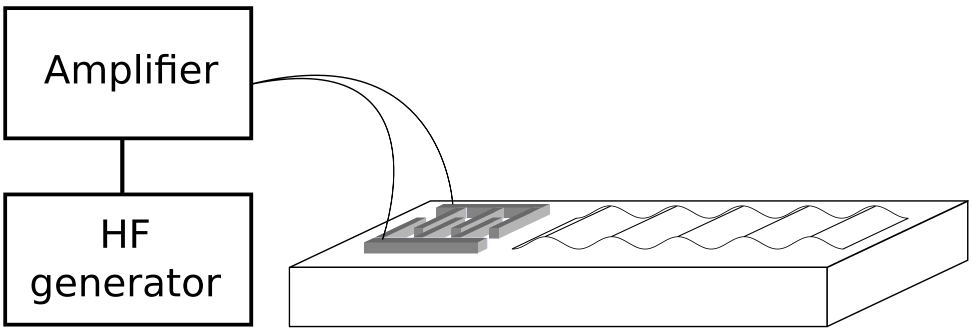

FIGURE 3.7: The SAW device. The IDT are connected to a high frequency generator.

3.2.4 Sample mounting

The sample was connected to a high frequency generator and an amplifier as described in section 3.2.1. The second Bragg reflection was used, with $\theta_B = 12.55°$. The sample was mounted inside a big vacuum chamber on a six axes goniometer, perpendicularly to ground, see Fig. 3.6. The reason for it is that the vertical divergence is much better than the horizontal one at the XPP-KMC3 beamline. The reason for using the second reflection, and not the first one that would be more intense, is due to the experimental chamber. To use the first reflection the detector should have been mounted inside the experimental chamber, see Fig. 3.9. This was not possible.

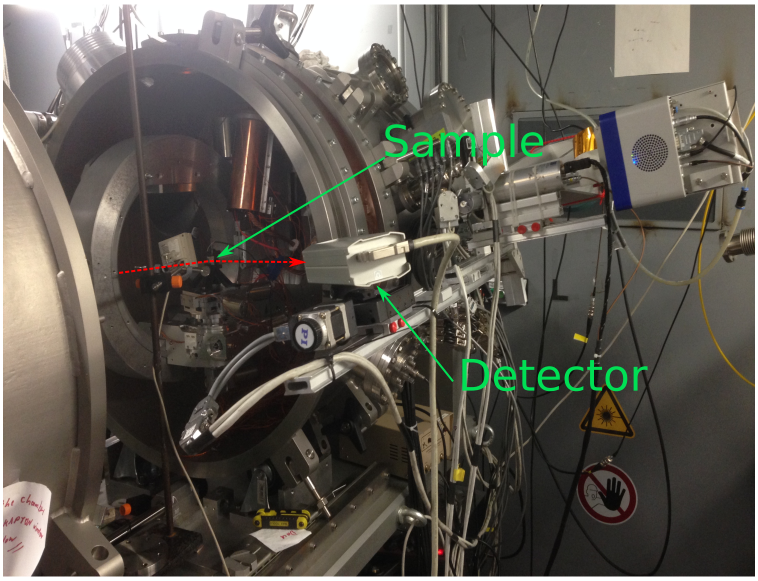

FIGURE 3.8: Picture of the diffraction setup at the endstation of the XPP-KMC3 beamline

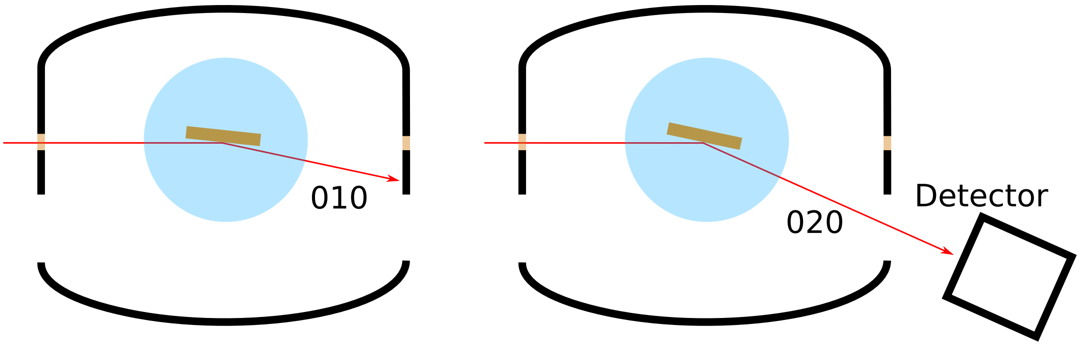

FIGURE 3.9: A schematic of the diffraction setup at the endstation of the XPP-KMC3 beamline, top view.

3.2.5 Simulations

The simulations were carried out with the GSolver software, see Appendix E. The results are shown in Fig. 3.10. On the Y axis is shown the intensity, normalized to one for the case of no SAW present on the crystal.

3.2.6 Results

The excitation of a SAW on the sample, a sinusoidal modulation of the crystal lattice, gives rise to diffraction satellites. The number and intensity of the satellites depends on the SAW amplitude. There is no need to rotate the crystal in sagittal geometry

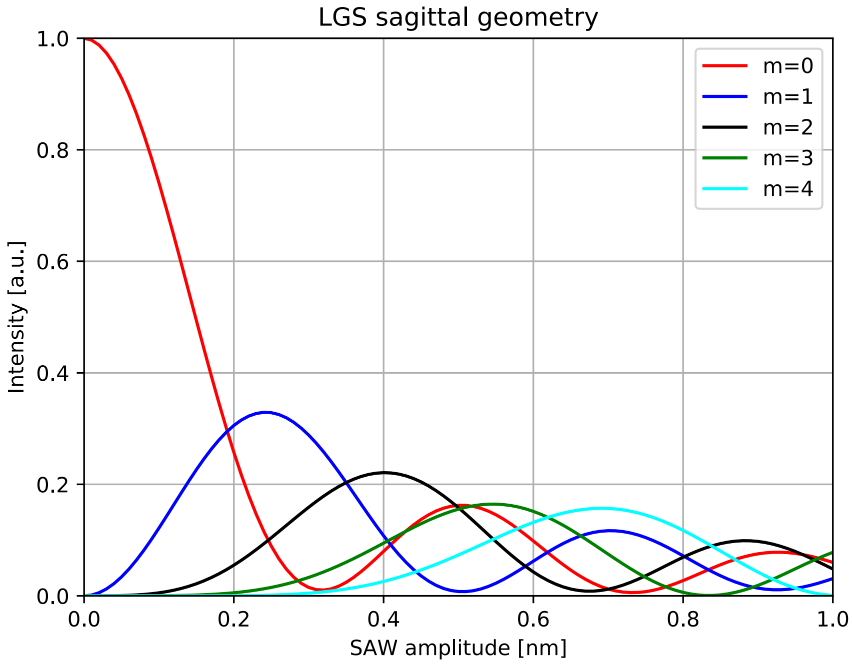

FIGURE 3.10: The diffraction efficiency for LGS depending on profile depth (SAW Amplitudes) calculated with GSolver for SAW grating with 3 μm period at the energy 8 keV in sagittal geometry.

since the satellites appear together with the Bragg peak. The amplitude of the SAW was varied by changing the voltage supplied to the IDT between 0 V and 40 V in steps of 10 V. The relative angular separation between the diffraction satellites depends exclusively on the ratio between the SAW and the radiation wavelength, as in eq. (1.39). Figure 3.11 shows the CCD camera images of X-ray Bragg diffraction on the SAW device. Increasing the amplitude of SAW more diffraction satellites are visible and with higher intensity. The angular separation between the diffraction satellites is $\delta\theta_{RC} = 9.7$ arcsec. Individual plots were obtained from each experimental image, considering only the pixel column in the center of the experimental image, Fig. 3.12 to 3.16. Finally the normalized intensities of the diffraction satellites vs the amplitude of the input signal are plotted in Fig. 3.17. The square of the Bessel function was added to the plot as a visual reference, according to the theoretical intensities as calculated with eq. (1.48). ImageJ [56] was used for a qualitative analysis of the images during the experiment. For the quantitative analysis I wrote a Python script that automatized the process, the *voltage scan class*, see Appendix C for the details. The intensity of the individual diffraction satellites was calculated by integration of selected regions.

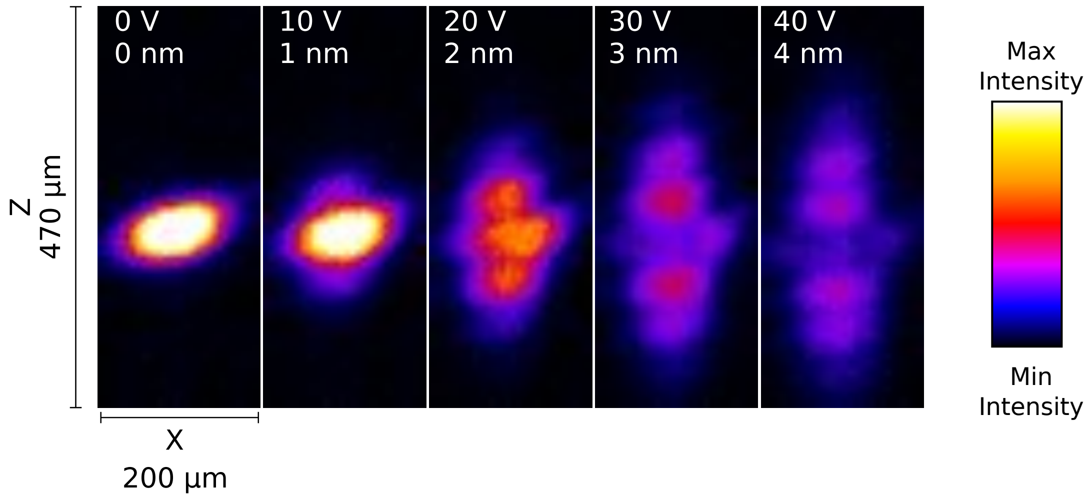

FIGURE 3.11: CCD camera images. The voltage supplied to the IDT was varied between 0 V and 40 V, and consequentially the amplitude of SAW changed. The orientation of the CCD camera is as shown in Fig. 3.8. The diffraction takes place along the z-axis.

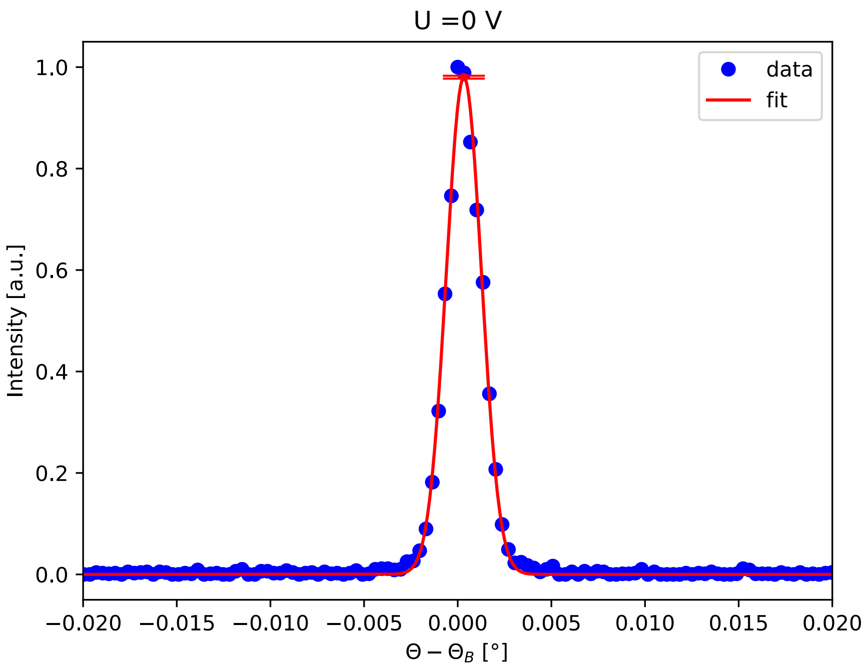

FIGURE 3.12: Diffraction pattern at 0 V. The standard deviation of the fit is shown at the position of the maximum.

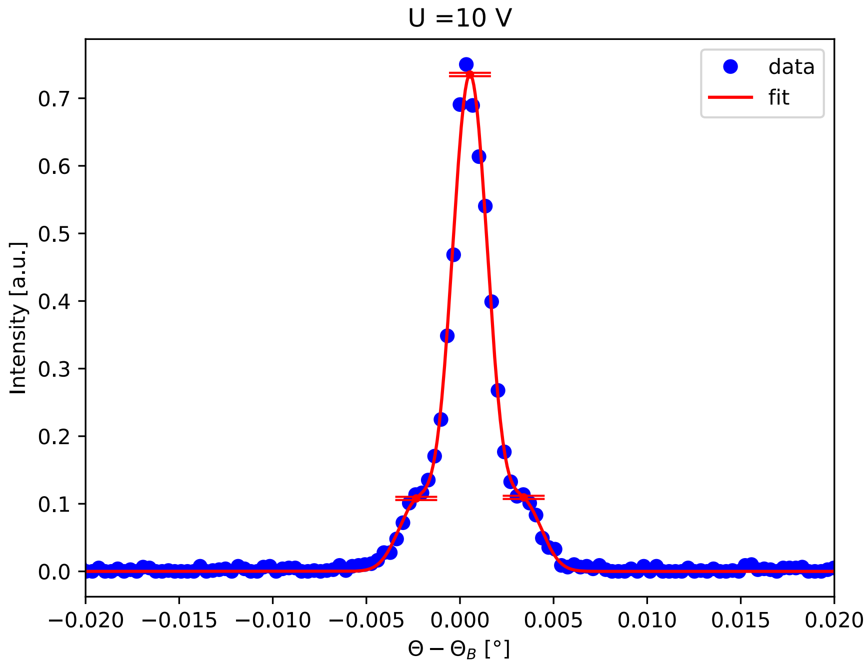

FIGURE 3.13: Diffraction pattern at 10 V. The standard deviation of the fit is shown at the position of the maxima.

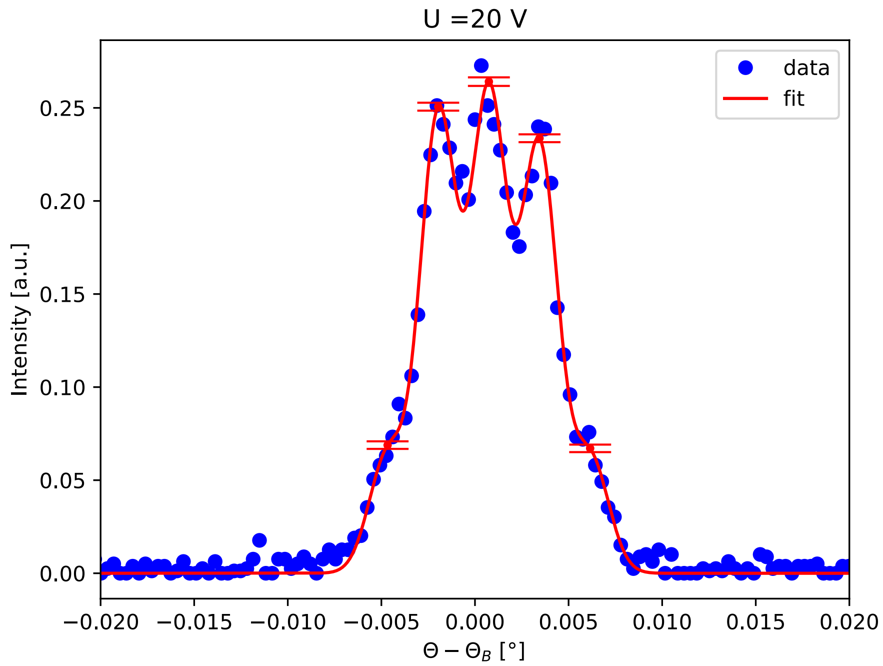

FIGURE 3.14: Diffraction pattern at 20 V. The standard deviation of the fit is shown at the position of the maxima.

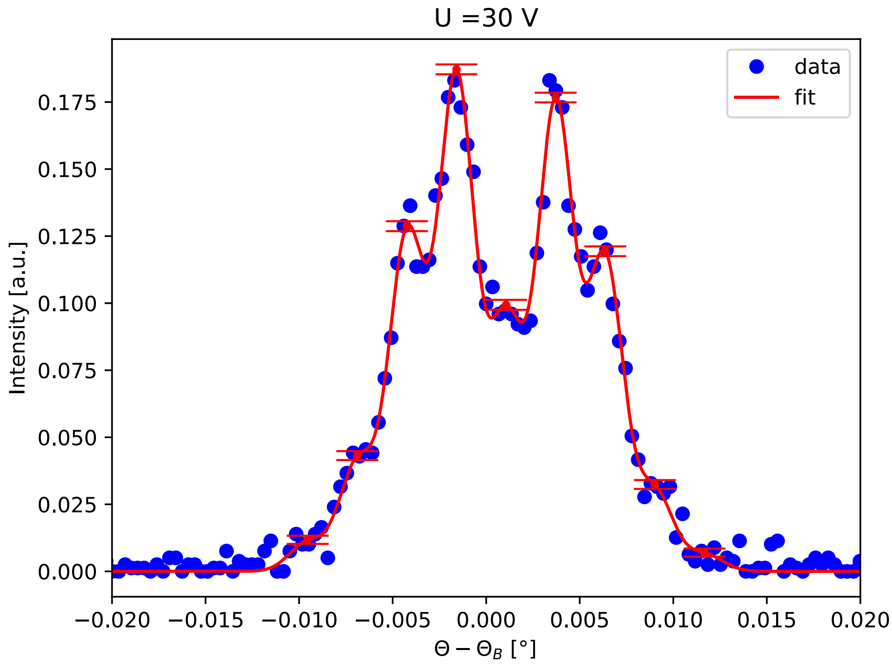

FIGURE 3.15: Diffraction pattern at 30 V. The standard deviation of the fit is shown at the position of the maxima.

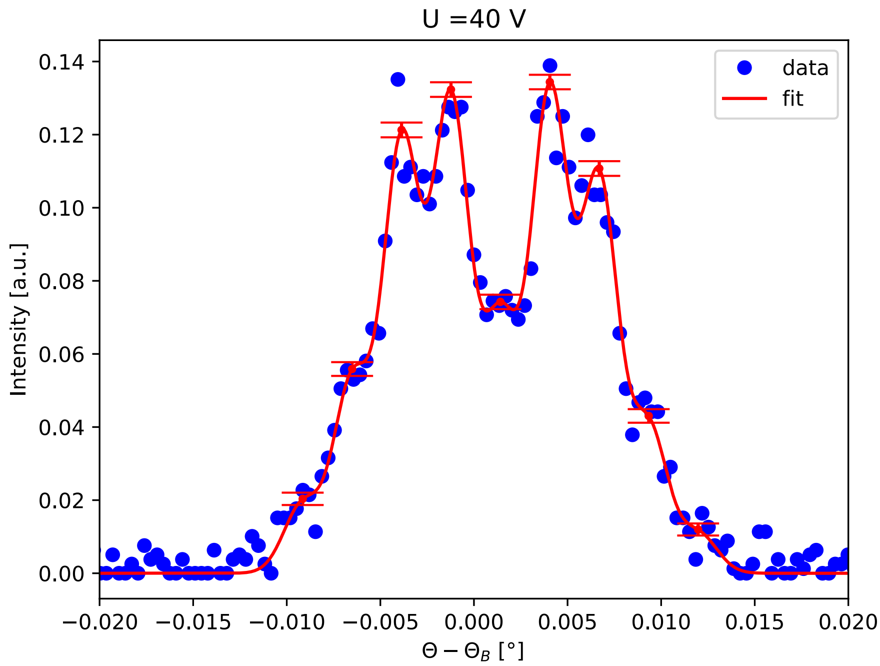

FIGURE 3.16: Diffraction pattern at 40 V. The standard deviation of the fit is shown at the position of the maxima.

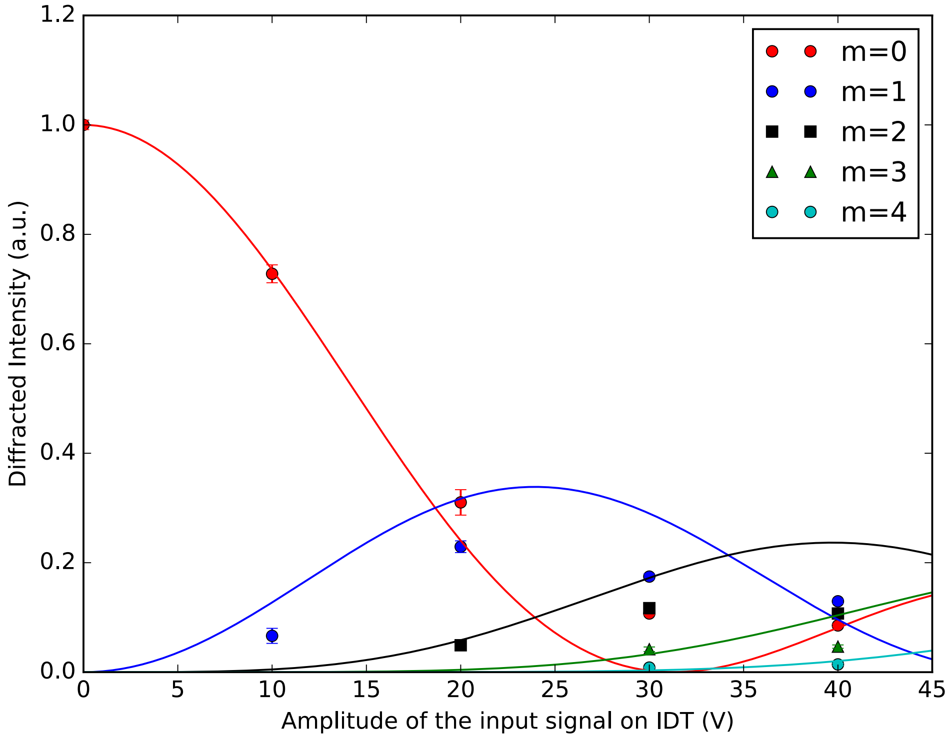

FIGURE 3.17: Intensities of the diffraction satellites (m=0,1,2,3,4) vs the amplitude of the input signal supplied to the IDT. The circles, squares and triangles are the experimental data. The solid lines are the Bessel function squared, plotted as a visual reference.

3.2.7 Discussion

In Fig. 3.11 the Bragg peak (m=0), and the diffraction satellites up to the third order are clearly visible, while the fourth order is revealed only after quantitative analysis. The Bragg peak and the satellites shift to lower z values when increasing the voltage. This is because the sample physically bends when SAW are excited. The measured angular separation between the diffraction satellites has 8% discrepancy with the theoretical value of $\delta\theta_{theoretical} = 10.66$ arcsec calculated with eq. (1.39). The results shown in Fig. 3.17 were compared with the simulations done in GSolver, see Fig. 3.10. The voltage at which the maxima occur in our experiment were coupled with the position of the maxima as simulated in GSolver, that depends on the amplitude of the grating. In Fig. 3.18 are plotted one against each other . This allows to calculate the coupling constant C $\sim$ 0.001 nm/V, that simply relates the voltage applied to the IDT with the amplitude of the generated SAW. Using this constant it was possible to calculate the amplitude of SAW depending on the applied voltage, see Fig. 3.11. Note that this constant is not universal, but it has an intrinsic dependency on the setup. Many parameters may vary the C factor, as the devices that are used to excite the SAW, the high frequency generator and the amplifier, as well as the cables and their length and the IDT design.

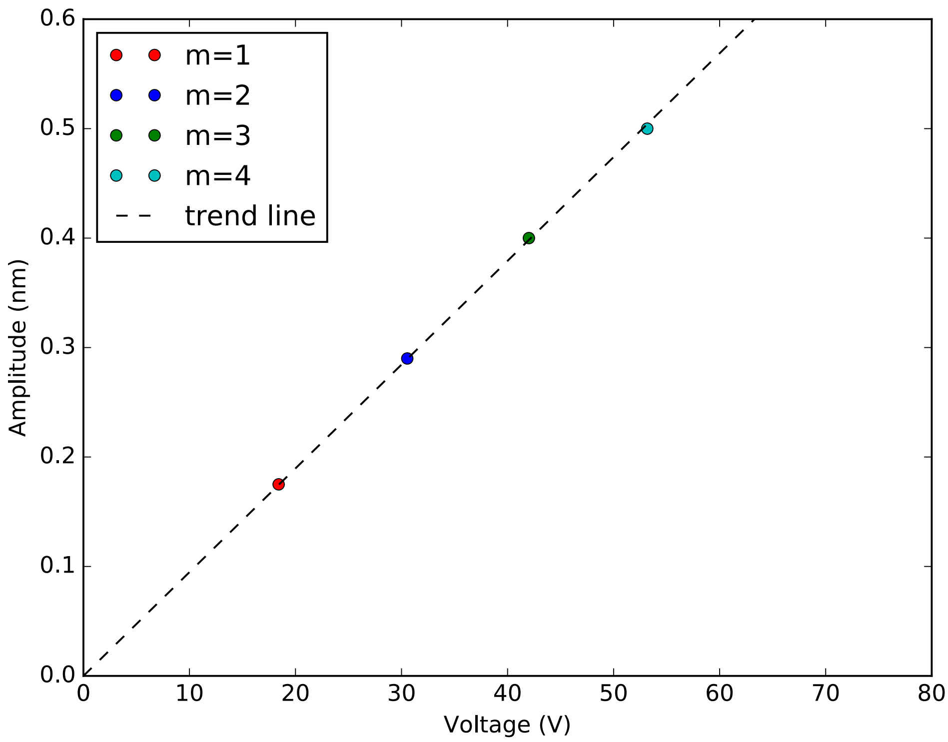

FIGURE 3.18: Amplitude of the SAW plotted vs the voltage supplied to the IDT.

3.3 Soft X-rays/SAW interaction

Diffraction of X-ray radiation on an acoustically modulated Si/W multilayer at E = 1000 eV and E = 600 eV was studied in Bragg and total external reflection conditions in meridional geometry at the Optics beamline [57] at the BESSY II synchrotron radiation facility.

3.3.1 SAW setup

The experimental setup presented is identical to the one presented in section 3.2.1. Additionally, to connect the sample to the HF generator the RF signal was brought inside a vacuum chamber using a floating shield (grounded) feedthrough.

3.3.2 Optics beamline at BESSYII

The Optics beamline has a dipole as a source. In Fig. 3.19 is shown the beamline schematic. M1 is a toroidal collimating mirror. The desired X-ray energy was selected with a blazed plane grating monochromator. The beam is refocused with the mirror M2, a cylindrical mirror, and finally it is focused on the sample by toroidal mirror M3. The sample was mounted on a goniometer that could translate and rotate the sample around the three axis. The intensity of diffracted X-ray radiation was recorded with a GaAs photodiode, enough to see the order separation with a detector sample distance of 0.3 m. The beam size at the sample position can be varied

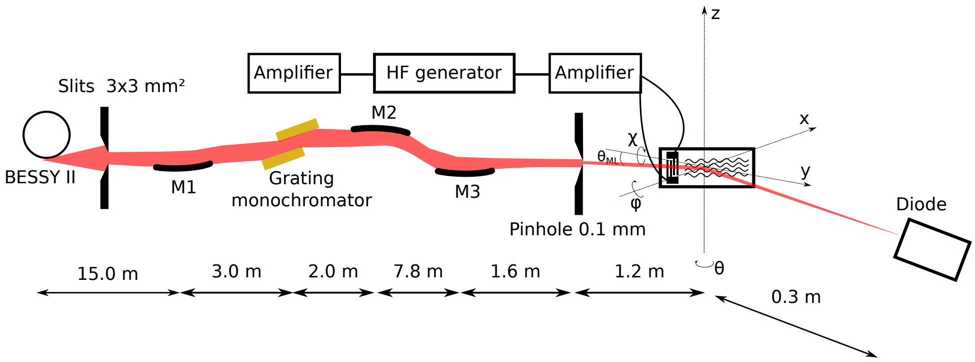

FIGURE 3.19: XPP-KMC3 beamline outline, picture not to scale.

using the a second pair of slits or pinholes of different size. The chosen pinhole had a diameter of 0.1 mm.

3.3.3 Sample – SAW device

For an overview of the sample and its properties see table A.1, at the voice S2. A scheme of the sample is shown in Fig. 3.20. The substrate was a 128° rotated Y-cut of black Lithium Niobate, a piezoelectric crystal. The surface roughness did not exceed 5 Å. To excite SAW two IDTs made of Aluminum were deposited on the surface of the LNB crystal by an external company, Avangard JSC. The IDTs were in split geometry configuration, see section 1.1.3, and were designed using the *IDT_DOUBLE_NEG* function as described in Appendix B. The acoustic aperture was w = 1.0 mm, see Fig. 3.20. A Si/W multilayer was deposited on the central part of the sample by an external company, INCOATEC. It is composed of 100 bilayers with 3 nm period and γ=0.5. The SAW wavelength was $\Lambda = 4\ \mu$m, the propagation velocity on LNB was $v_{SAW} = 3992$ m/s. The resonance frequency was estimated with eq. (1.1.3) to be 998 MHz and it slightly differ from the experimental value, that was found to be 978 MHz. The sample was tested with the VNA, which showed a resonance frequency of 985 MHz, see Fig. 3.21.

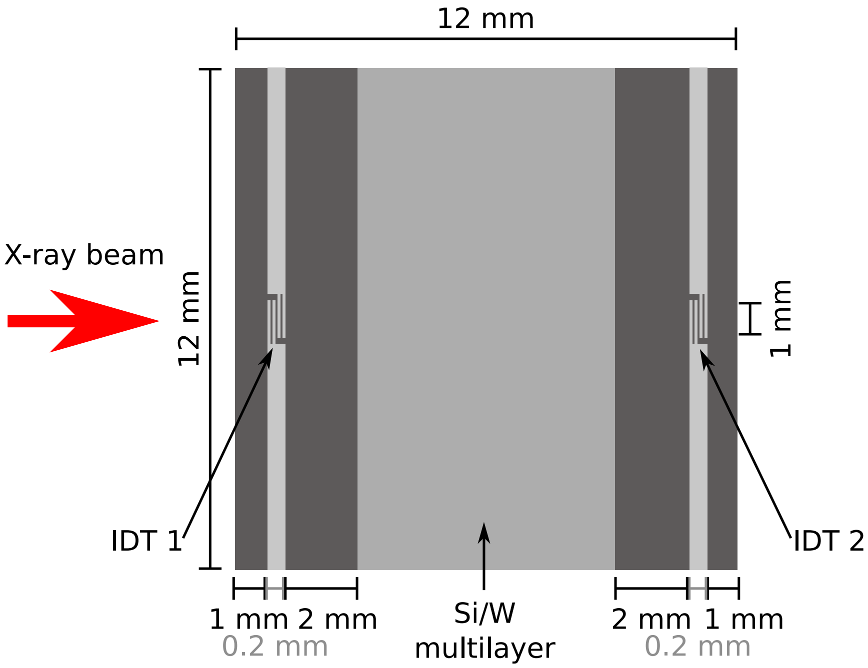

FIGURE 3.20: The schematic of sample studied at the Optics beamline.

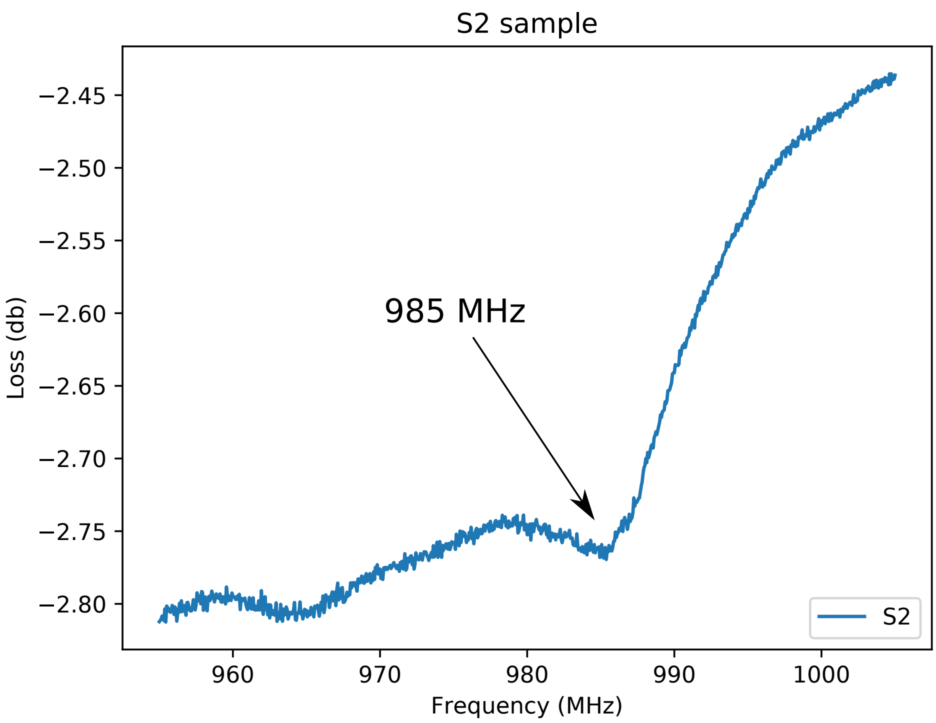

FIGURE 3.21: VNA measurement for the sample used during the experiment

3.3.4 Sample mounting

The sample was mounted inside a big vacuum chamber on a tripod installed on a three axes goniometer (sample azimuth and Θ and detector 2Θ), parallel to ground, see Fig. 3.22.

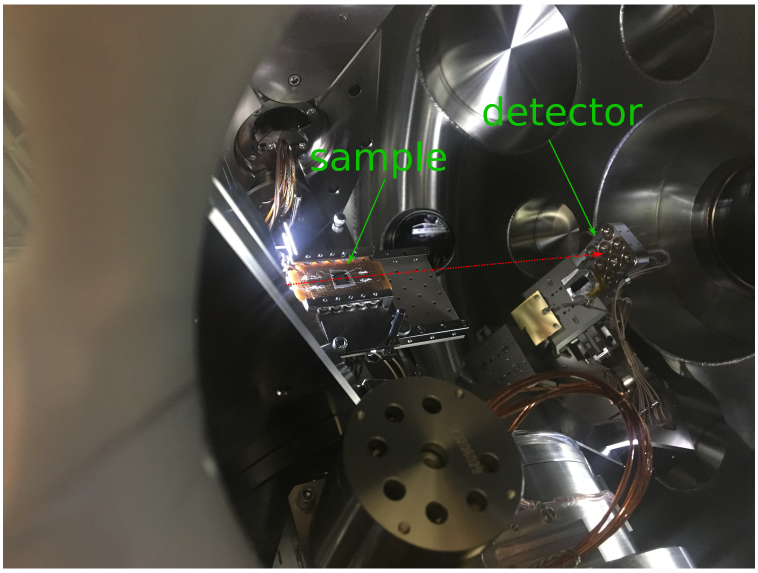

FIGURE 3.22: Picture of the diffraction setup at the endstation of the Optics beamline

3.3.5 Results at E = 1000 eV

In Fig. 3.23 are shown two reflectometry scans, one aligned at the multilayer Bragg peak, and the other one aligned at $\Theta = 2\Theta = 0$, compared to the theoretical reflectometry curve. In Bragg diffraction geometry, the multilayer reflection was used, with $\theta_B(E = 1keV) = 12.2°$. A voltage scan was taken at f = 980 MHz , varying the voltage between 2 V and 22 V in steps of 2 V. Each scan was fitted with the Python module described in Appendix C and in Fig. 3.24 the diffracted intensity of the m=± 1 is shown. The intensity is normalized to the intensity of the multilayer Bragg peak without SAW. In Fig. 3.25 three Θ-2Θ maps at different voltages (0,5,12 V) are shown. When SAW are off, Fig. 3.25 a), only the multilayer Bragg peak is visible. The satellites are barely visible at V = 5 V, Fig. 3.25 b), and clearly visible at v= 12 V, Fig. 3.25 c).

3.3.6 Results at E = 600 eV

A voltage scan was taken at f = 980 MHz, varying the voltage between 0 V and 19.5 V in steps of 0.5 V. The voltage scan was taken at the multilayer Bragg angle $\Theta_B(E = 600eV) = 20.5°$. Each scan was fitted and in Fig. 3.24 is shown the diffracted intensity of the m=± 1. The intensity is normalized to the intensity of the multilayer Bragg peak without SAW. In Fig. 3.26 a Θ-2Θ map at V = 15 V is shown. The map was taken around the multilayer Bragg peak. In Fig. 3.27 a Θ-2Θ map just above the total external reflection angle are shown. The same plots can be transformed into reciprocal space maps, and the result is shown in Fig. 3.28. The central and vertical bright line, in the two plots is due to the total external reflection. The peaks due to the SAW on the multilayer region are indicated with green arrows. The

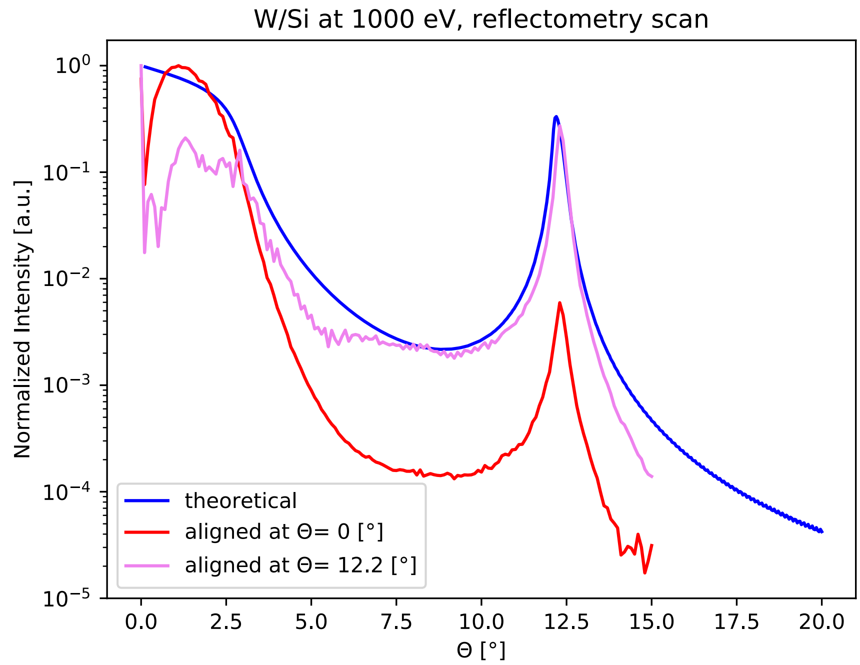

FIGURE 3.23: Two reflectometry scans, with the sample aligned at $\Theta = \Theta_B$ and at $\Theta = 0$ at E = 1000 eV, compared with the theoretical curve.

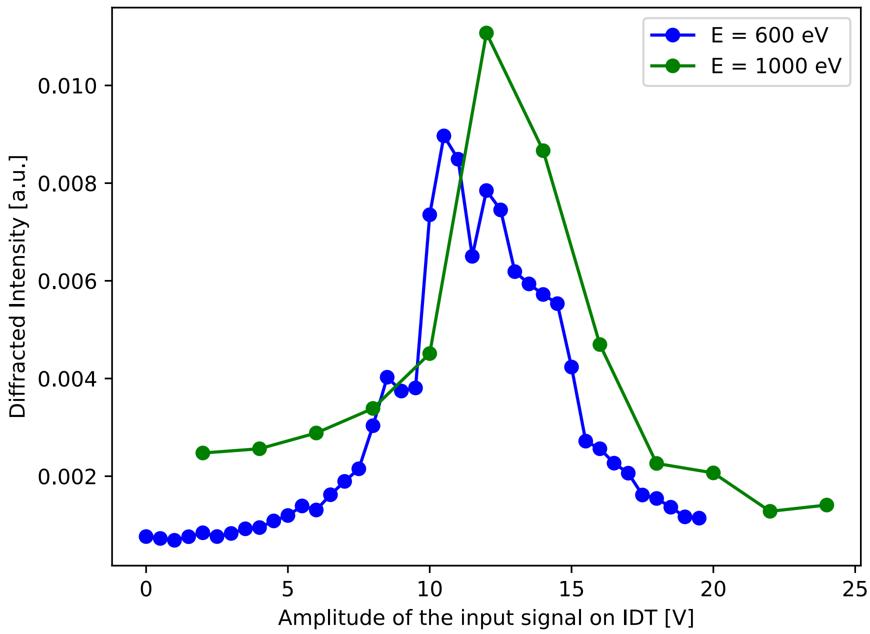

FIGURE 3.24: Intensity of the first diffraction satellite (m=$\pm$1) vs the amplitude of the input signal supplied to the IDT.

peaks due to the SAW on $LiNbO_3$ are indicated by orange arrows, and the peak due to the IDT are indicated by the blue arrow. It is possible to distinguish the different

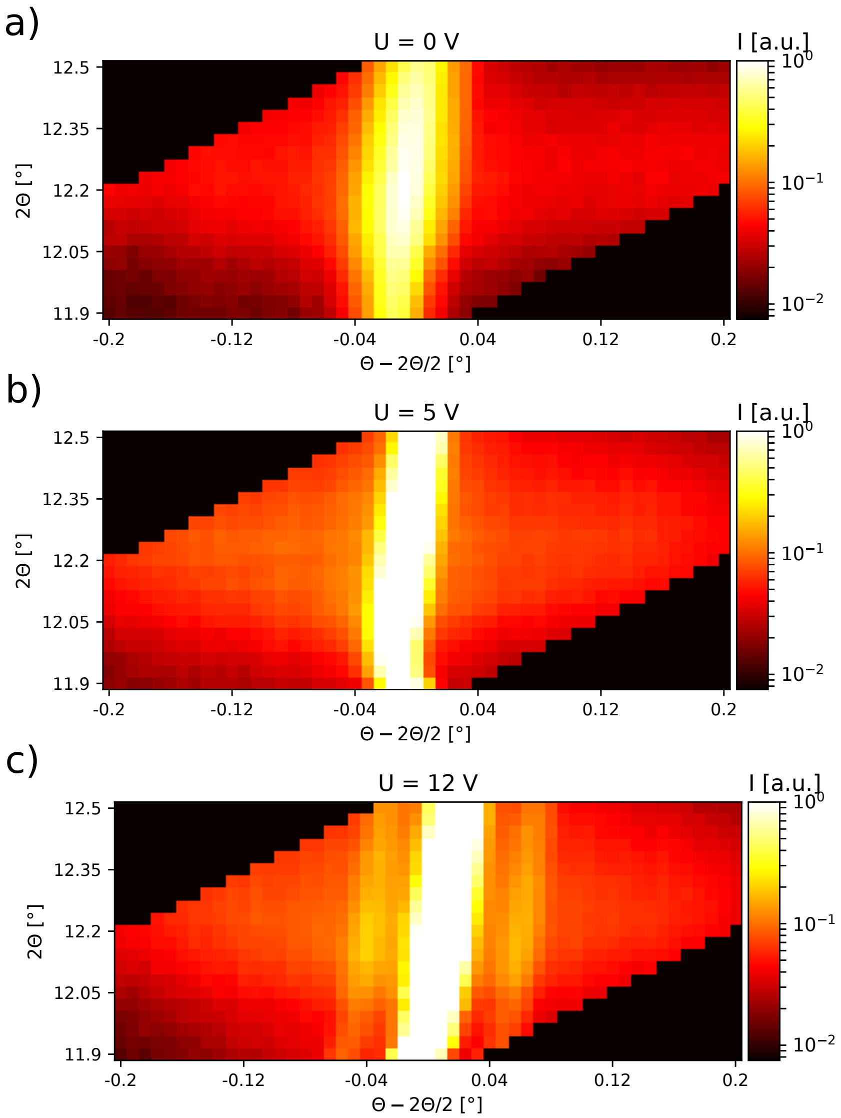

FIGURE 3.25: Three Θ-2Θ maps taken at three different voltages at E = 1000 eV. a) V = 0 V, b) V = 5 V and c) V = 12 V. The satellites appear with very low intensity at 5 V and are clearly visible at 12 V. The black regions were not scanned.

peaks because the SAW have different speeds in different part of the sample. The speed on the $LiNbO_3$ substrate is approximately 4 μm/ns. The SAW slows down when it propagates on the multilayer, and therefore its wavelength Λ gets smaller. A smaller Λ means higher angular separation of the diffraction satellites, see eq. (1.37). To confirm that the peak indicated by the blue arrow is due to the IDT, the geometry of the IDT must be considered. The IDT was in split geometry configuration. This means that its periodicity is four times higher than the SAW wavelength produced on $LiNbO_3$. The satellites peaks appear at approximately four time larger distance from the multilayer Bragg peak, compared to the satellite peaks due to the interaction of X-rays with a SAW on the $LiNbO_3$ substrate. The approximation comes from the fact the wavelength of SAW in $LiNbO_3$ is not exactly 4 μm. This because when a SAW is excited by the IDT, initially it travels at the interface between $LiNbO_3$ and Al, the material that constitutes the IDT. Their speed is therefore slightly different in the IDT region and in the substrate region, and a SAW with different speed results

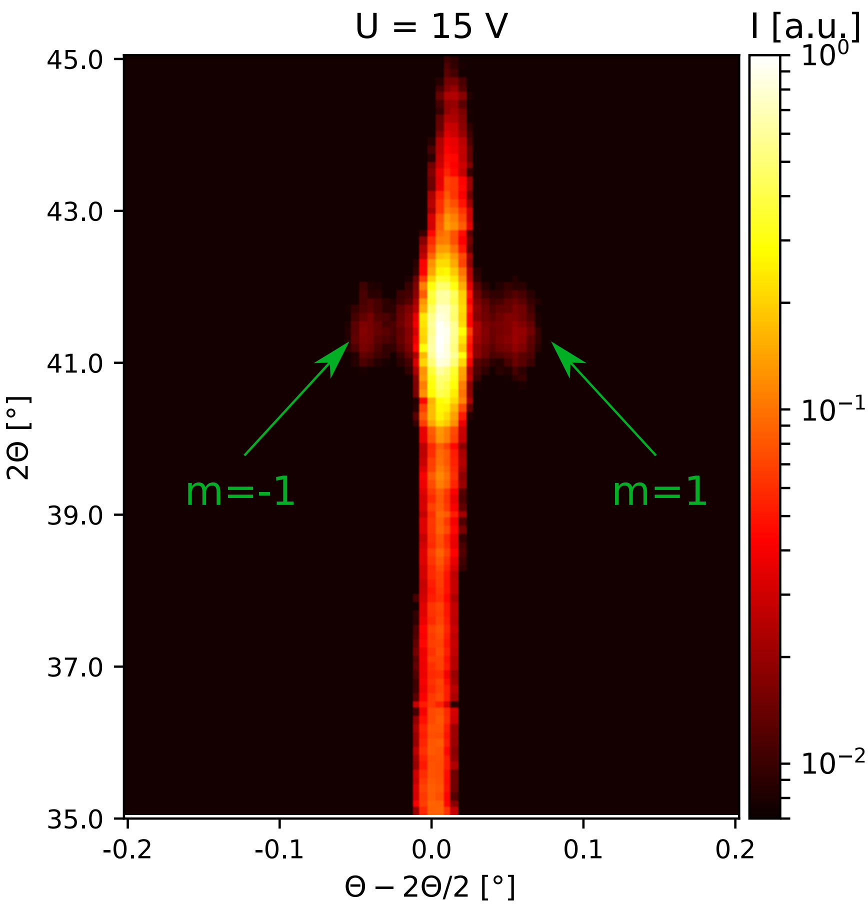

FIGURE 3.26: Θ-2Θ map at E = 600 eV at the multilayer Bragg peak at V = 15 V. The first order satellite peaks are clearly visible and indicate by green arrows.

in a SAW with a different wavelength.

3.3.7 Discussion

For the first time, the interaction of a SAW with X-rays of energy below 1 keV was investigated. This experiment had many technical difficulties that had to be overcome in order to get an efficient diffraction process. Most of all, since the experiment was performed in a vacuum chamber, a diagnostic system able to confirm the presence of the waves on sample was needed. A vector network analyzer was used to this scope, and proved to be an essential tool for the success of the experiment. While in air it is easy to correct eventual mistakes on the go, when working in vacuum the possibilities to take action are drastically reduced. The intensity of the first order satellites is low. At voltage 12 V for E = 1000 eV, it reaches a maximum intensity of 1.1% of the multilayer Bragg peak , and a maximum of 0.9% for E = 600 eV. Intuitively it makes sense that for lower photon energy the diffraction satellites maximal intensity reaches a lower value. This because lower energy photons have longer wavelength. Thus for the same amplitude of the SAW the diffraction satellites exhibit lower intensity. On the other hand, the plot in Fig. 3.24 shows that the first order diffraction satellite reaches its maximum at voltage 12 V. What is not clear then is why the second order diffraction satellites are not visible. The best way to approach

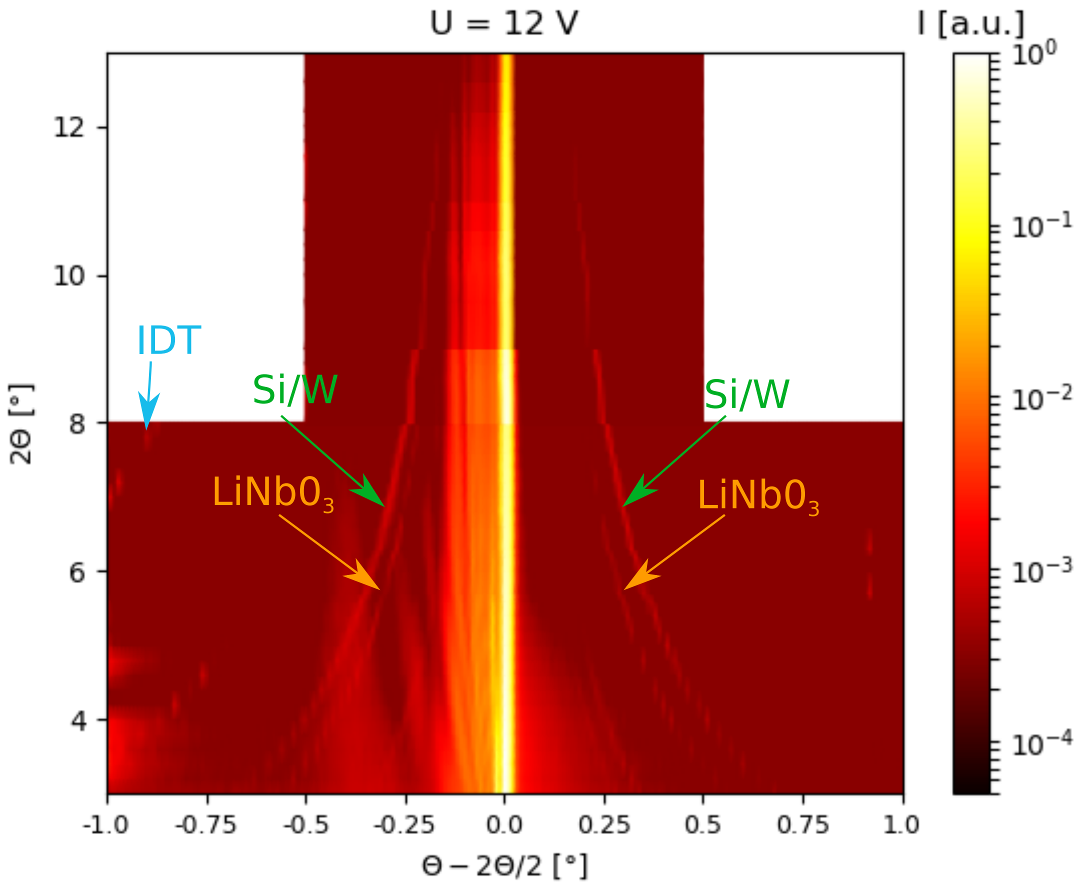

FIGURE 3.27: Θ-2Θ map at E = 600 eV in total external reflection condition at V = 12 V. The satellites due to the interaction of X-rays with the SAW on the substrate are indicated by orange arrows, the ones due due to the interaction on the Si/W multilayer are indicated by green arrows, and the ones due to the interaction of X-rays with the IDT with a blue arrow.

this problem would be to make a simulation. This is at the moment not possible, because the commercial software that we use to make this kind of simulation, GSolver, can not accept multilayered structure. Even though it is possible either to buy other commercial software able to make this kind of simulation, or, even better, it is possible to write a customized software to make this kind of simulation, this is either economically not possible or beyond the scope of this work. Nevertheless, one could compare this result with the simulation done for LGS crystal and plotted in Fig. 3.10. The only thing that would change if this simulation was done for the case of a Si/W multilayer at E=600 eV,E=1000 eV, it is only the maximal intensity reached by the satellite, and the amplitude needed. What it would not change is that when the first order reaches the maximum, the second order should be visible and should reach its maximum before that the first order disappears again. It is then plausible to think that the first order did not reach its maximum, but that the amplitude of the waves started to decrease. A possible explanation could be that the sample heats up due to the high voltage, and due to the fact that it is mounted and it is operating in vacuum it can not cool down with air convection. Such a phenomenon could interfere with the generation of SAW and reduce its amplitude. This is a possible explanation of this weird behavior, that need to be confirmed with further investigations.

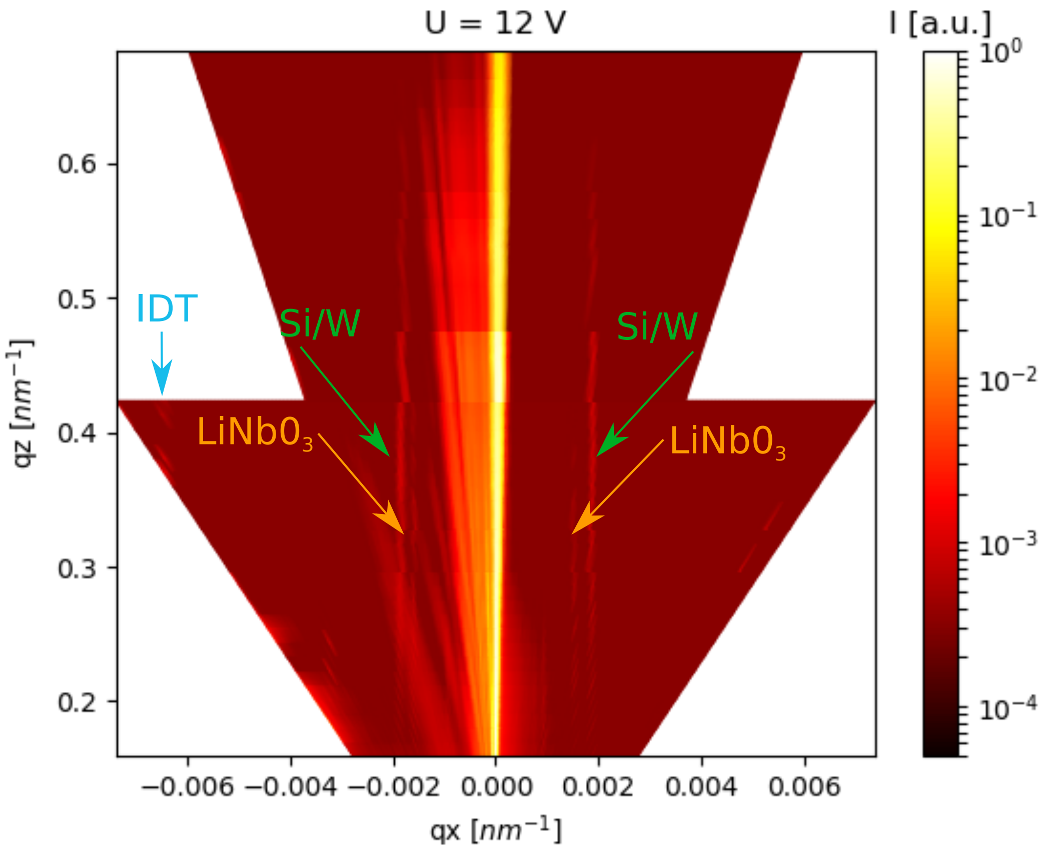

FIGURE 3.28: Reciprocal space map at E = 600 eV obtained by coordinate transformation from the same data used to plot the Θ-2Θ map in Fig. 3.27. In reciprocal space the trace of the diffraction satellites appear parallel next to trace of the multilayer Bragg peak. The diffraction satellites that arise due to the interaction of X-rays with the SAW on the substrate are indicated by orange arrows, the ones due due to the interaction on the Si/W multilayer are indicated by green arrows, and the ones due to the interaction of X-rays with the IDT with a blue arrow.

The Θ-2Θ maps taken around the multilayer Bragg peak at either at E = 1000 eV, Fig. 3.25, and at E = 600 eV, Fig. 3.26, show the diffraction satellites that appear as straight lines at the sides of high intensity line due to the multilayer Bragg peak.

The most interesting results is the Θ-2Θ maps taken between $2\Theta = 3° - 13°$ once it has been transformed into a reciprocal space map, Fig. 3.28. From simple geometrical considerations in reciprocal space, the speed of the SAW can be calculated, and it is easy to understand which interaction gave rise to the different lines visible in the plot. Consider the picture in Fig. 3.29.
In reciprocal space, the distance of the satellites from the specular reflection is inversely proportional to the period of the grating:

$$q_x^{LNB} = \frac{2\pi}{\Lambda_{SAW}^{LNB}}, \quad q_x^{Si/W} = \frac{2\pi}{\Lambda_{SAW}^{Si/W}}, \quad q_x^{IDT} = \frac{2\pi}{d^{IDT}/2} \tag{3.11}$$

where d is the periodicity of the IDT as defined in section 1.1.3. Given this distances in reciprocal angstrom $q_x^{LNB} = 0.0016 \pm 0.05nm^{-1}$, $q_x^{Si/W} = 0.0019 \pm 0.05nm^{-1}$, $q_x^{IDT} = 0.0065 \pm 0.05nm^{-1}$ it is easy to calculate the wavelength of the SAW and the periodicity of the IDT $\Lambda_{SAW}^{LNB} = 3.95 \pm 0.2$ μm, $\Lambda_{SAW}^{Si/W} = 3.3 \pm 0.16$ μm and $d^{IDT}/2 = 1.00 \pm 0.05$ μm. The corresponding speed of the SAW in $LiNbO_3$ and in the multilayer are $v_{SAW}^{LNB} = 3850 \pm 200$ m/s and $v_{SAW}^{Si/W} = 3230 \pm 150$ m/s.

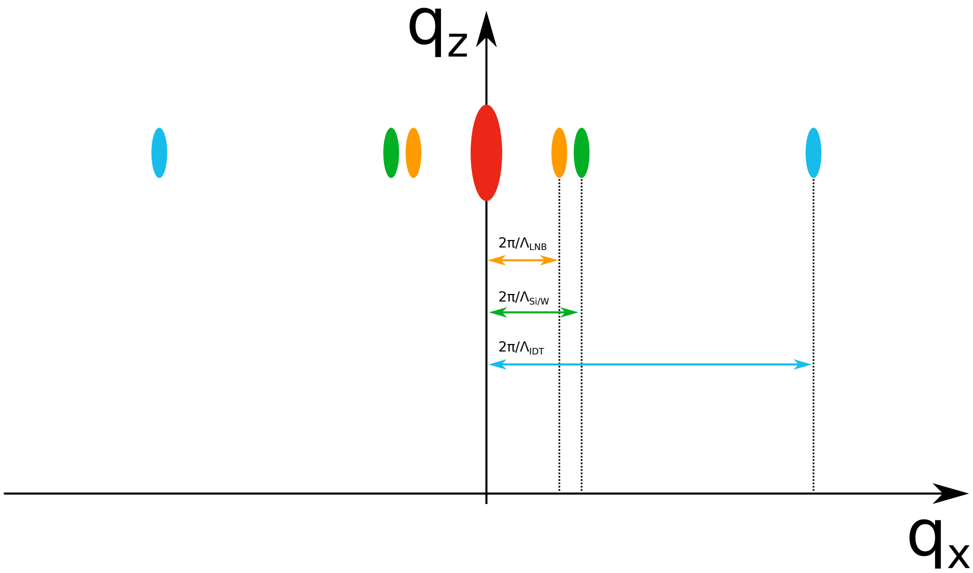

FIGURE 3.29: Total external reflection representation in reciprocal space of the reflections of sample used in the experiment. The picture in not to scale. The red dot represent the specular reflection, the orange dots represent the satellites due to the SAW on the $LiNbO_3$ substrate, the green dots represent the satellites due to the SAW on the Si/W multilayer, and the light blue dots represent the satellites due to the IDT. The distance of the satellites from the specular reflection is inversely proportional to the periodicity of the grating, whether the grating is made by a SAW or by the fingers of the IDT.

3.4 Time resolved experiment in sagittal geometry

X-ray diffraction from a SAW modulated W/B_4C multilayer was studied in a four circle diffractometer at the B16 beamline [58] at DLS. The term time resolved comes from the fact that, in contrast to the experiments described in section 3.2, a SAW is not excited continuously on the sample surface, and the time structure of the beam is taken into account and investigated by studying the interaction of the X-ray beam with pulses of SAW.

3.4.1 SAW Setup

The experimental setup presented in Fig. 3.30 is used to perform time resolved measurements. The SAW were excited using a high-frequency generator (Hameg, HM8134/5), and a wideband radio frequency (RF) amplifier with 5 W power (AR, KAW1020). SAW are emitted in trains of a certain duration, set to 100 ns. The emission of the SAW is correlated with the storage ring in order to scatter the x rays emitted from the selected electron bunches. Delay, and consequently the selected bunches, are varied by a delay generator (DG645, Stanford Research System).

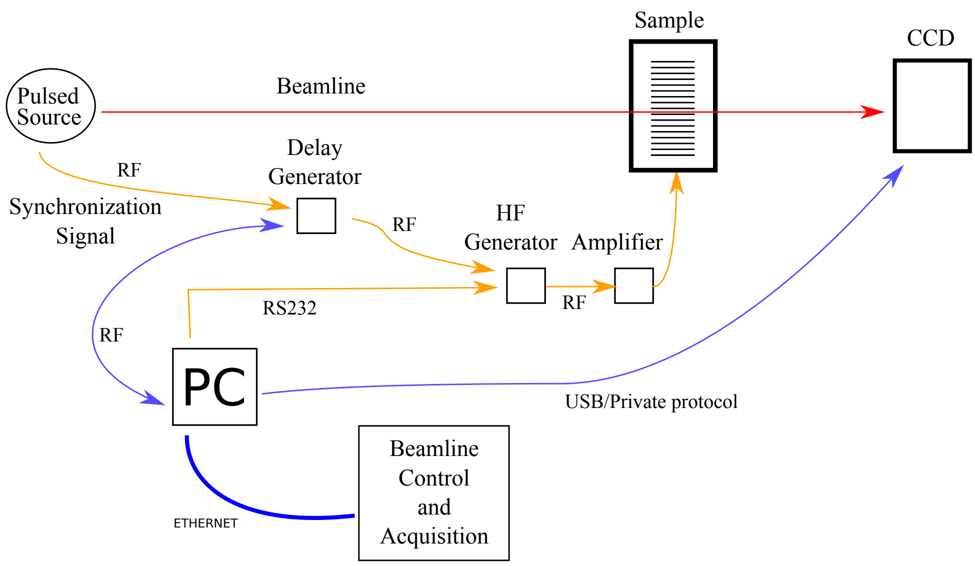

FIGURE 3.30: Experimental setup for SAW time resolved experiment.

3.4.2 B16 beamline at DLS

The X-ray energy of 8 keV was selected by a double Si 111 crystal monochromator. The beam was focused on the detector using 10 compound refractive Be lenses. The focal spot on the detector was 6 μm. This allow to resolve the Bragg peak from the diffraction satellites due to SAW, and the footprint of the beam on the sample is large enough to have a good scattering of the beam by SAW. A CCD camera detector (Photonic Science Ltd) was used to measure the diffracted intensity, with a pixel size of 6.5 μm. This corresponds to an angular resolution of 0.1 arcsec. This was enough to resolve the satellite peaks with a CCD sample distance of 1.5 m. The SAW were excited using the setup shown in section 3.4.1. The Bragg angle at the W/B_4C multilayer was $\Theta_B = 1.83°$ for the energy 8 keV, and the sample was tilted about the x-axis by $\phi = 70°$. Surface acoustic waves were emitted in trains of 100 ns duration. The emission of the SAW was correlated with the DLS storage ring

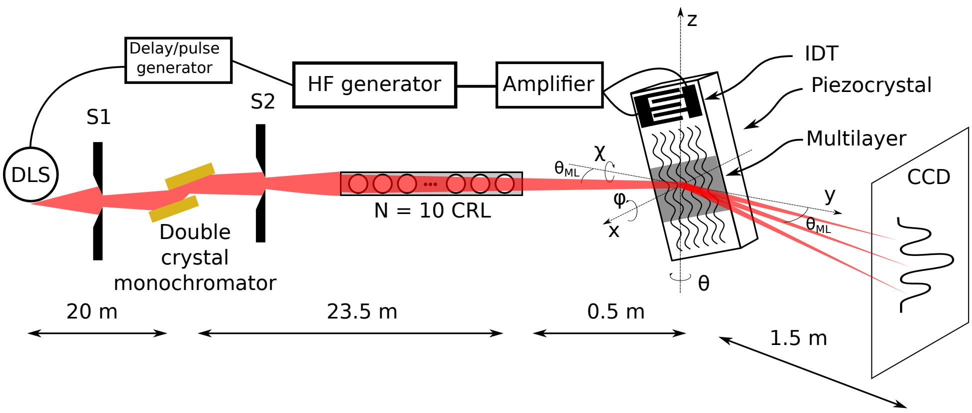

FIGURE 3.31: Experimental setup, picture not to scale. The sample is rotated for $\phi = 70°$ and $\Theta_B = 1.83°$.

in order to scatter the X-rays emitted from the selected electron bunch. Delay, and consequently the selected bunch, were varied by a delay generator (DG645, Stanford Research System). The bunch structure at DLS at the time of the experiment is shown in Fig. 3.32.

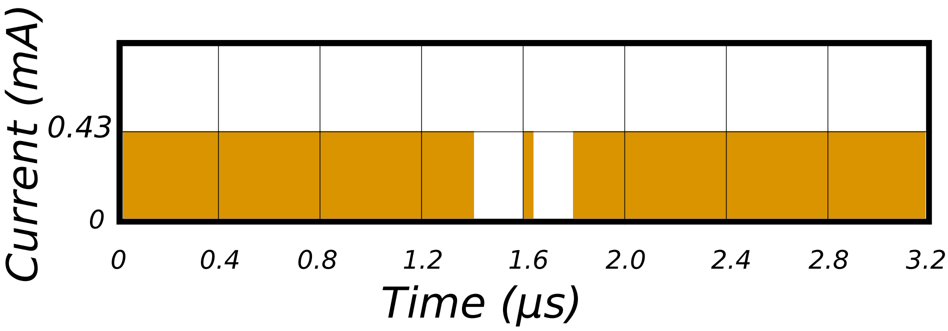

FIGURE 3.32: The bunch structure at DLS during the measurements. There are 686 contiguous bunches, 2 ns apart, each with a charge of 0.81 nC (0.43 mA), plus a single bunch of 0.81 nC (0.43 mA) in the middle of the gap in the bunch train of 500 ns.

3.4.3 Sample – SAW device

For an overview of the sample and its properties see table A.1, at the voice ML. The substrate was a Y-cut of Lithium Niobate (LNB), a piezoelectric crystal. The surface roughness did not exceed 5 Å. To excite SAW an IDT made of Aluminum was deposited on the surface of the LNB crystal. The IDT structure was fabricated on the LNB substrate coated with PMMA resist by e-beam lithography. The IDT was a in single configuration, see section 1.1.3, the acoustic aperture was w = 0.3 mm, see Fig. 1.2. The SAW wavelength was $\Lambda = 12\ \mu$m, the propagation velocity was $v_{SAW} = 3468$ m/s. The resonance frequency was estimated with eq. (1.1.3) to be 289 MHz and it coincided with the experimental value. The sample was tested with the VNA, which showed a slightly different activation frequency, see Fig. 3.33. A W/B_4C multilayer with period d = 2.7 nm (0.9 nm W, 1.8 nm B_4C, 200 bilayers) was deposited on the surface of the LNB crystal, see Fig. 3.31.

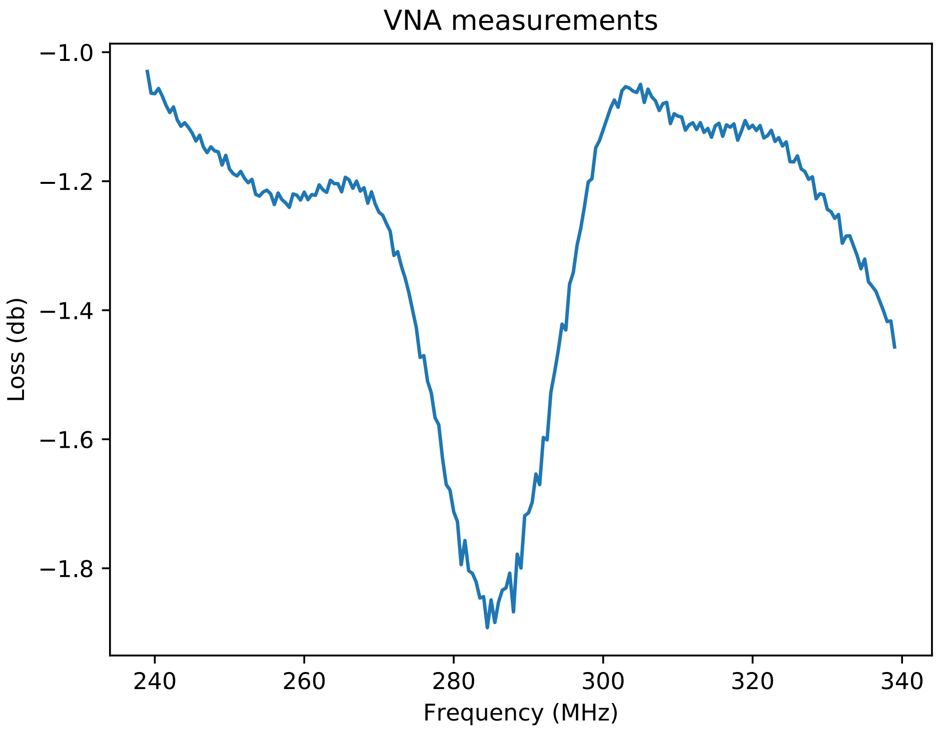

FIGURE 3.33: VNA measurement for the sample used during the experiment, LNB with a W/B_4C multilayer.

3.4.4 Delay scan in sagittal geometry

The SAW emission was electronically pulsed and synchronized with the arrival of the X-ray pulses, it was possible to select the X-ray pulse which will be diffracted in the satellites by varying the delay between the synchronization signal and the SAW pulse, see Fig. 3.34. The diffraction satellites appear only when the SAW train goes through the irradiated area of the crystal surface. Varying the delay between the synchronization signal and the emission of the SAW train allow to measure on the detector the diffraction pattern due to the interaction of the pulse train with different X-ray pulses, produced by either the multibunch or by the single bunch.

3.4.5 Results

Fig. 3.35 are Bragg topography images, with and without SAW. When SAW are activated it is visible their trace on the sample. The intensity on the SAW trace is lower than in the surrounding regions, this because the intensity of the Bragg reflection m=0, once the SAW are activated, is redistributed to the diffraction orders. In the CCD camera image in Fig. 3.36 the peaks are rather well separated, even though they are not entirely decoupled from the halo of the main beam. The very high intensity of the main beam originates from the crystal areas not affected by the SAW. The sample used for the measurements had rather narrow SAW path, w=0.3 mm, while the beam footprint on the sample was in the order of 15 mm. Thus a large portion of the incoming beam was hitting sample areas which were not covered by the SAW. The choice of $\phi = 70°$ represents a balance between the peak separation and the time resolution, defined as the time that the SAW train needs to cross and leave the X-ray beam footprint. The integrated intensity from the satellites was correlated to the delay time. The integration area in the CCD image was automatically selected

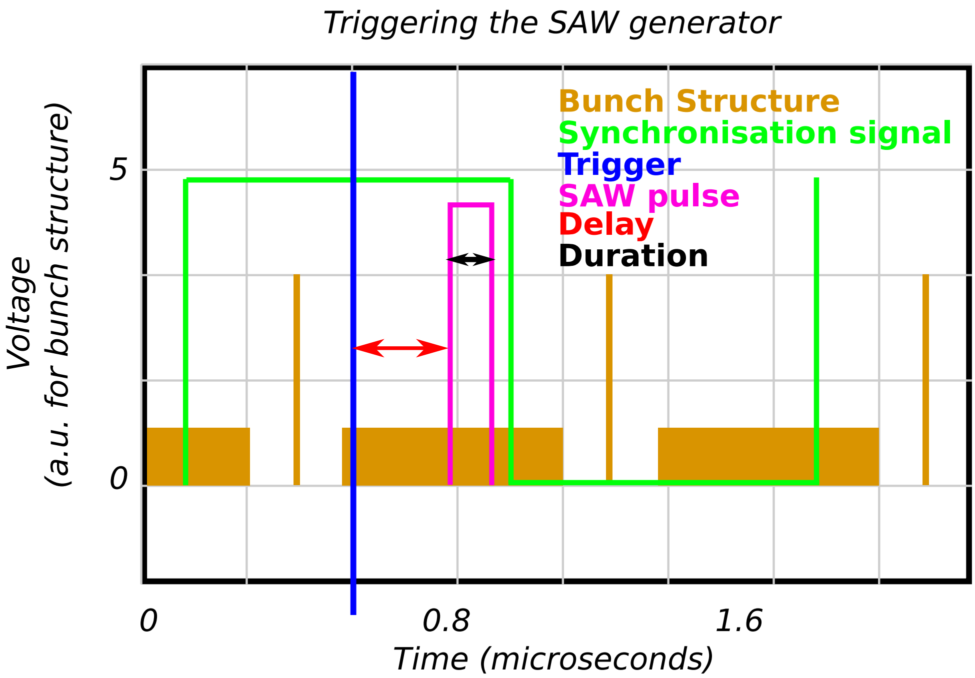

FIGURE 3.34: Triggering the SAW generator: the synchrotron time structure is represented in yellow. Here is shown the time structure of the Diamond Light Source when running in the Hybrid mode. The synchronization signal, in green, is used as a trigger for a short train of SAW. The delay between the synchronization signal and the trigger is due to the long cable that synchronization signal has to travel to reach the experimental station. The delay and the duration of the SAW train can be varied.

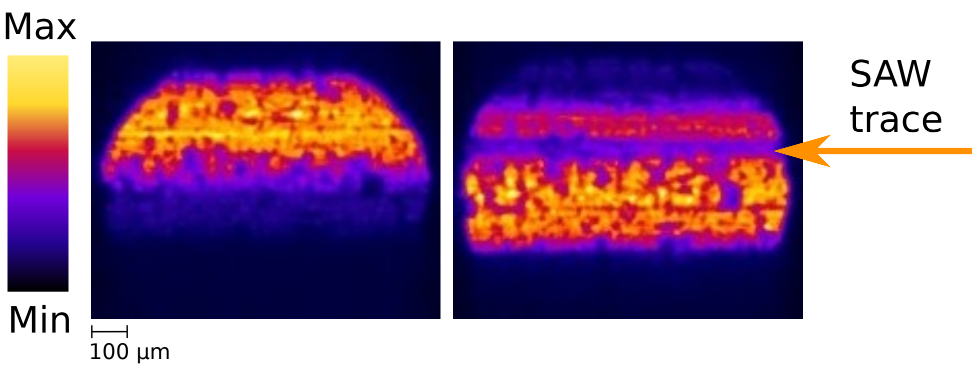

FIGURE 3.35: Bragg topography. Left: no SAW. Right: SAW with V=10 V. It is visible the SAW trace.

by a numerical algorithm, more details in appendix D. Due to different time dependencies, the algorithm is able to distinguish between the multilayer Bragg diffraction and the SAW diffraction satellites. It extracts and averages the delay scan for the two peaks, m=$\pm$1. Then it averages the two of them, differentiate them, and fit the edges with a simple gaussian curve, see Fig.3.37. Finally it fits the peak due to the single bunch, and combines the data, the fit of the single bunch and of the edges, and the calculated theoretical curve in one plot, see Fig. 3.38.

For a a given delay between the storage ring signal and the SAW trigger, SAW is crossing the footprint of the X-ray beam in the moment when a specific bunch is

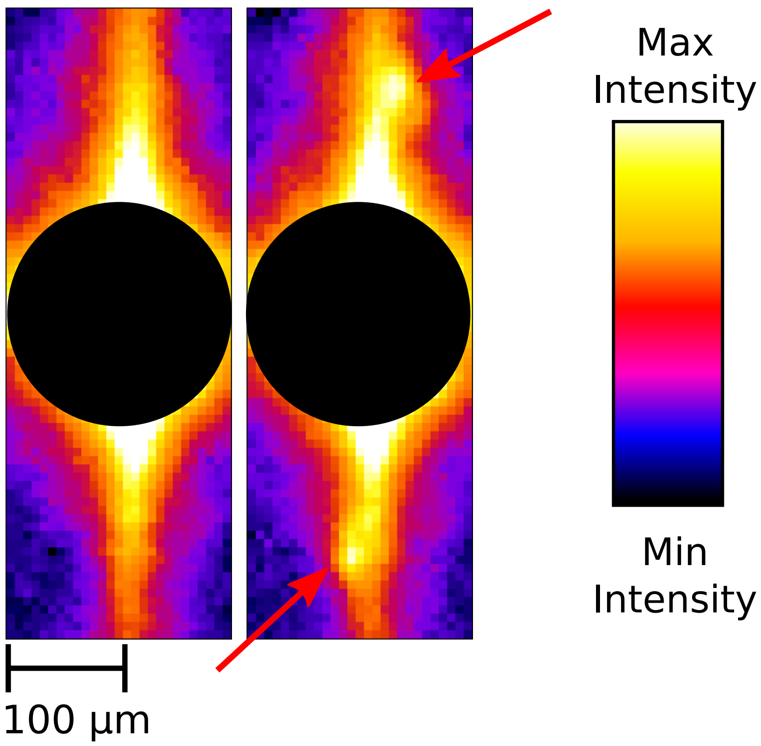

FIGURE 3.36: Experimental CCD camera images. The exposure time was 1 s. Surface plane is horizontal, scattering plane vertical. The saturating multilayer Bragg reflection in the middle was covered by a filled circle to avoid the distraction from the important parts of the image. **Left image:** SAW are off. **Right image:** the two small peaks (arrows) are the $m = \pm 1$ diffraction satellites due to the scattering on the SAW grating. They are separated from the main peak horizontally, as well as vertically, which facilitates the detection. The color scale was adjusted to emphasize the diffraction satellites

being scattered. When the SAW train reaches the beam footprint and interacts with the multibunch the intensity is maximal, normalized to 1 in the plot. The intensity decreases when the delay is such that the SAW train reaches the footprint during the ion gap, and it has a relative maximum in the middle of the gap due to the interaction with the single bunch. We estimated the time resolution at three different positions: at the single bunch position (delay = 1.6 μs), and at the falling and rising edge, respectively at 1.4 μs and 1.8 μs. The FWHM of the peak at the single bunch position is FWHM = 117 ns. To obtain the cross and leave time from the falling and rising edge we differentiate the spectra and fit the two peaks. The FWHM is FWHM$_l$ = 114 ns for the left slope and FWHM$_r$ = 118 ns for the right slope.

3.4.6 Discussion

The SAW device was rotated about the x-axis of $\phi = 70°$ to optimize the spatial resolution without spoiling the time resolution. It was shown that the rotation of the SAW device about the x-axis of $\phi = 70°$ optimizes the spatial resolution without spoiling the time resolution. The value of the angle ϕ is a balance between the peak separation and the time resolution: rotating the angle ϕ to lower values would allow for a better separation of the diffraction satellites, but at the same time it would spoil

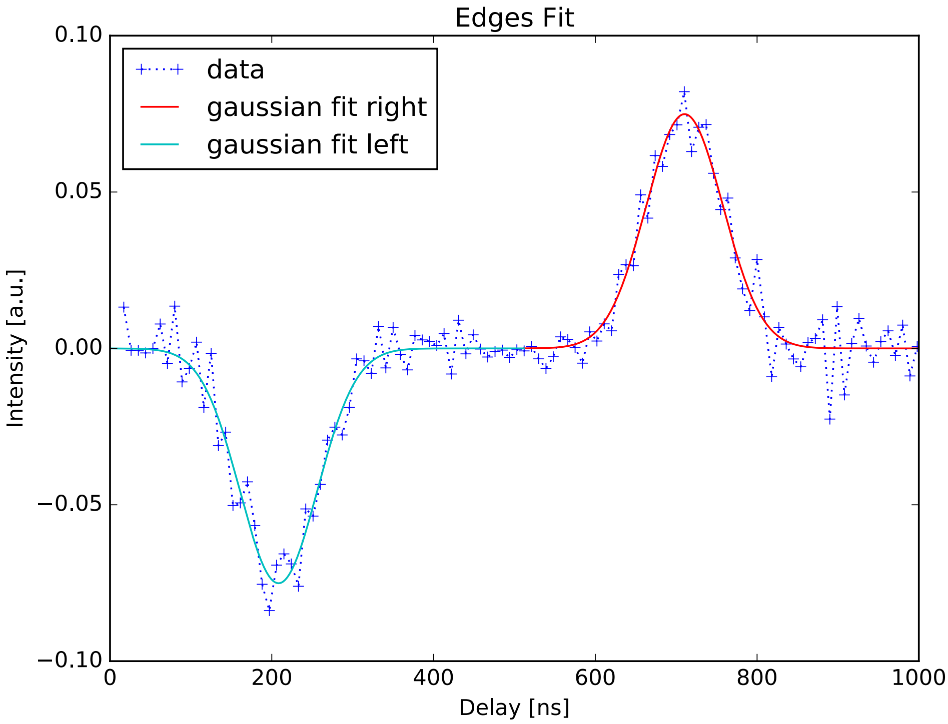

FIGURE 3.37: Differential spectra obtained averaging all the spectra due to the m=±1 diffraction orders. The two fit are done using a gaussian function.

the time resolution. This allowed to resolve the diffraction satellites on the detector. The angular separation of the diffraction satellites, as calculated in eq. (1.39), would have not been enough to distinguish the diffraction satellites from the Bragg peak with a sample detector distance of 1.5 m in sagittal geometry. The SAW train generated by our device has a duration of 118 ns, as discussed above. This means that when the SAW train interacts with the multibunch, it interacts with 59 bunches (each bunch is 2 ns apart). Calculation of the intensity shows that the peak intensity of the isolated pulse is about 3% of the maximal intensity. The calculation is the convolution of the synchrotron time pattern with the Gaussian curve having the width of the measured time resolution (green curve in Fig. 3.38). It matches the measured intensity.

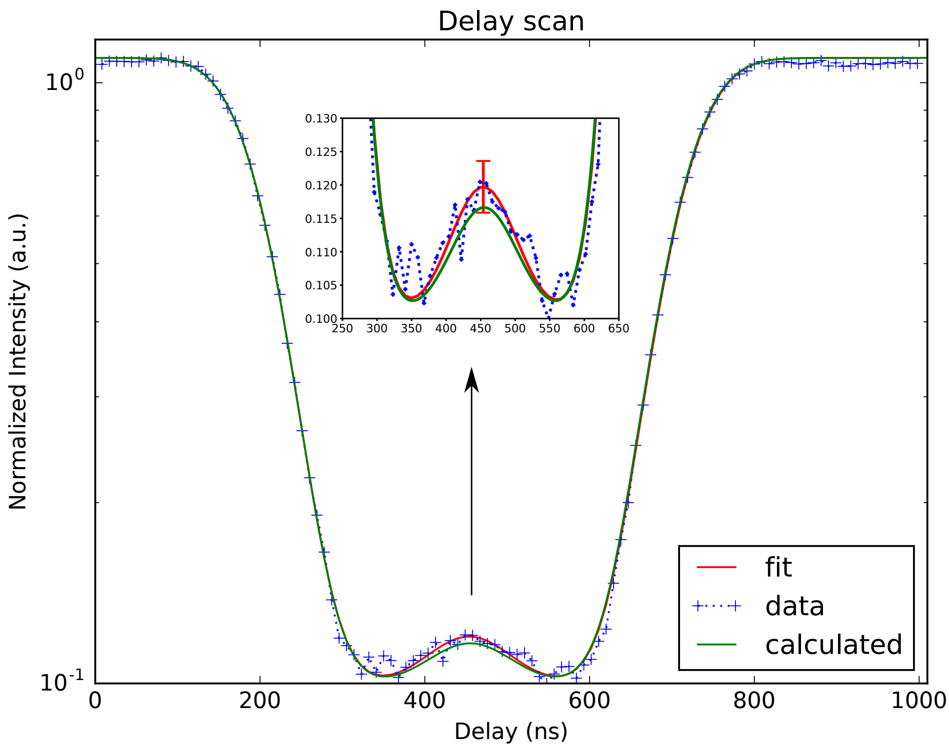

FIGURE 3.38: Measured data (blue), the gaussian fit (red), and the calculated shape of the curve (green). The arrow indicates a zoom in the region of the single bunch with the standard deviation of the fit at the single bunch position. The resolution of the measured curve is 10 ns.

3.5 Time resolved experiment in meridional geometry

X-ray diffraction in meridional geometry from a SAW modulated $LiNb0_3$ crystal was studied in a diffractometer at the mySpot beamline [59] at BESSY II. The term time resolved comes from the fact that, in contrast to the experiments described in section 3.2, SAW are not excited continuously on the sample surface, and the time structure of the beam is taken into account and investigated by studying the interaction of the X-ray beam with pulses of SAW.

3.5.1 SAW Setup

The SAW setup is identical to the one described in section 3.4.1.

3.5.2 mySpot at BESSYII

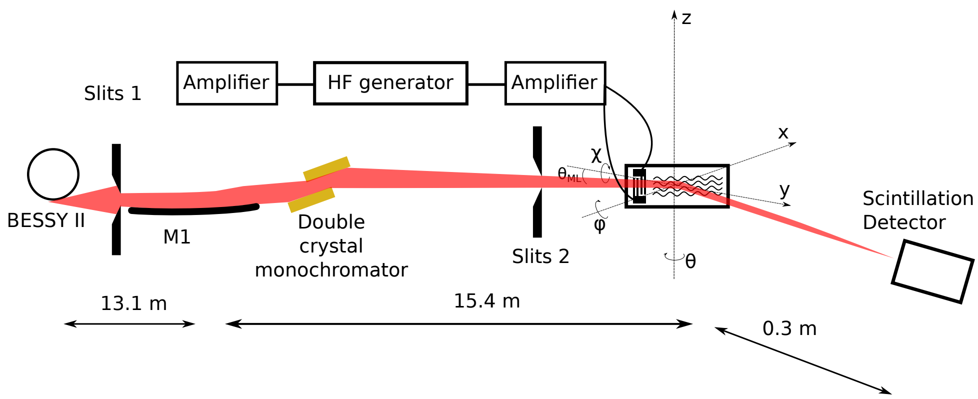

FIGURE 3.39: Experimental setup for SAW time resolved experiment.

The X-ray energy of 8 keV was selected by a double Si 111 monochromator. The beam was focused on the sample with M1 mirror, see Fig. 3.39. The beam was made parallel through a pair of slits and a pinhole aligned to each other. Slits 1 were closed down to 5×1 mm^2, Slits 2 were closed down to 0.5×0.5 mm^2. Additionally in front of the sample there was a pinhole of 10 μm diameter (pinhole is not present in the picture). This allowed to resolve the Bragg peak and the diffraction satellites due to SAW. A scintillation detector was used to measure the diffracted intensity, with motorized slits that were closed down to 0.01 mm approximately. This corresponds to an angular resolution of 3.5 arcsec. This was enough to resolve the satellite peaks with a detector sample distance of 0.3 m. The Bragg angle at the LNB crystal was θ =16.45° for the energy 8 keV. Surface acoustic waves were emitted in trains of 100 ns duration. The emission of the SAW was correlated with the BESSY II storage ring in order to scatter the X-rays emitted from the selected electron bunch. Delay, and consequently the selected bunch, were varied by a delay generator (DG645, Stanford Research System). The bunch structure at BESSY II at the time of the experiment is shown in Fig. 3.3. Additionally, one day the sychrotron storage ring was operated in the so called Few Bunch mode, shown and described in Fig. 3.40

3.5.3 Sample – SAW device

For an overview of the sample and its properties see table A.1, at the voice S1. A scheme of the sample is shown in Fig. 3.41. The substrate was a 128° rotated Y-cut of black Lithium Niobate, a piezoelectric crystal. The surface roughness did

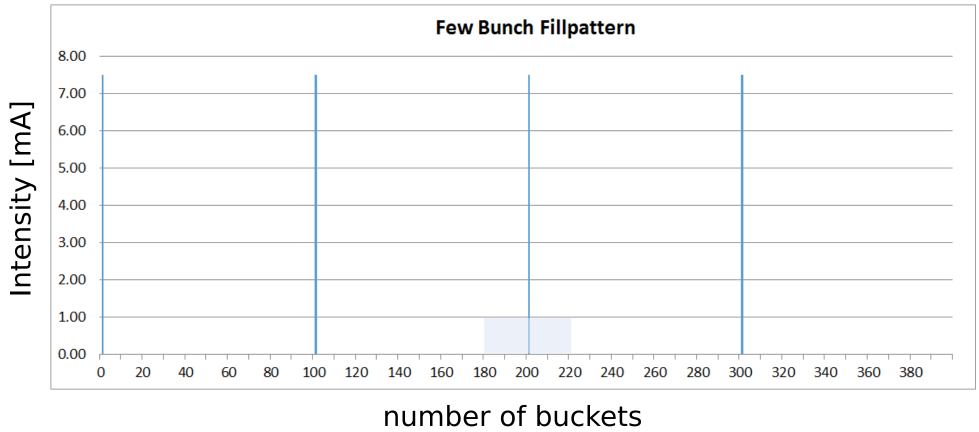

FIGURE 3.40: The few bunch operation mode at BESSY II. The bunches are stored on the bucket positions 1, 101, 201 and 301 providing a photon pulse repetition rate of 5 MHz (200 ns). The total current of 30 mA is equally distributed on all four bunches.

not exceed 5 Å. To excite SAW two IDTs made of Aluminum were deposited on the surface of the LNB crystal by an external company, Avangard JSC. The IDTs were in split geometry configuration, see section 1.1.3, and were designed using the *IDT_DOUBLE_NEG* function as described in Appendix B. The acoustic aperture was w = 1.0 mm, see Fig. 3.41. The SAW wavelength was $\Lambda = 4\ \mu$m, the propagation velocity was $v_{SAW} = 3992$ m/s. The resonance frequency was estimated with eq. (1.1.3) to be 998 MHz and it slightly with the experimental value, that was found to be 980 MHz. The sample was tested with the VNA, which showed a resonance frequency of 985 MHz, see Fig. 3.42.

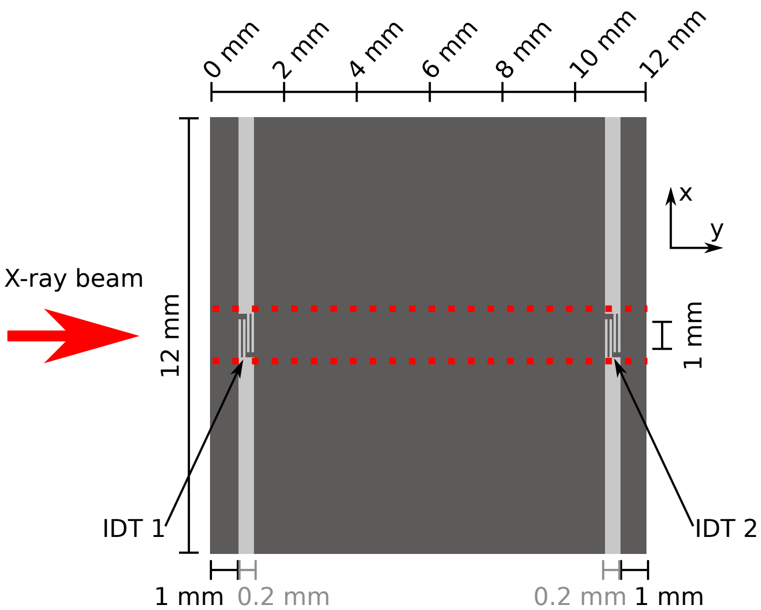

FIGURE 3.41: The sample studied at mySpot beamline. The measurements were performed at different y positions, in the region delimited by the two red dotted lines.

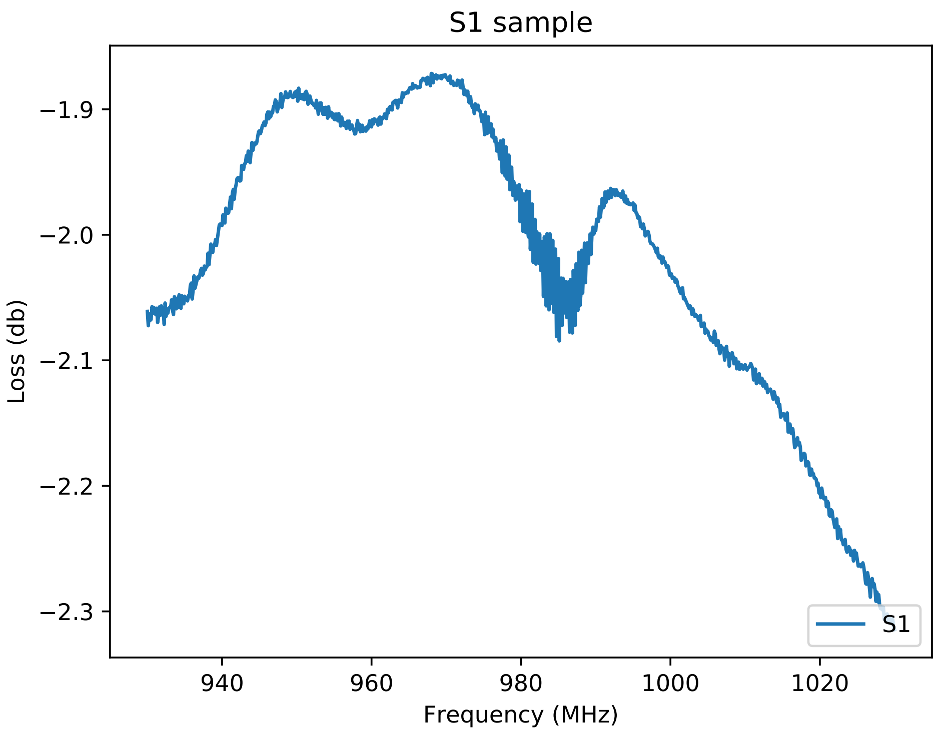

FIGURE 3.42: VNA measurement for the sample used during the experiment

3.5.4 Results

In Fig. 3.43 are shown two delay scans. The storage ring was operating in Few Bunch mode. One was recorded and position y = 1.5 mm, close to the IDT, and the second one was recorded at position y = 2.5 mm. Since the speed of the SAW on $LiNbO_3$ is approximately 4 μm ns^{-1} and the two delay scans are taken 1 mm apart in y direction, the same X-ray pulse is supposed to appear at a delay distance of 250 ns. This is indeed the case. The same X-ray pulse appears approximately at delay = 150 when the delay scan is performed at y=2.5 mm, and at delay = 400 ns when the delay scan is performed at position y = 1.5.

In Fig. 3.44 four Y scan recorded at different delays are shown. The storage ring was operating in Single Bunch mode. The edge of the sample is at y=0 mm, where the reflectivity drops to zero. The IDT is approximately at position y = 1, and it is emitting SAW pulses in both positive and negative y direction. It is particularly clear taking a look at the scan recorded at delay 590 ns and 640 ns. Even though it could be somehow counter intuitive, the longer the delay, the shorter distance has the SAW pulse traveled. At delay = 690,740 ns, the SAW pulse is still partially overlapping with the IDT, and this results in a broadening of the peak. This is true also for the scans at delay = 590, 640 ns, but the effect is less evident because the SAW pulse already partially left the IDT region.

In Fig. 3.45 five y scan recorded at five different delays are shown. The storage ring was operating in Single Bunch mode. The scan at delay 0 ns and 400 ns show zero values around y = 9 mm and y = 6 mm, respectively. This is due to beam loss. The edge of the sample are approximately at 0 mm and 11.5 mm. The four X-ray pulses

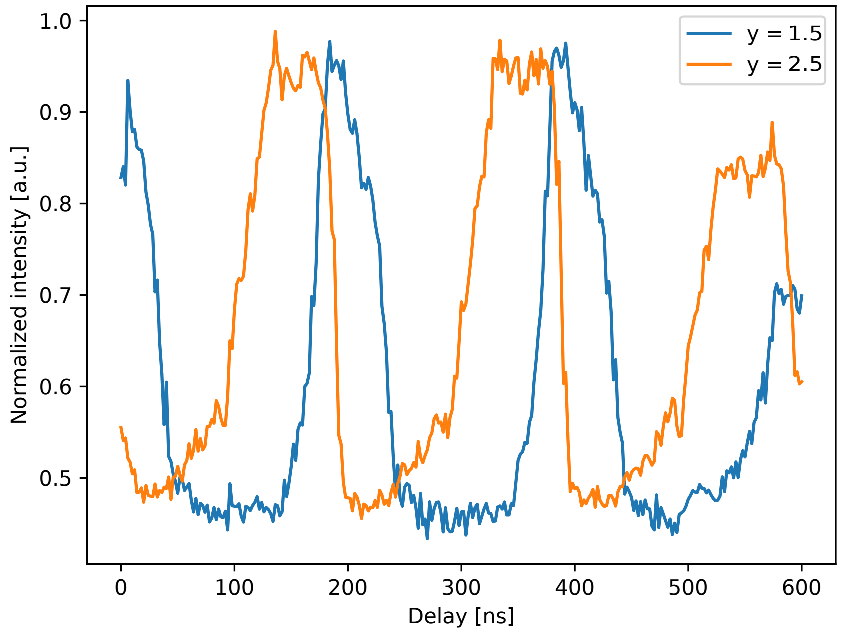

FIGURE 3.43: Delay scans at two different y position on the sample.

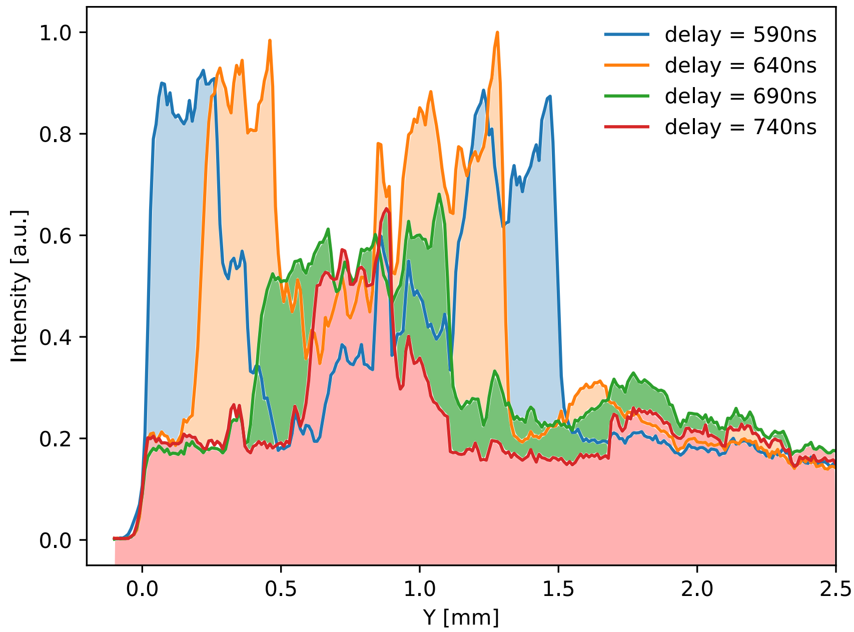

FIGURE 3.44: Y scans at different delays, the storage ring was operating in single bunch mode.

are correctly visualized while scanning on the sample when they interact with the SAW pulses. The different intensity does not depend on different intensity of the X-ray pulses and neither on different amplitude of the SAW pulses. The sample was not re-aligned for each point measured in y, but every 0.5 mm. Therefore the resulting intensity of the pulses, while it shows correctly the position of the SAW pulse, does not account for the amplitude of the SAW and neither for the intensity measured by the detector due to the interaction of the SAW pulse with the four X-ray pulses. Even though, comparing the shape of the peaks around position y = 3 mm, y = 6 mm and y= 9 mm, it can be noticed that each individual peak seems to suffer some sort of splitting. This might indicate that within the same SAW pulse there are different wavefront with slightly different speed.

Finally the shape of the peak at position y=10.5 mm recorded at delay = 0 ns differs from the shape of the other peaks. For a zoom around the region of interest see Fig. 3.46. A possible explanation for this peculiar shape, with two pronounced maxima so far apart from each other could be the following: around position y=10.5 lies the second IDT on the sample. When the wavefront of the SAW pulse reaches the second IDT, the fingers start vibrating. The mechanical movement of the fingers, coupled with the piezoelectric substrate, produces an electric field and consequently a current in the IDT itself. This electrical signal is faster than the SAW. It is possible that once the SAW pulse hit the first fingers of the IDT the signal is transmitted through the whole IDT, the fingers start vibrating and emitting a wave on the opposite side of the IDT. This would explain the presence of the second maximum.

In Fig. 3.47 the heat maps taken close to the IDT (A) and far (B) are shown. When

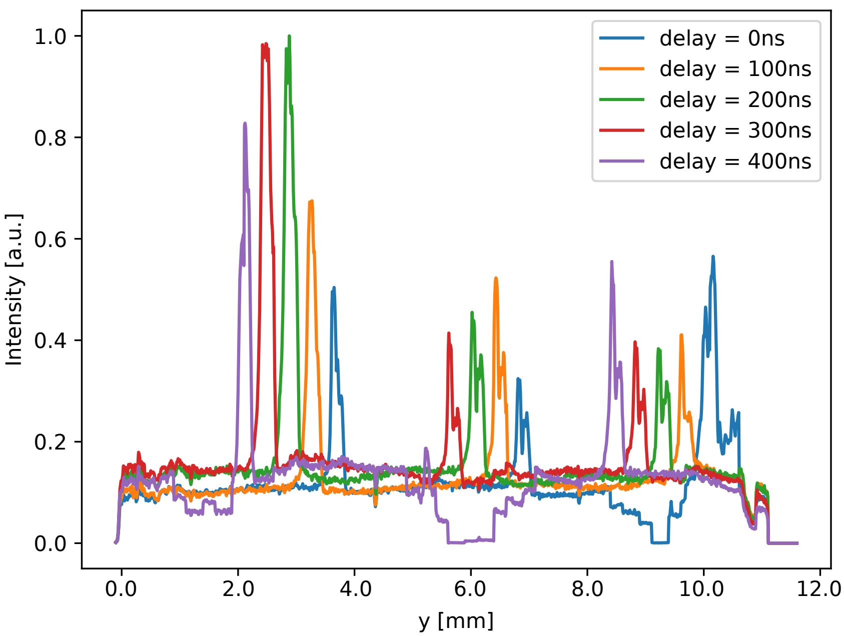

FIGURE 3.45: Y scans at different delays. The storage ring was operating in few bunch mode.

the SAW pulse is close to the IDT is quite compact and homogeneous. But once it travel far from the IDT (B) it seems to have a minimum in the middle (approximately at y = 2.12 mm), as if it is composed by two waves with slightly different speed. This would support and explain the peak splitting that can be observed in Fig. 3.45.

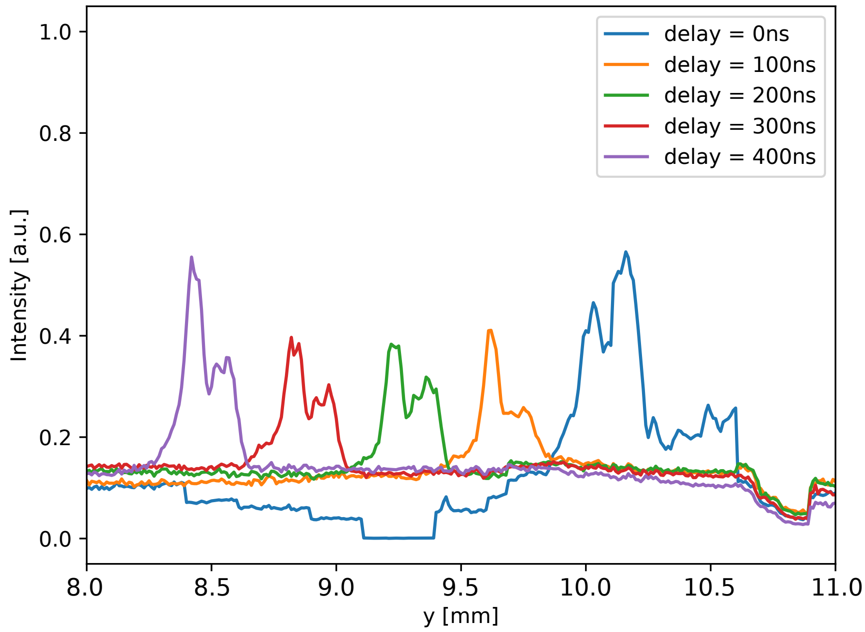

FIGURE 3.46: Y scans at different delay. Zoom around the second IDT.

3.5.5 Discussion

This series of measurements are extremely important to understand behavior of pulsed SAW. As a general comment it is important to underline that the absolute value of the delays reported in different plots, it is valid only within each plot. A number of events may change the value of the delay. A different cable used to connect the sample to the delay generator, or a beam loss, or a change of the operational mode of the storage ring. Delay scans at BESSY II with the storage ring operating in Single bunch mode and Few Bunch mode were performed for the first time. This allows a direct visualization of the fill pattern of the electron orbits via X-ray diffraction on pulsed SAW. The Y scans allow us to visualize how many SAW pulses are present on the surface of the sample, and at which position they are for a given delay. For the first time the shape of a SAW pulse was studied and visualized via a heat map. From the results it is clear that a SAW pulse is not a homogeneous pulse. It was confirmed that the width of the pulse corresponds to the width of the IDT, and it does not seems to be any spreading in this direction (z direction for the heat maps in Fig. 3.47). However the same heat maps of Fig. 3.47 clearly show that the SAW pulse has an internal structure. In particular it has a minimum in the middle and two wavefronts with different speed. It is not possible to state exactly what contributes to this internal structure, but it is possible to make some assumptions. It is known that the speed of the SAW is influenced by a number of factor, as impurity in the first layers of the crystal or on the surface of the crystal. Since the experiment was carried out in air, all sort of impurities might have deposited on the surface. The purity of the crystal has not been investigated, but impurities might contribute to it. Finally, imperfection in the manufacture of the IDT might also contribute to this behavior.

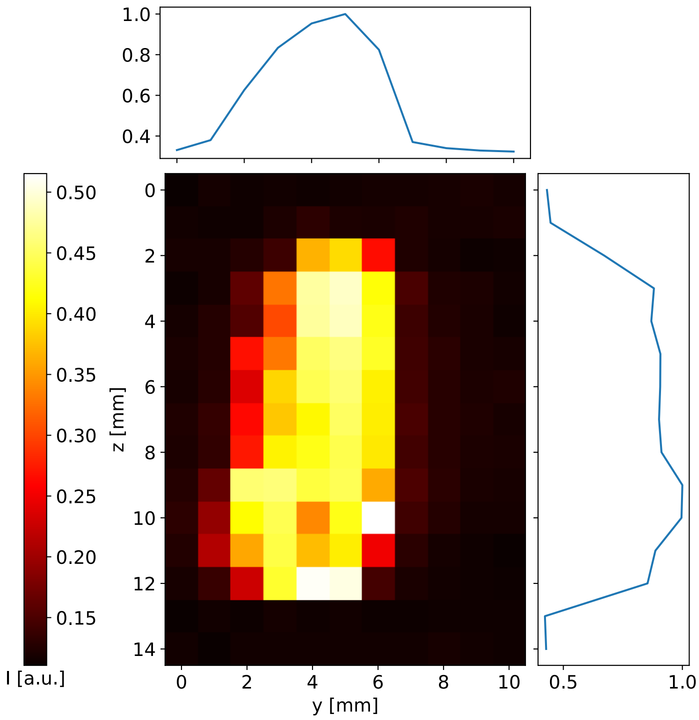

(A) close

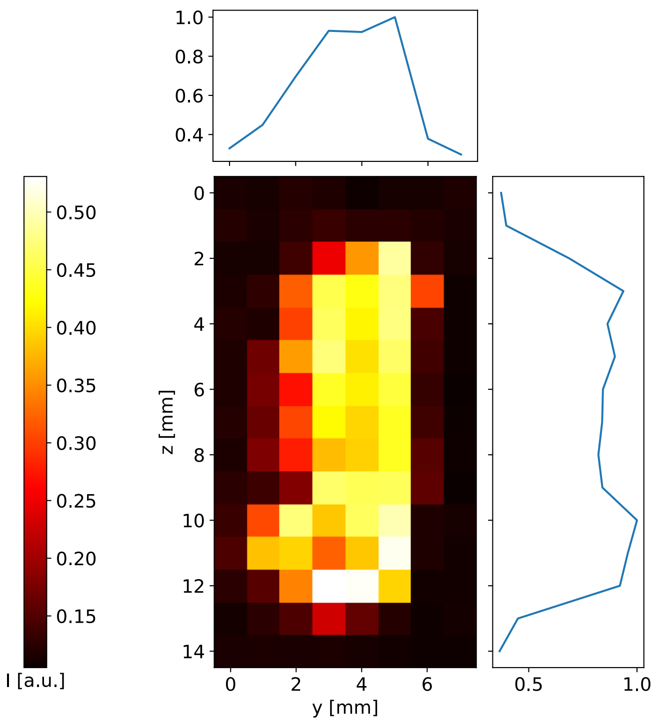

(B) far

FIGURE 3.47: Two heat maps recorded close and far from the IDT.

3.6 Summary

The results of the static experiment at the XPP_KMC3 beamline, X-ray Bragg diffraction in LGS crystal excited by SAW, demonstrated the possibility to achieve an effective diffraction of an X-ray beam in sagittal geometry. The proper theoretical model has been applied for calculation of SAW amplitude and wavelength based on the measurements of the electrical (amplitude of electrical signal) and diffraction (satellite intensity) parameters. The experimental result and theoretical predictions of kinematical theory are in a good agreement.

For the first time the interaction of X-rays with SAW at energy lower than E = 1 keV was investigated at the Optics beamline. The results of X-ray Bragg diffraction and total external reflection on a Si/W multilayer in meridional geometry are reported.

The results of the time resolved experiments show that it is possible to modulate a pulsed X-ray beam using pulsed SAW. For the first time it was shown that exciting a short enough trains of SAW on the surface of the crystal it is possible to select which pulse reaches the detector and which one is stopped. Moreover the structure of the SAW pulse was investigated and revealed inhomogeneity in the structure.

Chapter 4

Application: SAW Pulse Picker

X-ray time resolved experiments allow the investigation of the dynamics of chemical reactions or physical phenomena [1, 2, 3]. Various pump-probe experiments can be conceived, from measuring the fast structural changes (for an overview of recent X-ray diffraction experiments with time resolutions down to 100 fs see [60]) in dependence on external excitation to spectroscopic in-situ monitoring of chemical reactions using X-ray absorption spectroscopy (for an overview about picosecond and femtosecond XAS applied to molecular systems in solution see [61]). The studied processes span different time scales, from picosecond to millisecond. In pump-probe experiments, a fast change in the sample is triggered by external activation (pumping). Short time after the activation, a X-ray pulse is used to measure the state of the studied sample (probe). Ideally, no additional X-ray pulses should reach the sample, especially if the measurement hardware is not able discriminate the unwanted photons.

Synchrotron radiation facilities provide strong and stable X-ray beam pulses that can be used for time resolved measurements. The pulse sequence is the direct consequence of the filling pattern of electron bunches in the storage ring, see section 3.1.1. To be able to serve the experiments probing different time scales at the same time, a versatile modulator for the X-ray pulses time structure is needed. Since at synchrotron light sources many experiments are served simultaneously, such a device is preferably implemented in each experimental station.

BESSY II, a synchrotron radiation facility in Berlin, is preparing to upgrade to BESSY VSR [62], a variable-pulse-length storage ring. In its normal operating mode, the Hybrid Mode, BESSY II currently delivers high-brilliancy X-ray pulses having a duration of 17 picoseconds. Additionally, a few days per year BESSYII run in the some different modi, the *Single Bunch*, *Few Bunch* or the *Low-alpha Multi Bunch Hybrid Mode*, see [63] for the details, in order to study samples using extremely short pulses (about 3 picoseconds). To do so, however, the photon flux has to be greatly reduced. This will fundamentally change with BESSY-VSR. Thanks to a pair of superconducting radio frequency cavity the high proton flux will remain constant. BESSY-VSR will offer short pulses of 1.5 picosecond length and longer pulses of 15 picoseconds, see Fig 4.1. BESSY-VSR thus fills a gap between storage rings such as PETRA III and the free-electron lasers. Even though the operation modi in which BESSY-VSR will operate are still not well defined, it is conceivable that there will be the necessity to pick only certain X-ray pulses, either from a Hybrid Mode to allow for time resolved experiments through the whole year, or from a new *Few Bunch* mode.

Modern pulse pickers are mechanical choppers rotating at high velocities. This

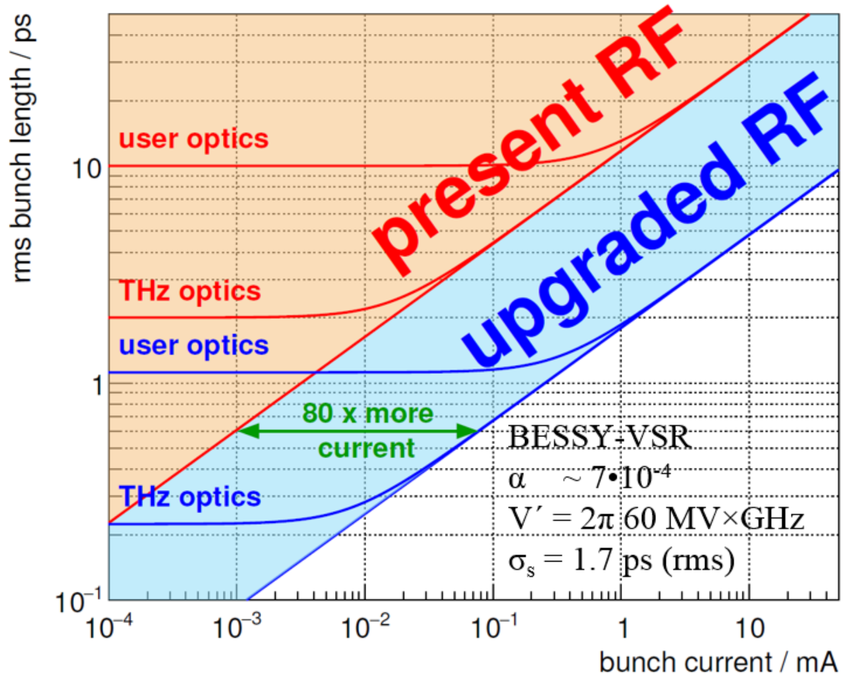

FIGURE 4.1: Bunch length as a function of bunch current at BESSY II for the present situation and with a 100 time stronger RF gradient [64].

comprises a wide range of different technical implementation, such as rotating crystals or mirrors [65], triangular shaped metal plates [66], rotating absorbers [67] and a wide range of variations of a rotating disk or cylinder [68, 69, 70, 71, 72, 73, 74, 75]. The open time window for each bunch picker depends on the design of the bunch picker itself. Mechanical bunch pickers are limited by the rotation speed and by the shape of the aperture, in the order of a few μs, while rotating crystals bunch pickers are limited by the rotation speed and by the distance of the mirrors to a defining aperture, in the order of a few hundred ns. Another limitation common to most of the pulse pickers actually in use, is that they operate at low repetition rate, in the KHz region. Nevertheless synchrotron sources operate with a repetition rates in the MHz region.

To overcome these problems, *Tucoulou et al.* presented a different kind of pulse picker based on the X-ray diffraction on a multilayer modulated by SAW) [76]. This device can be used for temporal modulation of X-rays by switching the grating structure on and off. If SAW are pulsed the diffraction satellites appear only when the SAW train goes through the irradiated area of crystal surface. The time resolution is defined as the time that the SAW train needs to cross and leave the X-ray beam footprint. *Tucoulou et al.* performed an experiment at the ESRF synchrotron facility, and managed to pick a single pulse in the middle of a gap of 1.8 μs using the grating produced by SAW in meridional geometry [76]. However such an implementation would not fit the requirements of smaller synchrotron sources such as BESSY II or Diamond Light Source (DLS). To be of practical value for BESSYII or DLS the time resolution has to be smaller than the wide ion clearing gap, 200 ns and 400 ns respectively. In this chapter is reported a possible implementation of an X-ray pulse picker built taking advantage of diffraction of SAW in sagittal geometry [**art:30**, 77]. In this geometry the wavefront is parallel to the scattering plane. This has the advantage to diminish the time resolution to values that are at least one order of magnitude lower compared to meridional geometry. The reason is that the SAW is traveling across and not along the footprint, which normally has much smaller transverse size than longitudinal. A functional test of the SAW pulse picker was reported by *Vadilonga et al.* in [78]. In this paper, unlike in [33, 77], a geometry close to sagittal, with a small inclination with respect to the SAW wavefront. This geometry takes advantage of the time resolution in sagittal geometry and at the same time it allows for a good separation of the diffraction satellites as in meridional geometry. The achieved time resolution, approximately 100 ns, is enough to pick the single bunch out of the *Hybrid Mode* of both BESSYII and DLS.

4.1 Time resolution of a SAW pulse picker

The time resolution of a pulse picker driven by a SAW is given by the time that the SAW pulse needs to cross and leave the beam footprint, see Fig. 4.2. Let's consider

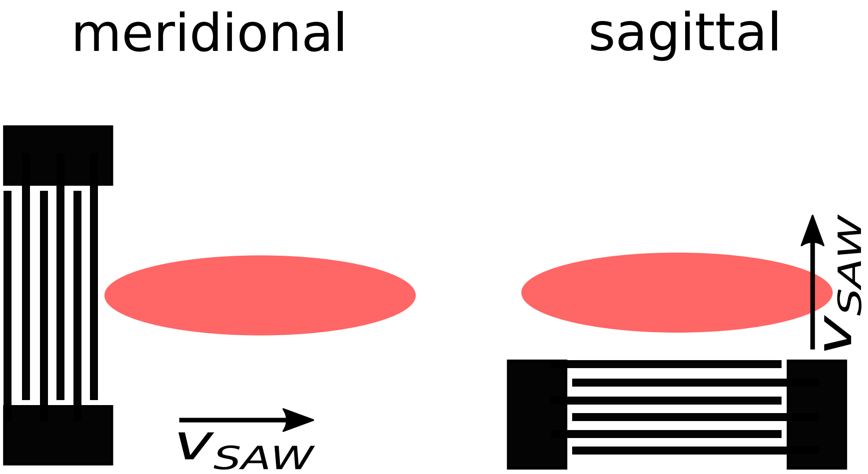

FIGURE 4.2: Time resolution in meridional (left) and sagittal (right) geometry.

the case of BESSYII as a target for the time resolution. The ion clearing gap duration is approximately 200 ns when the storage ring is working in the Hybrid Mode, see Fig. 3.4. Now consider the case of a beam size of 300×300 μm^2 (horizontal $\times$ vertical), and SAW running on a Si 111 crystal with a speed of approximately 5000 m/s as in reference [27]. The time resolution for the meridional and for the sagittal geometry case are plotted in Fig. 4.3. In meridional geometry the time resolution depends on the energy of the incoming X-rays, because the length of the footprint depends on the Bragg angle. The time resolution can be calculated as

$$\Delta T_{mer} = \frac{v_{beam}}{\sin(\Theta_B(E))} \frac{1}{v_{SAW}}, \tag{4.1}$$

where v_{beam} is the vertical size of the X-ray beam, $\Theta_B(E)$ is the Bragg angle and v_{SAW} is the speed of the SAW. The time resolution varies between 180 ns and 700 ns. In sagittal geometry the time resolution can be calculated as

$$\Delta T_{sag} = \frac{h_{beam}}{v_{SAW}}, \tag{4.2}$$

where h_{beam} is the horizontal size of the beam. In sagittal geometry the time resolution does not depend on the incident energy and is therefore constant with a value of approximately 60 ns. As reported in [78], using a B_4C/W multilayer with an incident angle of 1.83° and much slower speed than in the case of a Si substrate, a time resolution of 120 ns was achieved. This is enough to separate the single bunch from the Hybrid Mode in BESSY II.

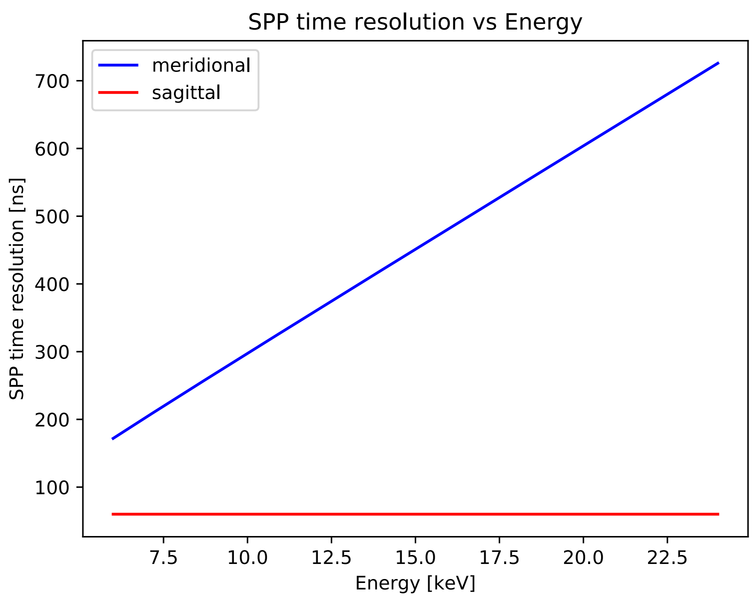

FIGURE 4.3: Time resolution of a SAW pulse picker in meridional and sagittal geometry depending on the X-ray energy, for a beamsize of $300 \times 300\ \mu m^2$.

4.2 Working principle – Possible implementation

One of the basic principle to keep in mind when implementing new optics for a beamline is that each optical element will reduce the overall flux reaching the experimental chamber, and increase the difficulty of aligning and manipulating the X-ray beam. The less optical element in the beamline, the better it is. A great advantage of such a SAW pulse picker lies in the fact that no additional optical element should be implemented in a beamline. It could potentially be implemented directly into an existing optical element, since the only requirements are to have parallel and monochromatic beam, e.g. on the second crystal of a double crystal monochromator, see Fig. 4.4. The working principle of the SAW pulse picker is shown in Fig. 4.5. A short SAW pulse is generated on the surface of a crystal, and it travel fast enough to cross and leave the beam footprint during the ion clearing gap (for a description of the time structure of a synchrotron radiation see section 3.1.1). The unique characteristic of such a pulse picker would be its repetition rate. It would be able to pick pulses separated by only 120 ns. Moreover such an implementation would be extremely flexible and versatile, and able to adapt to the necessity of the performed experiment. In fact it would not only be very fast, but also able to pick any pulse in a pulse train. Since it can be controlled electronically the repetition rate can be tuned to the requirement of each individual experiment. One could extract one X-ray pulse

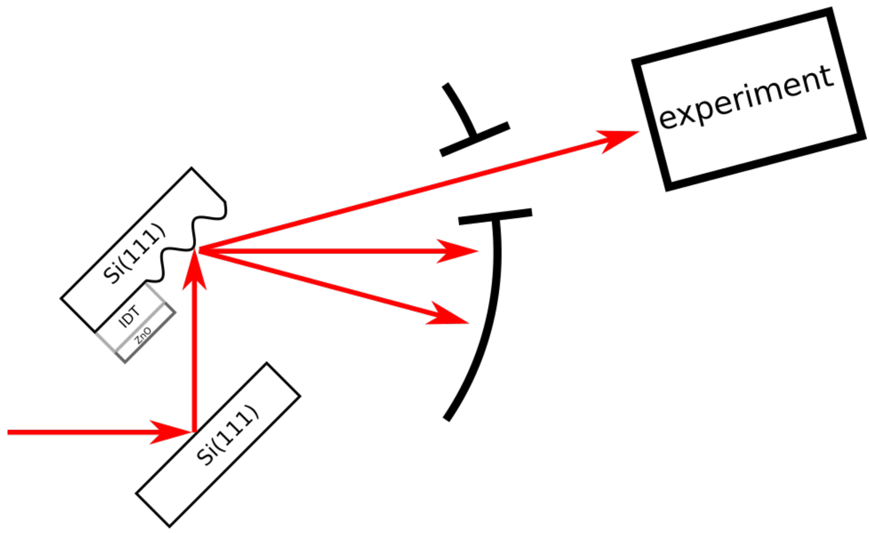

FIGURE 4.4: Possible implementation of a SAW pulse picker on the second crystal of a Si (111) monochromator.

per electron revolution, or two, or any combination of pulses separed by at least 120 ns.

4.3 Efficiency and Signal to Noise Ratio

The efficiency of such a pulse picker depends essentially on three factors. The first one is the overlap of the X-ray footprint with the SAW path. In sagittal geometry SAW travel across and not along the footprint, and this means that the path they have to travel to cross and leave the X-ray footprint does not depend on the X-ray incident angle, see eq. (4.2). As demonstrated in section 3.5, it is possible to stretch the acoustic aperture up to one millimeter, but it is not possible to stretch the acoustic aperture of an IDT indefinitely. The optimal value is recognized in literature to be approximately hundred times the acoustic wavelength. For a device with a SAW wavelength of 4 μm this means that the optimal aperture is approximately 400 μm. We managed to produce and test samples with an acoustic aperture up to 1 mm, see section 3.5. It is difficult to predict whether it is possible to stretch the acoustic aperture up to 3.5 mm to cover the whole hard X-ray range. In case it is not possible to stretch the acoustic aperture up to the desired value, an elegant solution could be applied . It consist in producing two or more IDT in the geometry showed in Fig. 4.6, called parallel IDT configuration. A similar design is already implemented in the python module to produce IDT designs described in appendix B, see the function IDT_DOUBLE_PARALLEL_NEG. Ideally the two IDT should excite two SAW pulse that would overlap with the X-ray footprint. Of course the feasibility of such a device should be further investigated. The second factor that influences the efficiency of the pulse picker is the reflectivity of the substrate on which the SAW are excited, which depends on the desired X-ray energy. In the hard X-ray region Bragg diffraction could be used, for example on a Si 111 substrate. Silicon is chosen because of its well known and good optical properties. Theoretical calculations suggest an efficiency of approximately 25%–40%. This depends on the maximal intensity that can be reached by the first diffraction order, and it can be estimated via equation (1.47). Finally, the Signal to Noise ratio (SNS), calculated from experimental data described in section 3.4, including the scattered intensity from non-disturbed area, is about 50% for our

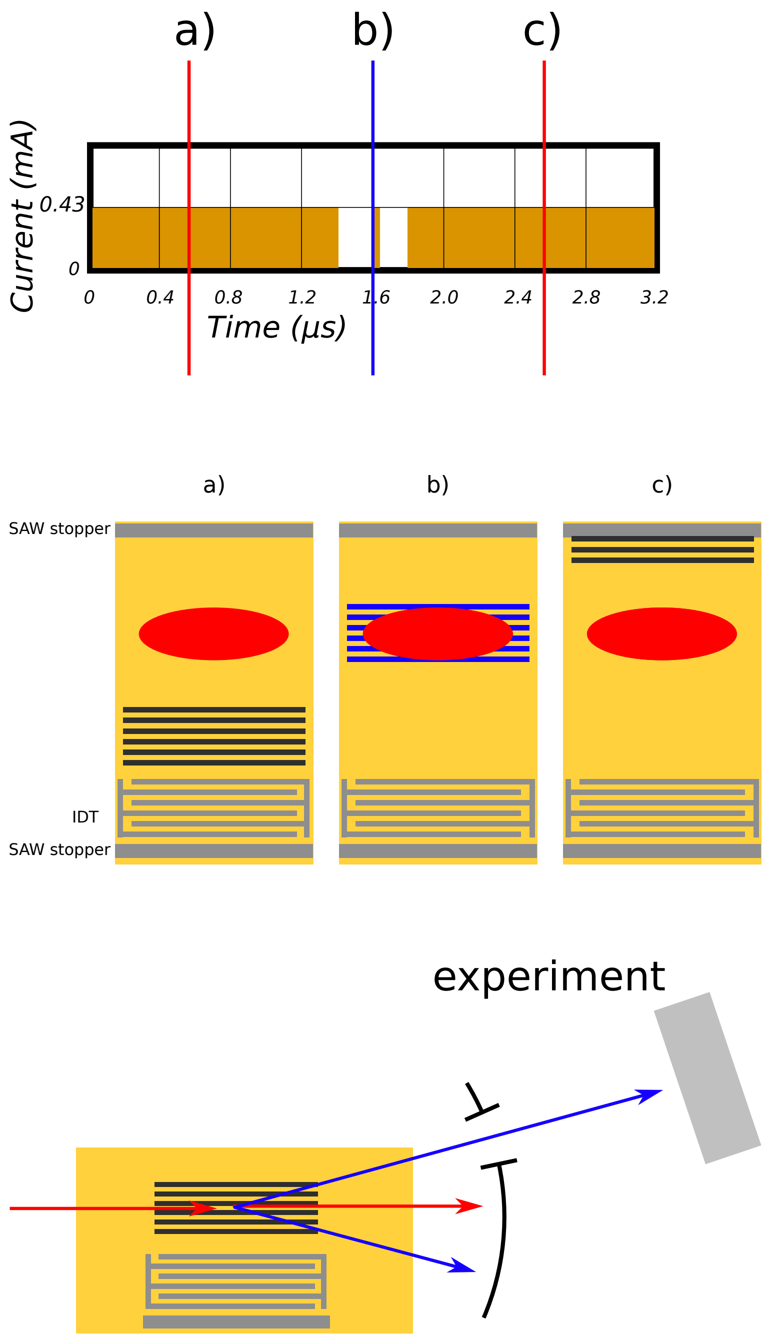

FIGURE 4.5: Working Principle of pulse picker driven by a SAW. A surface acoustic wave pulse is excited on the surface of a crystal. **a)** It starts travelling towards the position of the X-ray beam footprint. The Bragg diffracted beam is absorbed by a pair of slits, and no X-rays are delivered to the experimental chamber. **b)** The SAW pulse perfectly overlap with the X-ray beam footprint when the single bunch is coming. The first diffraction satellite reaches the experimental chamber, while all the other orders are absorbed by the slits. **c)** The SAW pulse travels away from the position of the X-ray beam footprint and it is absorbed by a SAW stopper.

measurements at E = 8 keV. However this does not reflect the real rejection ratio of a SAW pulse picker, which is proven in static experiments to be around 0.1% [10]. In the Soft X-ray region, where Bragg reflection is either very weak or completely

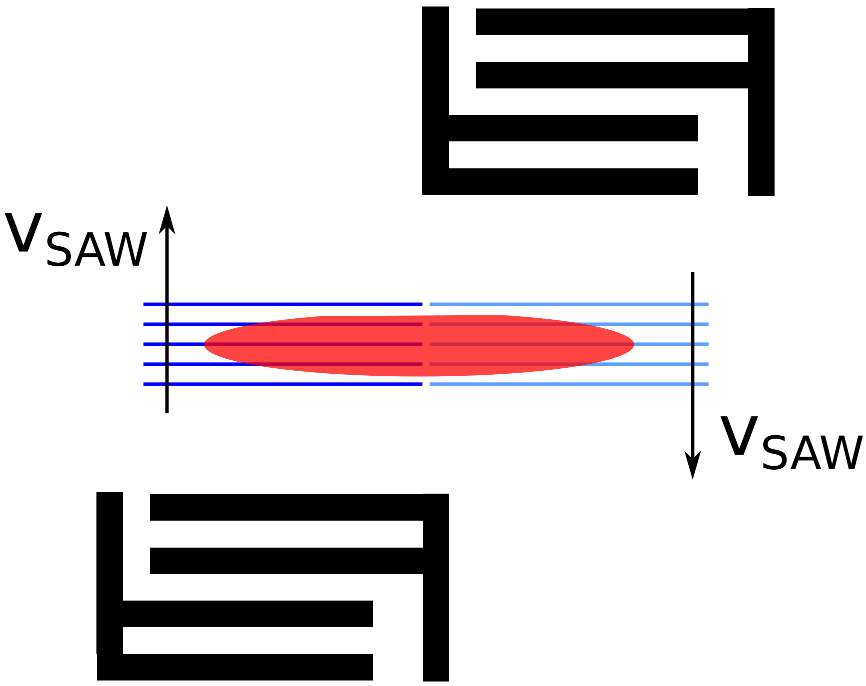

FIGURE 4.6: Parallel IDT configuration. Two IDT emit short SAW pulses that overlap with the X-ray beam footprint. In such a configuration the SAW path would be the double than the one produced by a single IDT.

absent, a multilayer reflection could be used as in the experiment reported in section 3.3. It is not possible at the moment, without further investigations, to guess the efficiency or the SNS in the Soft X-ray region.

4.4 Summary

A possible direct application of SAW is proposed. A possible implementation of a pulse picker for synchrotron radiation driven by SAW is discussed, together with its advantages and disadvantages over the other pulse pickers in use. Its criticality are discussed, and possible workarounds are suggested.

Chapter 5

Discussion and Outlook

In summary, within this work, the potential of the interaction of the X-rays and SAW was explored. The first experiment aimed to study Bragg diffraction in sagittal geometry, and demonstrated the possibility to achieve an effective diffraction. The second experiment, performed in meridional geometry in Bragg and total external reflection conditions, investigated for the first time the interaction of X-rays with SAW in the soft X-ray region. The results of two time resolved experiments have been reported, analyzed and discussed. The measurements performed in Bragg sagittal geometry showed that it is possible to temporally modulate an X-ray beam. Simply changing the scattering geometry lead to drastically reduce the time resolution and proved that the single bunch could be picked from the Hybrid Mode of DLS.

The four experiments reported in the thesis delivered promising results for the application of SAW as grating whose presence can be electronically controlled. Applying the SAW to a new generation of optics is an intriguing and promising possibility. To effectively manipulate an X-ray beam with SAW three issues must be addressed.

The scattering geometry plays an important role when manipulating an X-ray beam with a SAW. In meridional geometry the diffraction satellites appear one at a time when rocking the sample. Their angular separation is independent of the energy of the incoming photons, and it depends only on the ratio of the interplanar spacing of the substrate and the SAW wavelength. This makes it relatively easy to discriminate among the diffraction satellites. In sagittal geometry the diffraction satellites appear all at once. Their angular separation depends on the energy of the incoming photons and on the SAW wavelength. To discriminate among the diffraction satellites the detector must be placed at a certain distance and being provided of motorized slits, or in case of a CCD camera detector the pixels must be small enough. In both geometries, in order to obtain an effective diffraction process and in order to be able to resolve the diffraction satellites, the divergency of the X-ray beam should be lower than the angular separation of the diffraction satellites. Moreover the sample detector distance must such that the spatial separation of the diffraction satellites is smaller than the gap between the detector slits for a diode or scintillation detector, or smaller than the pixel size for a CCD camera. X-ray Bragg diffraction on SAW in sagittal geometry was investigated for the first time by *Roschupkin et al.* [33]. In this work the authors use a set of compound refractive lenses (CRL) to better resolve the diffraction satellites. To manipulate an X-ray beam it was important to proof that is it possible to resolve the diffraction satellites without the help of CRL, and this was done in the experiment reported in section 3.2.

When performing time resolved experiment with pulsed SAW, the time resolution is defined as the time that a SAW pulse needs to cross and leave the X-ray footprint. In meridional geometry the SAW pulse travels along the X-ray beam footprint, which is usually a longer path than travelling across it as it happens in sagittal geometry. To obtain maximal efficiency and be sure that the X-rays are scattered only by a portion of the substrate whose surface is modified by SAW, the SAW pulse must be at least as long as the X-ray beam footprint, but not longer. A longer SAW pulse would make the time resolution worse. In meridional geometry the length of the X-ray footprint depends on the incident angle of the X-ray beam. In the experiment performed by *Tucoulou et al.* [76], performed in meridional geometry, the time resolution was in the order of microseconds. Changing the geometry to sagittal, as in section 3.4, lead to a time resolution of only 120 ns, one order of magnitude lower. The spatial length of the SAW pulse, which depends on the SAW pulse duration, must be adjusted according to the dimensions of the X-ray beam footprint on the sample.

The efficiency of the diffraction process depends on four factors. First, the X-rays should not penetrate in the substrate more than one acoustic wavelength, to avoid interaction with layers that are not distorted by the SAW. Second, the X-ray beam footprint should overlap with the SAW path. In meridional geometry it is easy to overlap completely the X-ray beam footprint with the SAW path. The only precaution that must be taken is that the horizontal size of the beam does not exceed the acoustic aperture of the IDT. The vertical size of the beam is not really important as long as the footprint of the beam does not exceed the length of the sample. In sagittal geometry it is not easy to overlap the X-ray footprint with the SAW path. In this case the horizontal size of the beam must be smaller than the sample. The vertical size of the beam must be small enough, so that once it is projected on the sample surface the length of the footprint does not exceed the acoustic aperture of the IDT. In the experiment described in section 3.4, the acoustic aperture of the IDT was smaller than the X-ray beam footprint. Not all the photons interacted with portions of the sample distorted by SAW. To solve this problem new samples were produced and tested, with an acoustic aperture of 1 mm, as in the experiment described in section 3.5. Third, the reflectivity of the sample. In the hard X-ray region Bragg diffraction is an extremely efficient process. In the soft X-ray region Bragg diffraction is not an efficient process or it is even forbidden. That is the reason why to perform the experiment described in section 3.3 a $LiNbO_3$ crystal was coated with a Si/W multilayer. Finally one must take into account that the intensity of the diffraction satellites is proportional to the amplitude of the SAW via the relation expressed by eq. (1.48). Since SAW act as a phase grating when illuminated by X-rays, intuitively X-rays with shorter wavelength will achieve higher phase shift for a given amplitude, compared to X-rays with a longer wavelength. For hard X-rays this is not a concern, since it is easy to achieve an amplitude of the SAW such that the first diffraction order reaches its maximum intensity, usually between 25% and 40% of the reflectivity of the Bragg peak. For soft X-rays, with longer wavelength, the situation is more complicated, since not only the radiation wavelength is considerably longer, but also the diffraction process must take place in a multilayer, that has a periodicity in the order of magnitude of the nanometer, one order of magnitude higher than the interplanar distance in single crystals, in the order of amplitude of angstroms. Diffraction of soft X-rays was demonstrated in section 3.3 with a maximum reflectivity of the first diffraction order of about 1%. Further testing is required to establish if the intensity of the first diffraction satellites observed in this measurements it is the real maximal intensity, or if the heating of the sample due to the lack of possibility to cool down via air convection influenced the excitation of the SAW.

Spatial manipulation and time manipulation of an X-ray beam have been studied and characterized within this thesis. The time resolution can be further improved in two simple ways. The first one is to use pure sagittal geometry, contrary to what it was done in the time resolved experiment described in section 3.4. The second one is to use a substrate that increases the speed of the SAW. The efficiency of the diffraction process can be increased. For the hard X-ray region the primary concern is to overlap the X-ray beam footprint and the SAW path. As explained in detail in Chapter 4, for high energy X-rays the footprint might increase up to 4 mm, while the IDT with the wider acoustic aperture that were tested had an aperture of 1 mm. It is not easy to predict how much this aperture can be enlarged. In case it is not possible to enlarge the acoustic aperture up to the desired value, a new design consisting of two or more IDT emitting SAW from different directions can be tested, see Fig. 4.6. In the soft X-ray region, to increase the efficiency two paths can be followed. The first option would be to decrease the period of the multilayer. This might decrease the overall reflectivity of the multilayer because the individual layer would have a higher roughness to thickness ratio. The roughness is subject to technological limit. The second one is to increase the wavelength of the SAW. The higher the wavelength, the higher the amplitude of the SAW that can be achieved. The drawback of increasing the wavelength is that the angular separation of the diffraction satellites would decrease, making it more difficult to resolve diffraction pattern. A workaround to this problem, would be to produce an IDT that is able to focus the SAW. Close to the focus the amplitude of the SAW should be much higher than one produced by a normal IDT.

The application proposed in Chapter 4 is only one of the possible applications of a SAW to a new generation of X-ray optics. An interesting application would be to study a SAW device equipped with a broadband IDT. A broadband IDT generates SAW with different frequencies, and therefore with different wavelengths. Essentially it creates a grating on the sample surface whose period can be changed electronically, simply supplying a signal with a different frequency to the IDT.

Chapter 6

Publications and contributions

Publications

Vadilonga S., Zizak I., Roshchupkin D., Evgenii E., Petsiuk A., Leitenberger W., Erko A., "Observation of sagittal X-ray diffraction by surface acoustic waves in Bragg geometry". In: *J. Appl. Cryst.* 50(2017), pp. 525-530
DOI: 10.1107/S1600576717002977

Vadilonga S., Zizak I., Roshchupkin D., Petsiuk A., Dolbnya I., Sawnhey K., Erko, A., "Pulse picker for synchrotron radiation driven by a surface acoustic wave" In: *Opt. Lett.* 42(2017), pp. 1915-1918
https://doi.org/10.1364/OL.42.001915

Vadilonga S., Zizak I., Roshchupkin D., Petsiuk A., Dolbnya I., Sawnhey K., Erko, A., "Fast Active Optics for Synchrotron Radiation". In: *Diamond Light Source annual review* Accepted for publication

I. Roshchupkin D., Ortega L., Plotitcyna O., Erko A., Zizak I., Vadilonga S., Irzhak D., Emelin E., Buzanov O., Leitenberger W., "Piezoelectric Ca3NbGa3Si2O14 crystal: crystal growth, piezoelectric and acoustic properties". In: *Applied Physics A* 122(2016), pp. 753/1-10
doi:10.1007/s00339-016-0279-1

Talks

XTOP, Brno (Czech Republic), 2016: *Observation of sagittal X-ray diffraction of surface acoustic waves in Bragg geometry*

XOPT, Yokohama (Japan), 2017: *Single bunch extraction by SAW driven bunch chopper*

EUROMAT, Thessaloniki (Greece), 2017: *Pulse picker for x-ray radiation driven by Surface Acoustic Waves*

Posters

Adlershofer Forschungsforum, Berlin (Germany), 2016: *Active optics for time resolved experiments*

BESSY II user meeting, Berlin (Germany), 2016: *Observation of sagittal diffraction of x-rays by surface acoustic waves in Bragg geometry* and *Single bunch extraction by SAW driven bunch chopper*

Workshop From Matter to Materials and Life, Hamburg (Germany), 2016: *Observation of sagittal diffraction of x-rays by surface acoustic waves in Bragg geometry* and *Single bunch extraction by SAW driven bunch chopper*

POFII RT4, Berlin (Germany), 2016: *Active optics for time resolved experiments*

Swedish German Workshop at BESSY II, Berlin (Germany), 2016: *Active optics for time resolved experiments*

ICXOM24, Trieste (Italy), 2017: *Pulse picker driven by Surface Acoustic Waves*

SRI 2018, Taipei (Taiwan), 2018: *Pulse picker driven by a Surface Acoustic Wave*

Appendix A

Samples used in this work

	LGS_1	**S2**	**ML**	**S1**
Substrate	$La_3Ga_5SiO_{14}$	$LiNbO_3$	$LiNbO_3$	$LiNbO_3$
Cut	Y	128°Y	Y	128°Y
$V_{substrate}$ [m/s]	2343	3992	3992	3992
Λ [μm]	3	4	12	4
f [MHz]	781	978	289	980
IDT configuration	single	double	single	double
IDT aperture [mm]	0.3	1	0.3	1
IDT length [mm]	0.1	0.2	0.1	0.2
Multilayer	No	Si/W	No	W/B_4C
Experiment in sec.	3.2	3.3	3.4	3.5

TABLE A.1: The samples used in this work and their properties.

Appendix B

Python module for IDT design

Four functions that allow for the creation of single, double, parallel and series IDTs were defined in the *idt_lib.py*. A short description of each function and a schematic of the output are given below.

Simple IDT The *IDT_SIMPLE_NEG(idt_cell_name, period, x_pad_size, y_pad_size, aperture, number_of_pads)* function creates and IDT as in Fig. B.1.

Parameters:

- *idt_cell_name*, *string*, a unique name for the IDT.
- period, *float*, the period of the SAW to be generated.
- x_pad_size, *float*, the horizontal (x) size of the connecting pad
- y_pad_size, *float*, the vertical size of the contact pad (note: the higher this number, the more finger pairs. # *of finger pairs = y pad size* / 2
- aperture, *float*, the acoustic aperture
- number_of_pads, *float*, number of right pads. The right contact pads can be divided in several contact pads.

Returns:

- The function creates a cell containing a simple IDT and returns its name, the string "*idt_cell_name*".

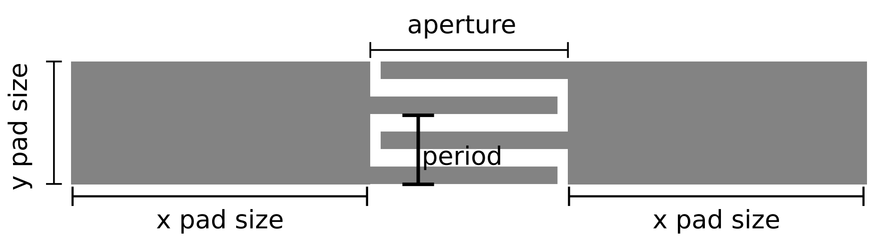

FIGURE B.1: Schematic of a simple IDT with the parameter to pass to the functions to create a GDS file.

Double IDT The *IDT_DOUBLE_NEG(idt_cell_name, period, x_pad_size, y_pad_size, aperture, number_of_pads)* function creates and IDT as in Fig. B.2. It needs the following parameters:

Parameters:

- *idt_cell_name*, *string*, a unique name for the IDT.
- period, *float*, the period of the SAW to be generated.
- x_pad_size, *float*, the horizontal (x) size of the connecting pad
- y_pad_size, *float*, the vertical size of the contact pad (note: the higher this number, the more finger pairs. *# of finger pairs = y pad size* / 2
- aperture, *float*, the acoustic aperture
- number_of_pads, *float*, number of right pads. The right contact pads can be divided in several contact pads.

Returns:

- The function creates a cell containing a simple IDT and returns its name, the string "*idt_cell_name*".

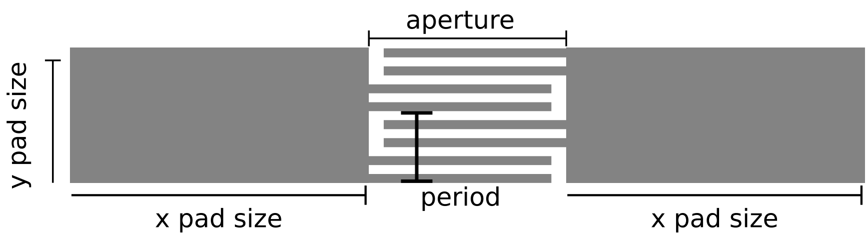

FIGURE B.2: Schematic of a double IDT with the parameter to pass to the functions to create a GDS file.

Parallel IDT The *IDT_DOUBLE_PARALLEL_NEG(idt_cell_name, period, x_pad_size, y_pad_size, aperture, number_of_pads)* function creates and IDT as in Fig. B.3.

Parameters:

- *idt_cell_name*, *string*, a unique name for the IDT.
- period, *float*, the period of the SAW to be generated.
- x_pad_size, *float*, the horizontal (x) size of the connecting pad
- y_pad_size, *float*, the vertical size of the contact pad (note: the higher this number, the more finger pairs. *# of finger pairs = y pad size* / 2
- aperture, *float*, the acoustic aperture
- number_of_pads, *float*, number of right pads. The right contact pads can be divided in several contact pads.

Returns:

- The function creates a cell containing a simple IDT and returns its name, the string "*idt_cell_name*".

Note that the function creates only one IDT. The second one should be created calling the function a second time, and placed in front of it.

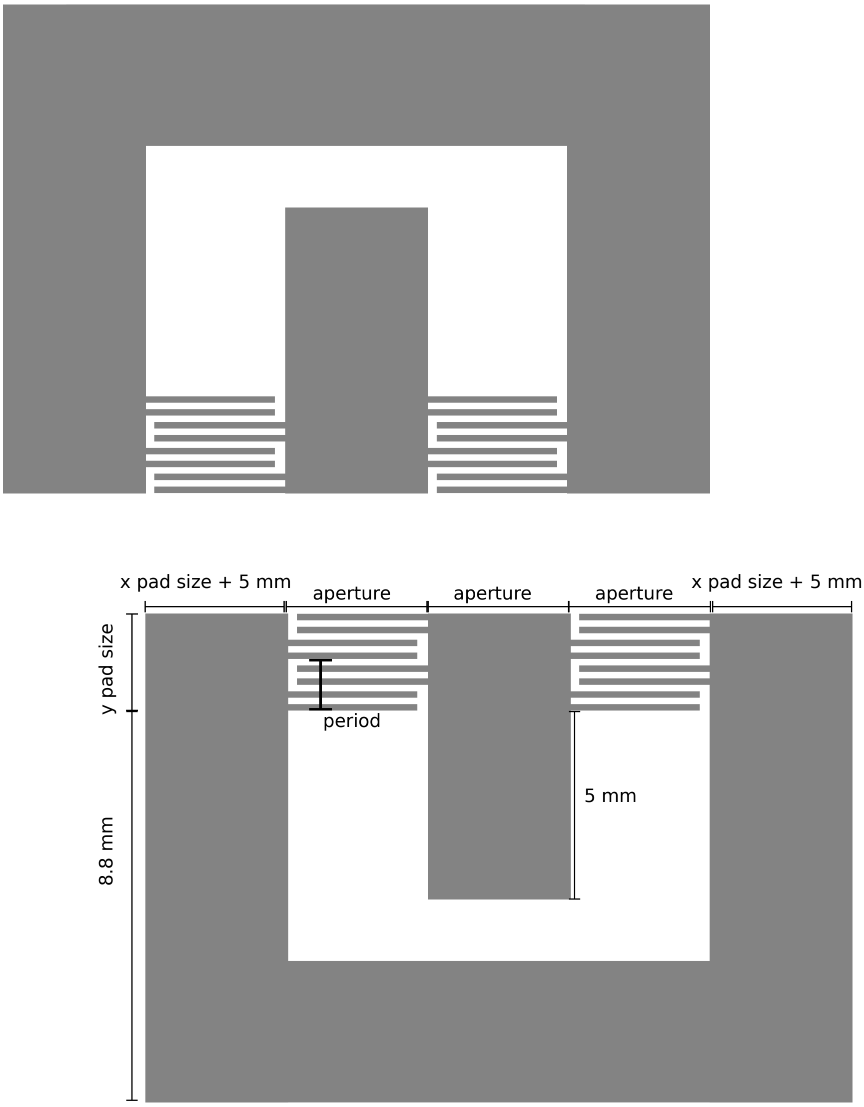

FIGURE B.3: Schematic of a parallel IDT with the parameter to pass to the functions to create a GDS file.

Series IDT The *IDT_DOUBLE_SERIE_NEG(idt_cell_name, period, x_pad_size, y_pad_size, aperture, number_of_pads)* function creates and IDT as in Fig. B.4.

Parameters:

- *idt_cell_name*, *string*, a unique name for the IDT.
- period, *float*, the period of the SAW to be generated.
- x_pad_size, *float*, the horizontal (x) size of the connecting pad
- y_pad_size, *float*, the vertical size of the contact pad (note: the higher this number, the more finger pairs. # *of finger pairs = y pad size* / 2

- aperture, *float*, the acoustic aperture
- number_of_pads, *float*, number of right pads. The right contact pads can be divided in several contact pads.

Returns:

- The function creates a cell containing a simple IDT and returns its name, the string "*idt_cell_name*".

Note that the function creates two IDTs. Additionally it creates two path to connect the IDT that are not represented in the figure, and whose parameters are fixed.

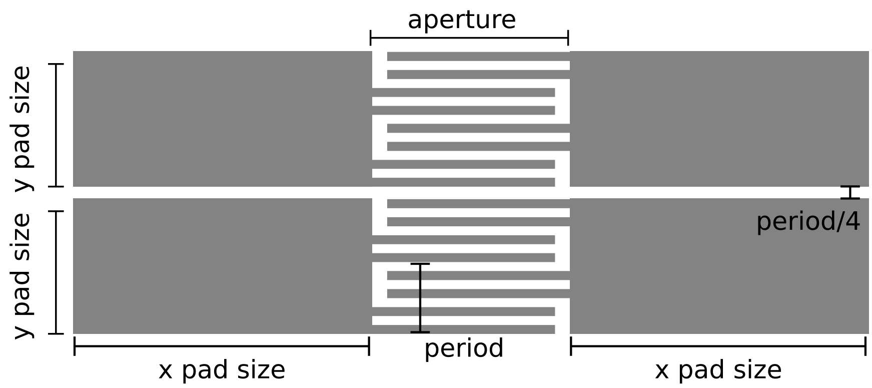

FIGURE B.4: Schematic of a two IDT in serie with the parameter to pass to the function to create a GDS file.

IDT library

```
import gdspy
import numpy as np

#implementation of the range function with float
def frange(start, stop, step):
    i = start
    while i < stop:
        yield i
        i += step


def IDT_SIMPLE_NEG (idt_cell_name, period, x_pad_size,\
                y_pad_size,aperture,number_of_pads):
        """
        Arguments:
        idt_cell_name=string 'name of the cell'
        period=integer, the period of IDT in micro m
        x_pad_size = integer, the width of the contact pads in micro m
        y_pad_size = integer, the length of contact pads in micro m
        aperture= integer, the space between the pads in micro m
        number_of_pads=integer, to split the left contact pads in more
        sections

        Return:
        idt_cell_name = cell containg the IDT
        """
        idt_cell_name = gdspy.Cell(idt_cell_name)
        #origin of the pad
        x0=0;
        y0=0;
        #fingers width
```

```
        fw=period/4.0
        #space occupied by the fingers(in legth), percentage of d
        finger_l=aperture-fw; ##lenght of the fingers
        finger_l2=fw;             ##for the left fingers..
        #number of fingers pairs
        finger_pairs_number=np.int((y_pad_size)/(period));
        #gap between contact pads
        gap=fw*4
        y_pad_size = (finger_pairs_number-1) * period + period/4*3

        for pad_n in range(0, number_of_pads, 1):
                x0=0;
                y0=y_pad_size*pad_n+gap*pad_n;
                #left contact pad(finger part)
                idt_cell_name.add(\
                        gdspy.Rectangle(\
                                (x0,y0),\
                                (x0+x_pad_size,y0+y_pad_size), 1))

                if pad_n == (number_of_pads-1):
                        #right contact pad(finger part)
                        idt_cell_name.add(\
                                gdspy.Rectangle(\
                                        (x0+x_pad_size+aperture,0),\
                                        (x0+2*x_pad_size+aperture,\
                                                y0+y_pad_size), 1))

                for displacement in frange(0, finger_pairs_number, 1):
                        #left fingers
                        idt_cell_name.add(\
                                gdspy.Rectangle(\
                                        (x0+x_pad_size,y0+displacement*period),\
                                        (x0+x_pad_size+finger_l,\
                                        y0+displacement*period+fw), 1))
                        #right fingers
                        idt_cell_name.add(\
                                gdspy.Rectangle(\
                                        (x0+x_pad_size+finger_l2,\
                                        y0+period/2+displacement*period),\
                                        (x0+x_pad_size+finger_l+finger_l2,\
                                        y0+period/2+displacement*period+fw), 1))

        return idt_cell_name



def IDT_DOUBLE_NEG (idt_cell_name, period, x_pad_size,\
                                y_pad_size,aperture,number_of_pads):
        """
        Arguments:
        idt_cell_name='name of the cell'
        period=the period of IDT in micro m
        x_pad_size = the width of the contact pads in micro m
        y_pad_size = the length of contact pads in micro m
        aperture= the space between the pads in micom m
        number_of_pads=if you want to have more contact pads

        Return:
        idt_cell_name = cell containg the IDT
        """
        idt_cell_name = gdspy.Cell(idt_cell_name)
        period = period/2.0
        #origin of the pad
        x0=0;
        y0=0;
        #fingers width
        fw=period/4
        #space occupied by the fingers(in legth), percentage of d
        finger_l=aperture-fw; ##lenght of the fingers
        finger_l2=fw; ##for the left fingers...
        #number of fingers pairs
        finger_pairs_number=(y_pad_size)/(period*2);
```

```
        remainder = np.remainder(y_pad_size, period*2)
        if remainder == 0:
                remainder = 4
        y_pad_size =y_pad_size - remainder

        #ridefining period
        period = period/2.0
        #gap between contact pads
        gap=fw*4

        pad_n=0;
        for pad_n in range(0, number_of_pads, 1):
                x0=0;
                y0=y_pad_size*pad_n+gap*pad_n;
                #left contact pad(finger part)
                idt_cell_name.add(\
                        gdspy.Rectangle(\
                                (x0,y0),\
                                (x0+x_pad_size,y0+y_pad_size-fw), 1))

                if pad_n == (number_of_pads-1):
                        #right contact pad(finger part)
                        idt_cell_name.add(\
                                gdspy.Rectangle(\
                                        (x0+x_pad_size+aperture,0),\
                                        (x0+2*x_pad_size+aperture,\
                                                y0+y_pad_size-fw), 1))

                for displacement in frange(0, finger_pairs_number-1, 1):
                        idt_cell_name.add(\
                                gdspy.Rectangle(\
                                        (x0+x_pad_size,y0+displacement*period*4),\
                                        (x0+x_pad_size+finger_l,\
                                                y0+displacement*period*4+fw),1))
                        idt_cell_name.add(\
                                gdspy.Rectangle(\
                                        (x0+x_pad_size,\
                                                y0+displacement*period*4+fw*2),\
                                        (x0+x_pad_size+finger_l,\
                                                y0+displacement*period*4+3*fw),1))

                        idt_cell_name.add(\
                                gdspy.Rectangle(\
                                        (x0+x_pad_size+finger_l2,\
                                                y0+displacement*period*4+fw*4),\
                                        (x0+x_pad_size+finger_l+finger_l2,\
                                                y0+displacement*period*4+5*fw),1))
                        idt_cell_name.add(\
                                gdspy.Rectangle(\
                                        (x0+x_pad_size+finger_l2,\
                                                y0+displacement*period*4+fw*6),\
                                        (x0+x_pad_size+finger_l+finger_l2,\
                                                y0+displacement*period*4+7*fw),1))


        return idt_cell_name


def IDT_DOUBLE_PARALLEL_NEG (idt_cell_name, period, x_pad_size, \
                                        y_pad_size,finger_lenght,number_of_pads):
        """
        Arguments:
        idt_cell_name = string, 'name of the cell'
        period = integer, the period of IDT in micro m
        x_pad_size = integer, the width of the contact pads in micro m
        y_pad_size = integer, the length of contact pads in micro m
        finger_lenght= integer, the space between the pads in micom m
        number_of_pads=integer, if you want to have more contact pads

        Return:
        idt_cell_name = cell containg the IDT
        """
```

```

        idt_cell_name = gdspy.Cell(idt_cell_name)

        period = period/2.0
        #origin of the pad
        x0=0;
        y0=0;
        #fingers width
        fw=period/4
        #space occupied by the fingers(in legth), percentage of d
        finger_l=finger_lenght-fw; ##lenght of the fingers
        finger_l2=fw; ##for the left fingers...
        #number of fingers pairs
        finger_pairs_number=(y_pad_size)/(period*2);
        #correct the y pad size to be compatible with the
        #number of fingers
        remainder = np.remainder(y_pad_size, period*2)
        if remainder == 0:
                remainder = 4
        y_pad_size =y_pad_size - remainder

        #ridefining period
        period = period/2.0
        #gap between contact pads
        gap=fw*4

        pad_n=0;
        for pad_n in range(0, number_of_pads, 1):
                x0=0;
                y0=y_pad_size*pad_n+gap*pad_n;
                if pad_n == (number_of_pads-1):
                        #left contact pad(finger part)
                        idt_cell_name.add(gdspy.Rectangle(\
                                (x0-50.e2,y0), \
                                (x0+x_pad_size,y0+y_pad_size-fw), 1))
                        #middle contact pad(finger both sides)
                        idt_cell_name.add(gdspy.Rectangle(\
                                (x0+x_pad_size+finger_lenght,- + 50.e2), \
                                (x0+x_pad_size+2*finger_lenght,\
                                        y0+y_pad_size-fw), 1))
                        #right contact pad(finger part)
                        idt_cell_name.add(gdspy.Rectangle(\
                                (x0+x_pad_size+3*finger_lenght,0), \
                                (x0+2*x_pad_size+3*finger_lenght+50.e2,\
                                        y0+y_pad_size-fw), 1))
                        #horizontal connecting line
                        idt_cell_name.add(gdspy.Rectangle(\
                                (x0-50.e2,y0-88.e2), \
                                (x0+2*x_pad_size+3*finger_lenght+50.e2,\
                                        y0+y0-78.e2), 1))
                        #left vertical pad
                        idt_cell_name.add(gdspy.Rectangle(\
                                (x0-50.e2,y0), \
                                (x0-40.e2,y0-78.e2), 1))
                        #right vertical pad
                        idt_cell_name.add(gdspy.Rectangle(\
                                (x0+2*x_pad_size+3*finger_lenght+40.e2,y0), \
                                (x0+2*x_pad_size+3*finger_lenght+50.e2,\
                                        y0-78.e2), 1))

                for displacement in frange(0, finger_pairs_number-1, 1):
                        #left IDT, left fingers
                        idt_cell_name.add(gdspy.Rectangle(\
                                (x0+x_pad_size,y0+displacement*period*4), \
                                (x0+x_pad_size+finger_l,\
                                        y0+displacement*period*4+fw), 1))
                        #left IDT, left fingers
                        idt_cell_name.add(gdspy.Rectangle(\
                                (x0+x_pad_size,y0+displacement*period*4+fw*2), \
                                (x0+x_pad_size+finger_l,\
                                        y0+displacement*period*4+3*fw), 1))
                        #left IDT, right fingers
```

```
                        idt_cell_name.add(gdspy.Rectangle(\
                                (x0+x_pad_size+finger_l2,\
                                        y0+displacement*period*4+fw*4), \
                                (x0+x_pad_size+finger_l+finger_l2,\
                                        y0+displacement*period*4+5*fw), 1))
                        #left IDT, right fingers
                        idt_cell_name.add(gdspy.Rectangle(\
                                (x0+x_pad_size+finger_l2,\
                                        y0+displacement*period*4+fw*6), \
                                (x0+x_pad_size+finger_l+finger_l2,\
                                        y0+displacement*period*4+7*fw), 1))
                        #right IDT, left fingers
                        idt_cell_name.add(gdspy.Rectangle(\
                                (x0+x_pad_size+2*finger_lenght,\
                                        y0+displacement*period*4), \
                                (x0+x_pad_size+2*finger_lenght+finger_l,\
                                        y0+displacement*period*4+fw), 1))
                        #right IDT, left fingers
                        idt_cell_name.add(gdspy.Rectangle(\
                                (x0+x_pad_size+2*finger_lenght,\
                                        y0+displacement*period*4+fw*2), \
                                (x0+x_pad_size+2*finger_lenght+finger_l,\
                                        y0+displacement*period*4+3*fw), 1))
                        #right IDT, left fingers
                        idt_cell_name.add(gdspy.Rectangle(\
                                (x0+x_pad_size+2*finger_lenght+finger_l2,\
                                        y0+displacement*period*4+fw*4), \
                                (x0+x_pad_size+3*finger_lenght,\
                                        y0+displacement*period*4+5*fw), 1))
                        #right IDT, left fingers
                        idt_cell_name.add(gdspy.Rectangle(\
                                (x0+x_pad_size+2*finger_lenght+finger_l2,\
                                        y0+displacement*period*4+fw*6), \
                                (x0+x_pad_size+3*finger_lenght,\
                                        y0+displacement*period*4+7*fw), 1))
        return idt_cell_name


def IDT_DOUBLE_SERIE_NEG (idt_cell_name, period, x_pad_size,\
                                y_pad_size,aperture,number_of_pads):
        """
        Arguments:
        idt_cell_name=string, 'name of the cell'
        period=integer, the period of IDT in micro m
        x_pad_size = integer, the width of the contact pads in micro m
        y_pad_size = integer, the length of contact pads in micro m
        aperture= integer, the space between the pads in micom m
        number_of_pads=integer, if you want to have more contact pads
        Return:
        idt_cell_name = cell containg the IDT
        """
        idt_cell_name = gdspy.Cell(idt_cell_name)
        period = period/2.0
        period_spacing = period

        #origin of the pad
        x0=0;
        y0=0;
        #fingers width
        fw=period/4
        #space occupied by the fingers(in legth), percentage of d
        finger_l=aperture-fw; ##lenght of the fingers
        finger_l2=fw; ##for the left fingers...
        #number of fingers pairs
        finger_pairs_number=(y_pad_size)/(period*2);
        remainder = np.remainder(y_pad_size, period*2)
        if remainder == 0:
                remainder = 4
        y_pad_size =y_pad_size - remainder

        y0list = [0, y_pad_size]

```

```
        #ridefining period
        period = period/2.0
        #gap between contact pads
        gap=fw*4
        for y0 in y0list:
                pad_n=0;
                x0=0;
                y0=y0 + y_pad_size*pad_n+gap*pad_n;
                if y0 != 0: #top idt

                                #left contact pad(finger part)
                                idt_cell_name.add(\
                                        gdspy.Rectangle(\
                                                (x0,y0),\
                                                (x0+x_pad_size,y0+y_pad_size-fw),\
                                                1))
                                #get away from active area(left)
                                idt_cell_name.add(\
                                        gdspy.Rectangle(\
                                                (x0,y0),\
                                                (x0+10.e2,y0-30.e2), 1))

                                if pad_n == (number_of_pads-1):
                                        #right contact pad(finger part)
                                        idt_cell_name.add(\
                                                gdspy.Rectangle(\
                                                     (x0+x_pad_size+aperture,y0),\
                                                     (x0+2*x_pad_size+aperture,\
                                                                y0+y_pad_size-fw),\
                                                                1))
                                        #get away from active area(right)
                                        idt_cell_name.add(\
                                                gdspy.Rectangle(\
                                                        (x0+2*x_pad_size+\
                                                                aperture-10.e2,y0),\
                                                        (x0+2*x_pad_size+aperture,\
                                                                y0-30.e2),\
                                                                1))
                else: #bottom idt

                                #left vertical pad(finger part)
                                idt_cell_name.add(\
                                        gdspy.Rectangle(\
                                                (x0+x_pad_size-10.e2,\
                                                        y0+y_pad_size-fw-10.e3),\
                                                (x0+x_pad_size,y0+y_pad_size-fw)\
                                                        , 1))
                                if pad_n == (number_of_pads-1):
                                        #right vertical pad(finger part)
                                        idt_cell_name.add(\
                                                gdspy.Rectangle(\
                                                        (x0+x_pad_size+aperture,\
                                                                y0+y_pad_size-\
                                                                        fw-10.e3),\
                                                        (x0+x_pad_size+\
                                                                aperture+10.e2,\
                                                                y0+y_pad_size-fw),\
                                                                1))
                                #left horizontal line(no finger part)
                                idt_cell_name.add(\
                                        gdspy.Rectangle(\
                                                (x0,y0-10.e3),\
                                                (x0+x_pad_size,\
                                                        y0+y_pad_size-fw-10.e3), \
                                                        1))

                                #right horizontal line(no finger part)
                                idt_cell_name.add(\
                                        gdspy.Rectangle(\
                                                (x0+x_pad_size+aperture,y0-10.e3),\
                                                (x0+2*x_pad_size+aperture,\
                                                        y0+y_pad_size-fw-10.e3), 1))
```

```
                #fingers
                for displacement in frange(0, finger_pairs_number-1, 1):
                        idt_cell_name.add(\
                                gdspy.Rectangle(\
                                        (x0+x_pad_size,y0+displacement*period*4),\
                                        (x0+x_pad_size+finger_l,\
                                                y0+displacement*period*4+fw),1))
                        idt_cell_name.add(\
                                gdspy.Rectangle(\
                                        (x0+x_pad_size,\
                                                y0+displacement*period*4+fw*2),\
                                        (x0+x_pad_size+finger_l,\
                                                y0+displacement*period*4+3*fw),1))

                        idt_cell_name.add(\
                                gdspy.Rectangle(\
                                        (x0+x_pad_size+finger_l2,\
                                                y0+displacement*period*4+fw*4),\
                                        (x0+x_pad_size+finger_l+finger_l2,\
                                                y0+displacement*period*4+5*fw),1))
                        idt_cell_name.add(\
                                gdspy.Rectangle(\
                                        (x0+x_pad_size+finger_l2,\
                                                y0+displacement*period*4+fw*6),\
                                        (x0+x_pad_size+finger_l+finger_l2,\
                                                y0+displacement*period*4+7*fw),1))


        return idt_cell_name
```

Example

```
#!/usr/bin/python

import gdspy
from idt_lib2 import *


print('Using gdspy module version ' + gdspy.__version__)

#       UNIT AND PRECISION
unit1=1.e-06;        ##units(micrometer), by default is meter
precision1=1.e-9;  ##precision(nanometer), by default is meter

#       CREATION OF A CELL THAT CONTAINS EVERYTHING
ALL_cell = gdspy.Cell('ALL')

#       Define parameters for IDT
period = 4.0
x_pad = 10.e2
y_pad_size = 35.e1
finger_length = 1.e3

IDT_1 = IDT_DOUBLE_PARALLEL_NEG('IDT4_cell', period, x_pad, \
        y_pad_size, finger_length, 1)
IDT_2 = IDT_DOUBLE_PARALLEL_NEG('IDT4_2', period, x_pad, \
        y_pad_size, finger_length, 1)

#       HERE I COMPOSE THE FINAL DRAW
dist = 2.e3
ALL_cell.add(gdspy.CellReference(IDT_1, (0, 0), rotation=0))
ALL_cell.add(gdspy.CellReference(IDT_2, (3*x_pad+finger_length, \
        dist+y_pad_size*2), rotation=180))
## ------------------------------------------------------------------ ##
##      OUTPUT
## ------------------------------------------------------------------ ##

## Output the layout to a GDSII file (default to all created cells).
## Set the units we used to micrometers and the precision to nanometers.
```

```
gdspy.gds_print('parallel_aperture_1mm_length_'+str(int(y_pad_size))+\
        '.gds', unit=unit1, precision=precision1)

## ------------------------------------------------------------------ ##
##      VIEWER
## ------------------------------------------------------------------ ##
## View the layout using a GUI.  Full description of the controls can
## be found in the online help at http://gdspy.sourceforge.net/
gdspy.LayoutViewer()
```

Appendix C

Python module for voltage scan analysis

This Python class is used to analyze the voltage scan with a SAW device. For a definition of a voltage scan see section 2.5. The class was tested with voltage scans where the m=0 order is always the most intense, even though it should work for a any voltage scan. Before using the class for evaluation one array containing the angles that have been scanned must be saved in a folder call *intermediate* as *SampleName_extracted_th.dat*, and the diffraction pattern should be saved in a file containing a matrix whose column represent each individual scan, with the name *SampleName_extracted_int.dat*. Once this is done the voltage scan object can be declared specifying the name of the sample *vs = voltage_scan('SampleName')*. The data can be normalized with *vs.normalize()*. This normalizes the Bragg peak with 0 V to one, and all the other scan consequently. When we apply a voltage to a SAW device, this creates stress and strain in the crystal, and the sample bends. This may lead to a small shift in the position of the rocking curve, this can be calculated with *vs.find_shift()*. If the Bragg peak is not the most intense, the method will not find the correct shift, and it is therefore necessary to either create an array by hand, or to implement some other method. All the maxima in each scan can be found with *vs.find_maxima()* and are saved in the intermediate folder. The scan can be fit through the *vs.fit_voltage_scan(self, delta_theta, show_plot)* method. The parameter *delta_theta* is the angular distance between maxima. This method does not guarantee exact results as it is. It might be necessary to change the fit routine depending on how many satellites appear in the diffraction pattern. It is implemented to be used with diffraction pattern with up to the m=±4 diffraction satellites. Finally the method *vs.intensity_vs_voltage(self,V_in,V_fin,V_step,show_plot)* can be used to produce a plot like the one in Fig. 3.17.

```python
#!/usr/bin/env python


import numpy as np
import numexpr as ne
import matplotlib.pyplot as plt
import pylab as plb
from scipy.optimize import curve_fit
from scipy.optimize import least_squares
import time
import matplotlib.colors as colors
import sys, os, re
sys.path.append('specscan')
import specscan as specscan
import string
from analysis_lib import *



```

```python

class extract_data():
        '''
        This class is used to extract data from specfiles.
        It uses the specfile class, writte by Ivo Zizak.

        Arguments:
        sample= string, the name of the sample
        first/last _scan= integers, first and last scan to be analyzed
        V_step = integer, the voltage step between two scans
        dir = string, the position of the data and name of the specfile
        x,y = strings, name of the motor used for the scan, and of the detector
        '''

        def __init__(self, sample, first_scan, last_scan, V_step, dir, x, y):
                self.sample = sample
                self.fs = first_scan
                self.ls = last_scan
                self.V_step = V_step
                self.dir = dir
                self.x = x
                self.y = y
                if not os.path.exists('intermediate'):
                        os.mkdir('intermediate')
        def voltage_array(self):
                '''
                Return:
                voltage = array, the voltages used to excite SAW
                '''
                V_fin = (self.ls-self.fs)*self.V_step
                voltage = np.arange(0, V_fin+self.V_step, self.V_step)
                np.savetxt('intermediate/'+self.sample+'_voltage.dat', voltage,\
                        fmt='%.18e', delimiter=' ', newline='\n')
                return voltage

        def extract_spec(self):
                '''
                This method extract the selected scan from a .spec file.

                Return:
                intensity_all = matrix, each column is a voltage scan
                theta = array,  angular position
                intensity_all and voltage are saved in the intermediate folder.
                '''
                spec=specscan.SpecFile(self.dir)
                for i in range(self.fs,self.ls):
                        print 'i', i
                        a=spec.get_scan_num(i)
                        #print 'a', a
                        if i == self.fs:
                                theta = a.data[self.x]
                        intensity = a.data[self.y]
                        try:
                                intensity_all = np.concatenate(\
                                (intensity_all,intensity), axis=0)

                        except NameError :
                                intensity_all = intensity
                intensity_all = intensity_all.reshape(\
                        (self.ls-self.fs,intensity.size))
                np.savetxt('intermediate/'+self.sample+'_extracted_int.dat', \
                        intensity_all, fmt='%.18e', delimiter=' ', newline='\n')
                np.savetxt('intermediate/'+self.sample+'_extracted_th.dat',\
                        theta, fmt='%.18e', delimiter=' ', newline='\n')
                return intensity_all.reshape((self.ls-self.fs,intensity.size)),\
                        theta

class voltage_scan():
        '''
        This class was tested only with data from sample where the 0-th order
        is always the stronger in the diffraction pattern.

```

```
        Arguments:
        sample = string, sample name
        '''
        def __init__(self, sample):
                self.sample = sample
                if not os.path.exists('intermediate'):
                        os.mkdir('intermediate')

                #loading the intensity and theta files
                self.theta = np.loadtxt(\
                        'intermediate/'+self.sample+'_extracted_th.dat')
                self.intensity = np.loadtxt(\
                        'intermediate/'+self.sample+'_extracted_int.dat')

        def normalize(self):
                '''
                This method normalize the previously extracted scan to one

                Return:
                intensity = matrix, each column is a scan, normalized to one
                '''
                first = self.intensity[0,:]
                max_int = np.amax(first)
                self.intensity = self.intensity/max_int
                np.savetxt('intermediate/'+self.sample+\
                        '_normalized_intensity.dat', self.intensity)
                print 'hi', self.intensity.shape
                return self.intensity

        def find_shift(self):
                '''
                Voltage scan shift due to surface bending of the sample when voltage
                is applied. This method measure the shift between the scan

                Return:
                shift = array, each each value correspond to the shift of the
                        corresponding scan
                '''
                first = self.intensity[0,:]
                max_th = np.argmax(first)
                shift = []
                for m in range(0,self.intensity.shape[0]):
                        mth = first = self.intensity[m,:]
                        maxm = np.argmax(mth)
                        shift.append(self.theta[maxm] - self.theta[max_th])
                np.savetxt('intermediate/'+self.sample+'_shift.dat', shift)
                return shift

        def find_maxima(self, plot):
                '''
                This method find all the maxima in the scan, a maxima is a point
                standing of minimum delta (set to 0.01)
                '''
                self.plot = plot
                delta = 0.01
                start = self.theta[0]
                stop = self.theta[len(self.theta)-1]
                step = (stop-start)/len(self.theta)
                shift = np.loadtxt('intermediate/'+self.sample+'_shift.dat')
                for m in range(0,self.intensity.shape[0]):
                        maxtab, mintab = peakdet(self.intensity[m,:],delta)
                        #~ print 'run', m
                        plt.figure(m)
                        #sel_max_x = theta[int(maxtab[:,0])]
                        sel_max_x = start + maxtab[:,0]*step
                        #~ print 'x', sel_max_x
                        sel_max_y = maxtab[:,1]
                        #~ print 'y', sel_max_y
                        #~ print sel_max_y

                        #saving the maxima to files
                        np.savetxt('intermediate/'+self.sample+'_int_max_'+\
```

```
                str(m*10)+' V'+'.dat', sel_max_y)
            np.savetxt('intermediate/'+self.sample+'_th_max_'+str(m*10)\
                +' V'+'.dat', sel_max_x)
            if self.plot == 1:
                plt.figure(m+100)
                plt.plot(sel_max_x-shift[m], sel_max_y, 'ko',\
                    label = 'maxima')
                plt.plot(self.theta-shift[m] , self.intensity[m,:],\
                    label = str(m*10)+' V')
                plt.title(str(m*10)+' V')
                plt.savefig('intermediate/'+self.sample+'_'\
                    +str(m*10)+' V'+'.pdf')
                plt.savefig('intermediate/'+self.sample+'_'\
                    +str(m*10)+' V'+'.png')
                plt.legend()
        #~ if self.plot == 1:
            #~ plt.show()
        #~ plt.clf()

    def fit_voltage_scan(self, delta_theta, show_plot):
        '''
        This methods works only if the data have been normalized,
        the shift has been calculated, and the maxima have been found

        Arguments:
        delta_theta= float, the distance between two satellites
        show_plot = 0/1, 0--no plot, 1--plot.
        '''
        self.delta_theta = delta_theta
        self.show_plot = show_plot
        #~ fitting the V=0 scan, just to find initial parameters for the fit
        intensity = self.intensity[0,:] #selecting the first scan, V=0
        mean = self.theta[np.argmax(intensity)]
        idx = (np.abs(intensity-0.5)).argmin()
        fwhm = 2*np.abs(mean - self.theta[idx])
        #~ print 'mean', mean
        guess_all = [0,0,0,0,1,0,0,0,0, mean, self.delta_theta*4,\
            self.delta_theta*3, self.delta_theta*2,
        self.delta_theta*1, self.delta_theta*1, self.delta_theta*2,\
            self.delta_theta*3, self.delta_theta*4, fwhm/2.35,fwhm/2.35]
        shift = np.loadtxt('intermediate/'+self.sample+'_shift.dat')
        m0 = []
        m1 = []
        m2 = []
        m3 = []
        m4 = []
        for m in range(0,self.intensity.shape[0]):
            #~ creating an array for plotting
            xplot = np.arange(self.theta[0],\
                self.theta[len(self.theta)-1]+shift[m], 0.00001)
            x = self.theta - shift[m] #shifting the array to be centered
            xplot = xplot - shift[m]  #shifting the array for plotting
            intensity = self.intensity[m,:] #select m-th scan to fit
            #loading the max in th and intensity
            max_int = np.loadtxt('intermediate/'+self.sample+\
                '_int_max_'+str(10*10)+' V'+'.dat')
            max_th = np.loadtxt('intermediate/'+self.sample+\
                '_th_max_'+str(10*10)+' V'+'.dat')
            #~ calculating the mean to guess it for the fit
            mean = max_th[np.argmax(max_int-1)] - shift[m]
            #~ FITTING
            [amp4l,amp3l, amp2l, amp1l,amp,amp1r,amp2r,amp3r,amp4r,\
                mean,c1,c2,c3,c4,c6,c7,c8,c9, sigma0, sigma],\
                    pcov=curve_fit(gaus9_all_2sigma, x,\
                        intensity, guess_all)
            #~ Updating guess for the next iteration
            guess = [amp4l,amp3l, amp2l, amp1l,amp,amp1r,amp2r,\
                amp3r,amp4r,mean,c1,c2,c3,c4,c6,c7,c8,c9,sigma0,\
                    sigma]
            #~ Plotting the results of the fit with the data
            plt.figure(m)
            plt.title(str(m*10)+' V')
```

```
                        plt.plot(xplot, gaus9_all_2sigma(xplot, amp4l,amp3l, amp2l,\
                                amp1l,amp,amp1r,amp2r,amp3r,amp4r,mean,c1,c2,c3,\
                                        c4,c6,c7,c8,c9,  sigma0, sigma), 'r',\
                                                label = 'gaussian fit')
                        plt.plot(x , self.intensity[m,:], label = str(m*10)+' V')
                        #~ Saving the values of the fit
                        m0.append(amp)
                        m1.append((amp1l+amp1r)/2)
                        m2.append((amp2l+amp2r)/2)
                        m3.append((amp3l+amp3r)/2)
                        m4.append((amp4l+amp4r)/2)
                        np.savetxt('intermediate/'+self.sample+'_m'+str(m*10)+\
                                '_par.txt',(amp4l,amp3l, amp2l, amp1l,amp,amp1r,\
                                amp2r,amp3r,amp4r,mean,c1,c2,c3,c4,c6,c7,c8,c9,\
                                        sigma0,sigma))
                        guess = [amp4l,amp3l, amp2l, amp1l,amp,amp1r,amp2r,amp3r,\
                                amp4r,mean,c1,c2,c3,c4,c6,c7,c8,c9,sigma0,sigma]

                np.savetxt('intermediate/'+self.sample+'_m0.dat', m0)
                np.savetxt('intermediate/'+self.sample+'_m1.dat', m1)
                np.savetxt('intermediate/'+self.sample+'_m2.dat', m2)
                np.savetxt('intermediate/'+self.sample+'_m3.dat', m3)
                np.savetxt('intermediate/'+self.sample+'_m4.dat', m4)
                #~ if self.show_plot == 1:
                        #~ plt.show()
                #~ plt.clf()

        def intensity_vs_voltage(self, V_in, V_fin,V_step,show_plot):
                '''
                This method produces the plot of the intensity of the satellites
                vs the voltage applied.

                Arguments:
                V_in/_fin/_step: integers, initial and final voltage of the scan,
                                        and the voltage step
                show_plot = 0/1, 0--no plot, 1--plot.
                '''
                self.V_in = V_in
                self.V_fin = V_fin
                self.V_step = V_step
                self.show_plot = show_plot
                voltage = np.arange(self.V_in,self.V_fin+1,self.V_step)

                m0 = np.loadtxt('intermediate/'+self.sample+'_m0.dat')
                m1 = np.loadtxt('intermediate/'+self.sample+'_m1.dat')
                m2 = np.loadtxt('intermediate/'+self.sample+'_m2.dat')
                m3 = np.loadtxt('intermediate/'+self.sample+'_m3.dat')
                m4 = np.loadtxt('intermediate/'+self.sample+'_m4.dat')
                #plotting
                fig = plt.figure(1000)
                ax = fig.add_subplot(111)
                ax.plot(voltage,m0, 'ro', label = 'm=0')
                ax.plot(voltage,m1, 'bo', label = 'm=1')
                ax.plot(voltage,m2, 'go', label = 'm=2')
                ax.plot(voltage,m3, 'mo', label = 'm=3')
                ax.plot(voltage,m4, 'co', label = 'm=4')
                plt.setp(ax.get_xticklabels(), visible=False)
                plt.legend()
                plt.title('Intensity/Voltage')
                plt.xlabel('Voltage [V]')
                plt.ylabel('intensity [a.u.]')
                plt.savefig('intermediate/'+self.sample+'_voltage_orders.png')
                #~ if self.show_plot == 1:
                        #~ plt.show()
                #~ plt.clf()



########################
#FUNCTIONS TO TEST THE CLASSES#
########################
def test_extract_data():
```

```python
        print 'Testing the class extract_from_spec'
        dir = 'data/2017-05-18_sample_M1_01.spec'
        extracted = extract_data('test',1,12,10,dir,'eta', 'cyber')
        intensity_all, th = extracted.extract_spec()
        print 'test complete'

def test_voltage_scan():
        print 'Testing the class voltage_scan'
        vs = voltage_scan('test')
        i = vs.normalize()
        shift = vs.find_shift()
        vs.find_maxima(plot = 1)
        vs.fit_voltage_scan(delta_theta = 0.004, show_plot = 0)
        vs.intensity_vs_voltage(0,100,10, show_plot = 0)
        plt.show()
        print 'test complete'


if __name__ == "__main__":
        test_extract_data()
        test_voltage_scan()
```

Appendix D

Python module for delay scan analysis

Analyzing the data manually is, in many circumstances, a slow, tedious and not accurate procedure. We scanned a delay of 1000 ns, taking on picture each ns. We collected in total 10 scans. Therefore I implemented a class in Python that automatize most of data analysis the process. First of all it is important to define what kind of data one can pass to the class, and there are two possibilities. The first one is to start with the *TIFF* file of the measurements. In our specific case we used a 2D detector, a CCD camera with 1368×1040 pixels. To each pixel was assigned a value between 0 and 256. The Bragg peak and the diffraction satellites lie in a very small region, of approximately 50×100 pixels. It is important, before feeding the *TIFF* files to the class, to open the data with an image processing program like ImageJ (or Fiji, a 'batteries included' distribution of ImageJ), and individuate the areas where there are the diffraction orders, surrounded by the black rectangles in Fig. D.1a, and write down the coordinates of the bottom left (x_1, y_1) and top right ($x_,y_2$) corner. This is not mandatory, the program is able to find on its own the area where there is an intensity modulation due to the diffraction orders, at cost of a very long computation time. Once the region of interest are set via the method *set_region(x1, x2, y1, y2, label)*, where *label* is a string that must be used to specify which diffraction order is being extracted, the delay scans can be extracted with the method *tiff_extract_n_scans()*. The method returns a matrix where each column is associated with a delay scan of a certain pixel in the region of interest. A delay scan where the intensity is modulated by a diffraction order, will have a shape as the one depicted Fig. D.1b. The user should select an appropriate rejection value via the method *set_rejection(rejection)*. This may vary depending on a number of factor, like the detector used, the noise, and beam parameters, therefore is given the possibility to vary it manually. The *select_good_scans(intensity, plot)* is used to select only the delay scan with a shape like in D.1b, and it returns the average of the selected scans. Since the measurements were noisy, a method to smooth the data was implemented. The *smooth(intensity)* method performs a simple moving average, an unweighted mean of the previous *n* data. The number of data points to average is set with the *set_Nsm(Nsm)* method. In our case the original data set showed an increasing intensity during the scan that is not related with the effect we were interested in. Thus the method *norm_line(delay, intensity)* have been defined. This average the value of the first and last five points of the delay scan, calculates a straight line that passes through this two points and normalize the scan to it. The scan can be further normalized to one with the *norm(delay, intensity)* method. To estimate the FWHM at the edges the intensity scan must be derived with the *derive(intensity)* method and then passed to *estimate_edge(delay, intensity_der, plot)*. To estimate the FWHM of the single bunch the *estimate_single_bunch(delay, intensity,left_edge, right_edge, fwhm,* *shift, plot)* can be used. Beyond the delay and intensity arrays, this method requires three more important parameter, the position of the falling and rising edges and the expected FWHM of the single bunch (the FWHM of the single bunch is similar to the FWHM of the peaks resulting from the edges in the derived intensity scan). Finally the whole scan can be fit via the *fit_delay_scan(delay, intensity, plot)* method once the proper initial parameters for the fit have been set via the method *set_fit_delay_scan_parameter(mean_l, mean_r, mean_sb, amp_sb, fwhm)*.

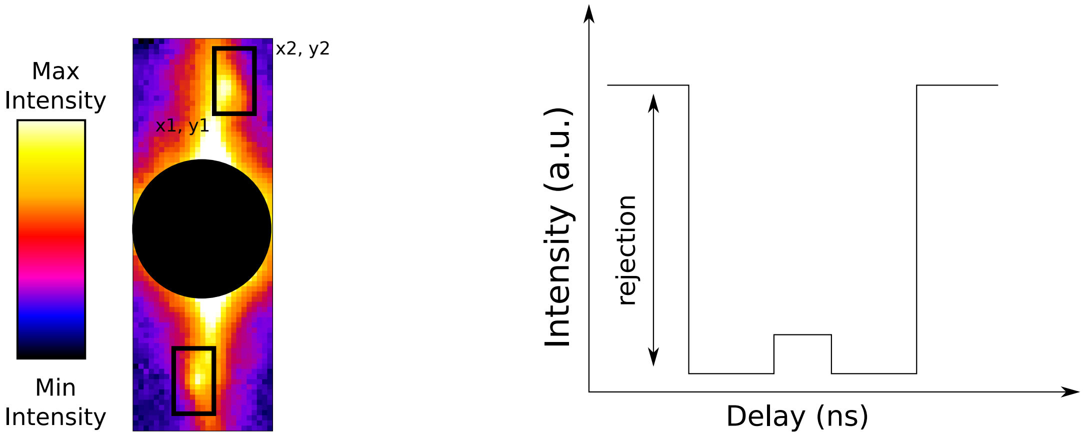

(A) (B)

FIGURE D.1: **A**: the experimental image **B** the kind of plot expected

```
import numpy as np
import matplotlib.pyplot as plt
from scipy.optimize import curve_fit
import os
from lib import *



class time_resolved_analysis():
        '''
        This class provides methods to do a complete analysis of pulse
        picker. The raw data consists of tif files. One scan consists of several
        .tif files recorded at different delay. In the example there are 10 scans,
        each one consisting of 1001 picture. The Tiff files to be analyzed must
        be in the data folder.

        Arguments:
        sample = string, the name of the sample
        pic_name = string,  'the name of the tif image without the number'
        first_im = int, number of the first image to analyze
        n_scans = int, number of stacks(number of scans)'''

        def __init__(self, sample, pic_name, first_im, scan_length, n_scans,\
                                pixel = 3):

                self.sample = sample
                self.pic_name = pic_name
                self.first_im = first_im
                self.scan_length = scan_length
                self.n_scans = n_scans
                #variables that will be defined later
                self.pixel = None
                self.xpix_in = None
                self.xpix_fin= None
                self.ypix_in = None
                self.ypix_fin = None
                self.up_down = None
                self.rejection = None
```

```

                if not os.path.exists('intermediate'):
                        os.mkdir('intermediate')
                return

        def set_region(self, x1, x2, y1, y2, label):
                '''
                Set the region of the image to be analyzed. This is a rectangle
                with one corner in (x1,y1) and (x2,y2)

                Arguments:
                x1 = integer, bottom left corner
                y1 = integer, bottom left corner
                x2 = integer, top right corner
                y2 = integer, top right corner
                '''
                self.xpix_in = x1
                self.xpix_fin = x2
                self.ypix_in = y1
                self.ypix_fin = y2
                self.up_down = label

        def set_rejection(self, rejection):
                '''
                Set the rejection value.

                Arguments:
                rejection= integer, rejection value
                '''
                self.rejection = rejection
        def set_Nsm(self, Nsm):
                '''
                Set number of consecutive points to average to smooth the data.

                Arguments:
                Nsm = integer
                '''
                self.Nsm = Nsm

        def create_name_array(self):
                '''
                Creates an array with the names of all the tiff files
                used for n scans. At the moment this method is not used by other
                classes, this will be implemented in future.
                '''
                file_names = []
                for m in range(0,self.n_scans):
                        for i in range(0, self.scan_length):
                                num = str((m*self.scan_length)+(self.first_im+i))
                                file_names.append(self.pic_name+num+'.tif')
                return file_names


        def tiff_extract_n_scans(self):
                '''
                Read n_scans composed  of scan_length tif files and
                extract the values of certain pixels and saves them in matrix.
                One needs to set the region with the set_region method

                Return:
                intensity_all = matrix, each column is one delay scan
                '''



                dir = 'data/'
                #coordinates of the pixel to analyze

                dx = self.xpix_fin - self.xpix_in + 1
                dy = self.ypix_fin - self.ypix_in + 1

```

```
        #declare two zeros array for later
        delay= np.zeros(self.scan_length)
        intensity= np.zeros(shape=(self.scan_length, dx*dy+1))
        for m in range(0,self.n_scans):
            for i in range(0, self.scan_length):
                num = str((m*self.scan_length)+(self.first_im+i))
                delay[i] = i
                im = Image.open(dir + self.pic_name+num+'.tif')
                pix = im.load()
                pos=0
                for x in range(self.xpix_in, self.xpix_fin+1):
                    for y in range(\
                    self.ypix_in,self.ypix_fin+1):
                        intensity[i,pos] = pix[x,y]
                        pos = pos +1
            try:
                intensity_all
            except NameError:
                print "extracted scan number 1"
                intensity_all = intensity
            else:
                print "extracted scan number", m+1
                intensity_all = np.concatenate(\
                            (intensity_all, intensity),\
                                axis=1)
        imarray = np.array(im)


        np.savetxt('intermediate/'\
            +self.sample+'_'+self.up_down+'_imarray.txt', (imarray))
        np.savetxt('intermediate/'\
            +self.sample+'_'+self.up_down+'_intensity.txt',\
                (intensity_all))
        return intensity_all#, imarray


    def select_good_scans(self, intensity, plot ):
        '''This method provides an easy way to differ between pixel scans.
        It differs between the pixels hit by the plus minus first order and
        the others. It return one single scan, which is the average of the
        selected scans.

        Arguments:
        file_names =  list of strings, the name of the images to be analyzed
                             this is still not used at the moment
        intensity = matrix, containing delay scans in column
        plot = 0/1, 0--no plot, 1--plot.

        Return:
        intensity = array, average of the selected delay scan
        '''
        self.intensity = intensity

        if self.rejection == None:
            sys.exit("Please define the rejection with set_rejection()")

        dx = self.xpix_fin - self.xpix_in + 1
        dy = self.ypix_fin - self.ypix_in + 1
        x_pas = np.zeros(dx*dy*(self.n_scans+1))
        y_pas = np.zeros(dx*dy*(self.n_scans+1))
        x_rej = np.zeros(dx*dy*(self.n_scans+1))
        y_rej = np.zeros(dx*dy*(self.n_scans+1))

        i_pas = 0
        i_rej = 0
        rej=0

        for i in range(0,dx*dy*(self.n_scans)):
            l_av = np.average(self.intensity[[0,5], i])
            c_av = np.average(self.intensity[\
                [self.scan_length/2-100,self.scan_length/2+100], i])
            r_av= np.average(self.intensity[\
```

```python
                [self.scan_length-6,self.scan_length-1], i])
            if l_av - c_av>self.rejection and \
                r_av - c_av>self.rejection and \
                np.amin(self.intensity[:, i])>100 and \
                np.amax(self.intensity[:, i])<500:
                    try:
                        intensity_sum
                    except NameError:
                        intensity_sum = self.intensity[:, i]
                        x_pas[0] = self.xpix_in+int(i)/dy
                        y_pas [0] = self.ypix_in+int(i)%dy
                        pas = 1

                    else:
                        intensity_sum=(self.intensity[:,i]\
                            + intensity_sum)
                        x_pas[pas] = self.xpix_in+int(i)/dy
                        y_pas [pas] = self.ypix_in+int(i)%dy
                        pas = pas + 1

            else:
                x_rej[rej] = self.xpix_in + i / dy
                y_rej [rej] = self.ypix_in + i % dy
                rej = rej+1

        intensity_sum = intensity_sum / len(x_pas)
        x_pas_short = x_pas[0:pas]
        y_pas_short = y_pas[0:pas]
        x_rej_short = x_rej[0:rej]
        y_rej_short = y_rej[0:rej]
        print '#################################'
        print 'selecting scans '+ self.up_down
        print 'rejected', rej
        print 'passed', pas
        print '#################################'
        np.savetxt('intermediate/'+self.sample+'_'+self.up_down+\
            '_selected_intensity.txt', (intensity_sum))
        if plot == 1:
            plt.figure(1)
            plt.title('Average of good scans '+self.up_down)
            plt.plot(intensity_sum[0: self.scan_length])
            plt.show()
        return  intensity_sum

    def smooth(self, intensity):
        '''This method provides an easy way to smooth the data.
        The data points of a signal are modified so that individual points
        (presumably because of noise) are reduced, and points that are
        lower than the adjacent points are increased leading to a
        smoother signal. Set the Nsm via the set_Nsm before using
        this method.

        Arguments:
        intensity =array, scan to smooth

        Return:
        delay_smooth = array, arbitrary delay array useful to plot the data
        intensity_smooth = array, the smoothed delay scan
        '''
        self.intensity = intensity

        delay_smooth = np.zeros(len(self.intensity)/self.Nsm+1)
        intensity_smooth = np.zeros(len(self.intensity)/self.Nsm+1)

        for x in range(0,len(self.intensity)):
            delay_smooth[int(x/self.Nsm)] = int(x)
            intensity_smooth[int(x/self.Nsm)] += self.intensity[x]

        np.savetxt('intermediate/'+self.sample+'_intensity_smooth.txt',\
            intensity_smooth)
        np.savetxt('intermediate/'+self.sample+'_delay_smooth.txt',\
            delay_smooth)
```

```
                return delay_smooth[0:len(delay_smooth)-1],\
                           intensity_smooth[0:len(delay_smooth)-1]

        def norm_line(self, delay, intensity):
                '''
                Original dataset shows an increasing amplitude during the scan
                that is not related width the effect we want to observe. Here are
                normalized: averaging five points to the left and 5 to the right
                and drawing a line

                Arguments:
                delay = array, the delay relative to intensity
                intensity, array, the scan to normalize with a line

                Returns:
                delay = array, delay as input
                intensity= array, delay scan normalized
                '''

                self.delay = delay
                self.intensity = intensity

                #calculating the line
                left_av = np.average(self.intensity[0:self.Nsm/3])
                right_av = np.average(self.intensity[-self.Nsm/3:-1])
                norm_line = left_av + (right_av-left_av)/\
                                        (len(self.delay)*self.Nsm)*self.delay

                #correcting for the pendenza della retta
                self.intensity = self.intensity/norm_line

                #shifting to zero
                self.intensity = self.intensity-np.amin(self.intensity)
                #print 'ss max', np.amin(ss)


                return self.delay, self.intensity

        def norm(self, delay, intensity):
                '''This class normalize an array scan to one.

                Arguments:
                delay = array, the delay relative to intensity
                intensity, array, the scan to normalize to one

                Returns:
                delay = array, delay as input
                intensity= array, delay scan normalized to oen
                '''

                self.delay = delay
                self.intensity = intensity

                #normalizing to 1
                self.intensity = self.intensity/np.amax(self.intensity)
                np.savetxt('intermediate/'+self.sample+'_intensity_norm.txt',\
                        self.intensity)

                return self.delay, self.intensity

        def derive(self, intensity):
                '''this method provides an easy way to derive a data set


                Arguments:
                intensity = array, the array to derive

                Return:
                intensity_der: array, derived array (also saved in intermediate)
                '''
                self.intensity = intensity
                intensity_der = np.empty(len(self.intensity))
```

```
                for x in range(1,len(self.intensity)):
                #for x in smooth:
                        #~ print 'x', x
                        #~ print self.intensity[x]
                        #~ print self.intensity[x-1]
                        #~ print self.intensity[x]-self.intensity[x-1]
                        intensity_der[x] = self.intensity[x]-self.intensity[x-1]
                #~ print sder
                np.savetxt('intermediate/'+self.sample+'_intensity_derived.txt',\
                                intensity_der)
                return intensity_der[1:len(intensity_der)+2]

        def estimate_edge(self, delay, intensity_der, plot):
                '''
                This method provides an easy way to fit the edges.
                If used to fit the delay scan, this has to be derived.

                Arguments:
                delay = array, the delay relative to intensity_der
                intensity_der = array, the intensity scan derived
                plot = 0/1, 0--no plot, 1--plot.

                Return:
                mean_l, fwhm_l =  float, position and the fwhm of the left edge
                mean_r, fwhm_r = float, position and the fwhm of the right edge
                the method returns the position and the fwhm of the left and right
                edge.

                It saves the parameters and the pcov matrix resulting from the fit
                in the
                intermediate folder
                '''
                self.delay = delay[1:len(delay)] #derived array has one less value
                self.intensity_der = intensity_der
                self.plot = plot

                #LEFT PEAK
                x_l = self.delay[0:len(self.delay)/2]
                y = self.intensity_der[0:len(self.intensity_der)/2] * -1
                n = len(x_l)            #the number of data
                amp = np.amax(y)
                mean = x_l[np.argmax(y)]                        #guessing mean value
                sigma = np.sqrt(sum(y*(x_l-mean)**2)/n )#guessing the fwhm

                #fitting
                [amp_l,mean_l,sigma_l],pcov_l = \
                        curve_fit(gaus,x_l,y,p0=[amp,mean,sigma])
                fwhm_l = sigma_l * 2.3548

                #RIGHT PEAK
                x_r = self.delay[len(self.delay)/2:len(self.delay)]
                y = self.intensity_der[len(self.intensity_der)/2:\
                                len(self.intensity_der)]
                n = len(x_r)
                amp = np.amax(y)
                mean = x_r[np.argmax(y)]
                #fitting
                [amp_r,mean_r,sigma_r],pcov_r = \
                        curve_fit(gaus,x_r,y,p0=[amp,mean,sigma_l])
                fwhm_r = sigma_r * 2.3548
                #SAVING FIT PARAMETER
                np.savetxt('intermediate/'+self.sample+'_left_edge_fit_param.txt',\
                        [amp_l,mean_l,sigma_l] )
                np.savetxt('intermediate/'+self.sample+'_left_edge_fit_pcov.txt',\
                        pcov_l )
                np.savetxt('intermediate/'+self.sample+'_right_edge_fit_param.txt',\
                        [amp_r,mean_r,sigma_r] )
                np.savetxt('intermediate/'+self.sample+'_right_edge_fit_pcov.txt',\
                        pcov_r )

                #PLOTTING
                if self.plot == 1:
```

```
                xplot_l = np.arange(0,self.delay[len(self.delay)/2], 0.001)
                xplot_r = np.arange(self.delay[len(self.delay)/2],\
                        self.delay[len(self.delay)-1], 0.001)
                plt.figure(10)
                plt.plot(self.delay,self.intensity_der,'b+:',label='data')
                plt.plot(xplot_r,gaus(xplot_r,amp_r,mean_r,sigma_r),\
                        color = 'red',label='gaussian fit right')
                plt.plot(xplot_l,-1*gaus(xplot_l,amp_l,mean_l,sigma_l),\
                        color = 'c',label='gaussian fit left')
                plt.legend(loc = 2)
                plt.title('Edges Fit')
                plt.xlabel('Delay (ns)')
                plt.ylabel('Normalized Intensity (a.u.)')
                plt.savefig('intermediate/'+self.sample+\
                        '_edge_fitting.pdf',bbox_inches="tight")
                plt.show()
        return mean_l, fwhm_l, mean_r, fwhm_r

    def estimate_single_bunch(self, delay, intensity,left_edge, right_edge,\
                                        fwhm, shift, plot):
        '''
        This method provides an easy way to fit the edges.
        If used to fit the delay scan, this has to be derived.

        Arguments:
        delay = array, the delay relative to intensity_der
        intensity_der =array, the intensity scan derived
        left_edge = int, the position of the left edge
        right_edge = int, the position of the right edge
        fwhm = int, the expected fwhm, use the average of the edges
                    if available
        shift = float, to plot logaritmic, shift the data to avoid zeros
        plot = 0/1, 0--no plot, 1--plot.

        Return:
        mean_sb, fwhm_sb, amp_sb = float, mean, fwhm, and intensity of
        the sb peak the method returns the position and the fwhm of single
        bunch. Additionally it saves the parameters and the pcov matrix
        resulting from the fit in the intermediate folder, as well as a
        graph with the fit if plot = 1
        '''

        self.delay = delay
        self.intensity = intensity
        self.left_edge = left_edge
        self.right_edge = right_edge
        self.fwhm = fwhm
        self.shift = shift
        self.plot = plot

        #defining the region to fit
        mean = np.int((self.left_edge + self.right_edge)/2/self.Nsm)
        h_w = fwhm/self.Nsm
        l = np.int(mean - h_w)
        r = np.int(mean + h_w)
        x = self.delay[l : r]
        y = self.intensity[l : r]

        #Guessing the parameter for the fit
        n = len(x)  #the number of data
        mean = (self.left_edge + self.right_edge)/2
        sigma = np.sqrt(sum(y*(x-mean)**2)/n )
        amp = np.amax(y)
        #fitting
        [amp_sb,mean_sb,sigma_sb],pcov_sb =\
                curve_fit(gaus,x,y,p0=[amp,mean,sigma])
        fwhm_sb = sigma_sb * 2.3548
        #SAVING FIT PARAMETER
        np.savetxt('intermediate/'+self.sample+\
                '_single_bunch_fit_param.txt', [amp_sb,mean_sb,sigma_sb] )
        np.savetxt('intermediate/'+self.sample+\
                '_single_bunch_fit_pcov.txt', pcov_sb )
```

```
			if plot ==1:
				plt.figure(11)
				plt.plot(self.delay, self.shift+self.intensity,'b+:',\
					label='data')
				plt.plot(x,self.shift+gaus(x,amp_sb,mean_sb,sigma_sb),\
					color = 'red',label='single bunch position')
				plt.legend(loc=9)
				plt.title('Delay scan')
				plt.xlabel('Delay (ns)')
				plt.ylabel('Normalized Intensity (a.u.)')
				#~ plt.yscale('log')
				plt.ylim(0.01,1+self.shift)
				plt.savefig('intermediate/'+self.sample+\
					'_single_bunch_fitting.pdf', bbox_inches="tight")
				plt.show()
			print 'fwhm', fwhm_sb
			return mean_sb, fwhm_sb, amp_sb


		def set_fit_delay_scan_parameter(self, mean_l, mean_r, mean_sb,\
								amp_sb, fwhm):
			'''
			Use this method to set the initial parameters for the fit delay
			scan. One can use the estimate_edges and estimate_single
			bunch to guess them.

			Arguments:
			mean_l  = int, position of the left edge
			mean_r  = int, position of the right edge
			mean_s  = int, position of the single bunch
			amp_sb = int, amplitude of the single bunch
			fwhm = int, fwhm of the sb or of the derivative of the edge'''

			self.mean_l = mean_l
			self.mean_r = mean_r
			self.mean_sb = mean_sb
			self.amp_sb = amp_sb
			self.fwhm = fwhm


		def fit_delay_scan(self, delay, intensity, plot):
			'''
			This method provides an easy way to fit the complete delay scan.
			Set the initial parameters for the fit using the
			set_fit_delay_scan_parameter method. The fit is carried out using
			the sb function defined in lib.py

			Arguments:
			delay = array, the delay array
			intensity = array, the intensity array to fit
			plot = 0/1, 0--no plot, 1--plot.+

			Return:
			fwhm = float, the average value of the FWHM
			Parameters and the pcov matrix are saved in intermediate folder.
			A pdf with the plot of the data and the fit is also saved
			'''
			self.delay = delay
			self.intensity = intensity

			sigma = self.fwhm / 2.3548
			[self.mean_l, self.mean_r, self.mean_sb,sigma, self.amp_sb],\
				pcov_del =curve_fit(sb,self.delay,self.intensity,\
					p0=[self.mean_l, self.mean_r, self.mean_sb,sigma,\
						self.amp_sb])
			np.savetxt('intermediate/'+self.sample+'_delay_scan_fit_param.txt',\
				[self.mean_l, self.mean_r, self.mean_sb,sigma, self.amp_sb])
			np.savetxt('intermediate/'+self.sample+'_delay_scan_fit_pcov.txt',\
				pcov_del )
			if plot ==1:
				gauss_sum_fit = sb(self. delay,self.mean_l, self.mean_r,\
							self.mean_sb,sigma, self.amp_sb)
```

```
                        plt.figure(12)
                        plt.plot(self.delay,gauss_sum_fit, 'r', label = 'fit')
                        plt.plot(self.delay, self.shift+self.intensity,'b+:',\
                                label='data')
                        plt.legend(loc=9)
                        plt.title('Delay scan')
                        plt.xlabel('Delay (ns)')
                        plt.ylabel('Normalized Intensity (a.u.)')
                        plt.ylim(0.01,1.3+self.shift)
                        plt.savefig('intermediate/'+self.sample+\
                                '_delay_scan_fit.pdf',bbox_inches="tight")
                        plt.show()
                fwhm = 2.3548 * sigma
                return fwhm





def test_time_resolved_analysis():
        '''
        Test function
        '''
        test = time_resolved_analysis('test', 'ipp', 2426, 1001, 10)
        file_names = test.create_name_array()

        xpix_in = 855
        xpix_fin = 859
        ypix_in = 211
        ypix_fin = 219
        test.set_region(xpix_in, xpix_fin,ypix_in,ypix_fin,'down')
        #~ intensity_down = test.tiff_extract_n_scans()
        intensity_down = np.loadtxt('intermediate/test_down_intensity.txt')
        test.set_rejection(140)
        intensity_down = test.select_good_scans(intensity_down, 1)

        xpix_in = 860
        xpix_fin = 864
        ypix_in = 156
        ypix_fin = 163
        test.set_region(xpix_in, xpix_fin,ypix_in,ypix_fin,'up')
        #~ intensity_up = test.tiff_extract_n_scans()
        intensity_up = np.loadtxt('intermediate/test_up_intensity.txt')
        test.set_rejection(150)
        intensity_up = test.select_good_scans(intensity_up, 1)

        intensity = (intensity_down + intensity_up)/2

        test.set_Nsm(9)
        delay_smooth, intensity_smooth = \
                test.smooth(intensity)
        delay_smooth, intensity_smooth = \
                test.norm_line(delay_smooth, intensity_smooth)
        delay_smooth, intensity_smooth = \
                test.norm(delay_smooth, intensity_smooth)

        #~ plt.plot(intensity_smooth)
        intensity_der = test.derive(intensity_smooth)
        mean_l, fwhm_l, mean_r, fwhm_r =\
                test.estimate_edge(delay_smooth, intensity_der, 1)
        fwhm_edges = (fwhm_l + fwhm_r)/2
        mean_sb, fwhm_sb, amp_sb =\
                test.estimate_single_bunch(delay_smooth, intensity_smooth,\
                        mean_l, mean_r, fwhm_edges,0.0, 1)
        print 'FWHM right edge, mean:', fwhm_r, 'ns', mean_r, 'ns'
        print 'FWHM left edge, mean:', fwhm_l, 'ns', mean_l, 'ns'
        print 'FWHM single bunch,mean, amp:', fwhm_sb, 'ns',\
                mean_sb, 'ns', amp_sb, 'ns'
        print 'FWHM average:', (fwhm_r+fwhm_l+fwhm_sb)/3, 'ns'
        test.set_fit_delay_scan_parameter(mean_l, mean_r, mean_sb,\
                                                                amp_sb, fwhm_sb)
        fwhm = test.fit_delay_scan(delay_smooth,intensity_smooth, 1)
```

```python
        print 'FWHM from delay scan:', fwhm, 'ns'



if __name__ == "__main__":
        test_time_resolved_analysis()
```

Appendix E

GSolver

GSolver is a full vector implementation of a class of algorithms known as Rigorous Coupled Wave Analysis(RCWA), whose principles are described in section 1.2.3. The program deliver a numerical solution of Maxwell's equations for a periodic grating structure that lies at the boundary between two homogenoeus linear isotropic inginite half spaces, see Fig. E.1. *Region I* is the superstrate, and *Region II* is the substrate. Maxwell's equation are solved with only two simplifying assumptions:

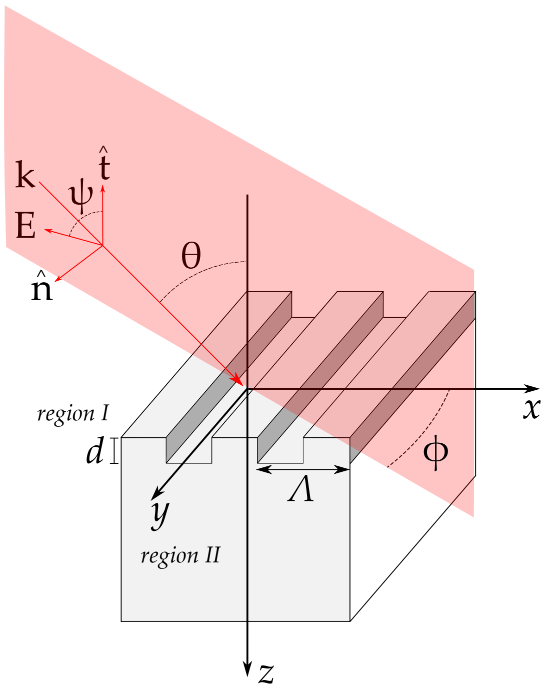

FIGURE E.1: Geometry for the binary rectangular groove grating diffraction problem. Without any loss of generality the normal to the boundary is in the z direction, and the grating vector is in the x direction

- the grating must be constructed with a piecewise-linear approximation;
- The infinite Fourier series representation of the permittivity of each layer is truncated.

When opening Gsolver for the first time, the screenshot shown in Fig. E.2 is displayed. The following parameters should be inserted:

- **Vacuum Wavelength**: the wavelength of the incident radiation
- **Grating Period or Lines/mm**

- θ: the Bragg angle for a given wavelength and a given material
- ϕ: the angle that determine the meridional or sagittal geometry
- **Units**: to choose the units used for the input parameters
- **Superstrate/Substrate index**: the refractive index of superstrate (air or vacuum) and substrate.
- **Polarization parameters**: for SAW simulations can be left as they are.

GSolver supports six refraction indexes models: Constant, Drude, Sellmeier, Herzberger, Schott, Polynomial and Table. If the substrate material is not in the predefined list, this can be manually added modifying the file *Gsolver/GSv52/GSolver.ini*. See reference [79] for detailed instructions.

A final and important observation about the simulations with GSolver. In section 1.2 the interaction of X-rays with SAW is described. This interaction is the result of two distinct diffraction problems. The first one is described by the Bragg law, and this happens independently from the presence of SAW. GSolver has no information about the Bragg law, and therefore is not able to calculate absolute values for the intensities of the diffraction orders depending on the amplitude of the SAW. It calculates only relative intensities, where the Bragg reflection in the case of no SAW present on the sample is normalized to one.

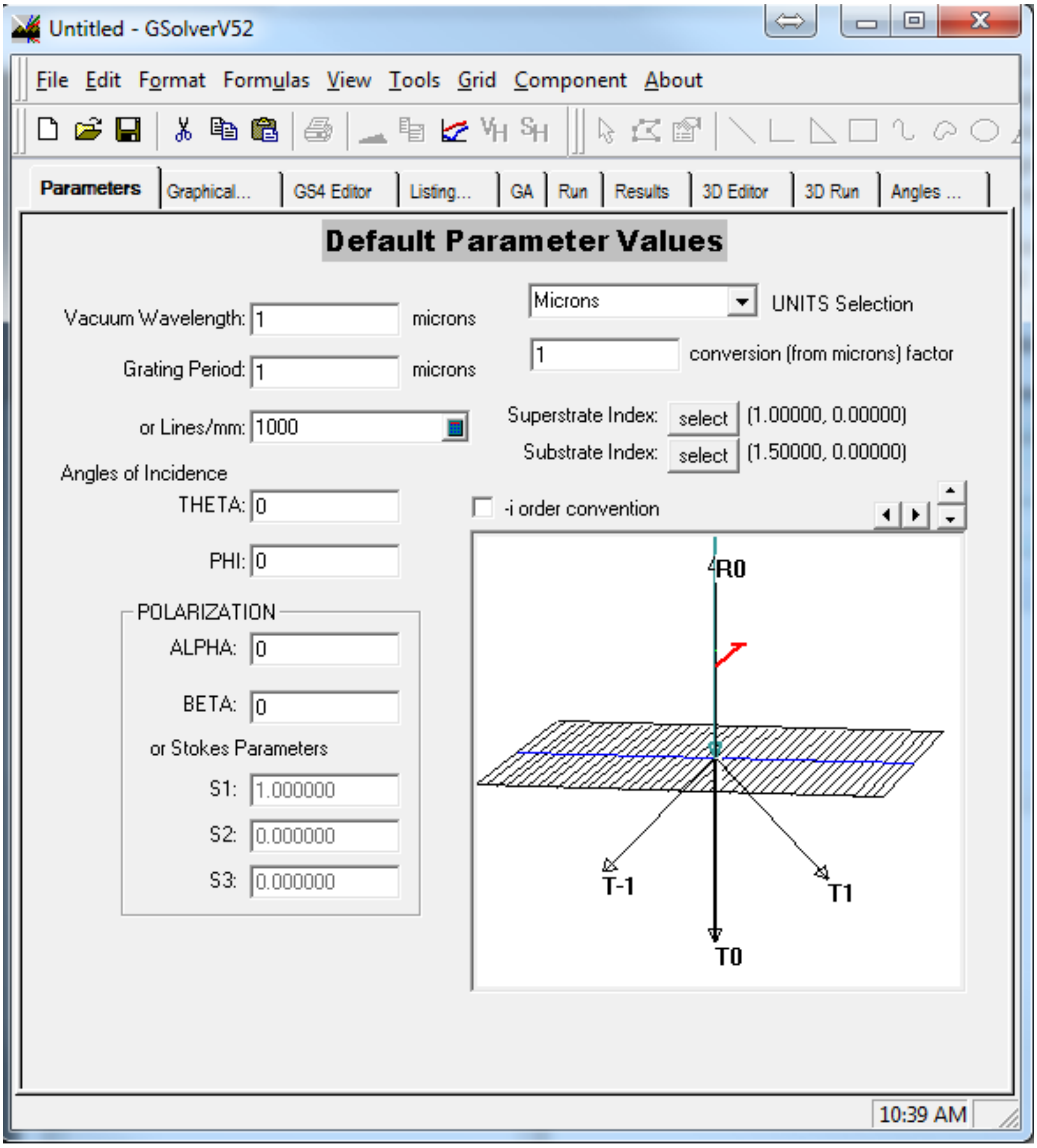

FIGURE E.2: Screenshot of GSolver showing the parameters to input.

Bibliography

[1] C. Rischel et al. "X-ray diffraction from laser-heated organic films". In: *Nature* 390 (1997), pp. 490 –492.

[2] V. Srajer et al. "Photolysis of the Carbon Monoxide Complex of Myoglobin: Nanosecond Time-Resolved Crystallography". In: *Science* 274 (1997), pp. 1726 –1729.

[3] R.W. Schoenlein et al. "Femtosecond X-ray Pulses at 0.4 A Generated by 900 Thomson Scattering: A Tool for Probing the Structural Dynamics of Materials". In: *Science* 274 (1996), pp. 236 –238.

[4] Rayleigh. "On waves propagating along the plane surface of an elastic solid". In: *Proc. London Math. Soc.* 7 (1885), pp. 4 –11.

[5] R. M. White and F. W. Voltmer. "Direct Piezoelectric coupling to surface acoustic waves". In: *Applied Physics Letters* 7.12 (1965), pp. 314–316. DOI: 10.1063/1.1754276.

[6] D. Morgan. *Surface Acoustic Wave Filters: With Applications to Electronic Communications and Signal Processing*. Studies in Electrical and Electronic Engineering. Elsevier Science, 2010. ISBN: 9780080550138. URL: https://books.google.de/books?id=ITLn6tj4SDQC.

[7] C. Campbell. *Surface Acoustic Wave Devices and Their Signal Processing Applications*. USA: Academic Press Inc., 1989.

[8] D. P. Morgan. "History of SAW devices". In: (1998), pp. 439–460. ISSN: 1075-6787. DOI: 10.1109/FREQ.1998.717937.

[9] Seishi Kikuta, Toshio Takahashi, and Shinichiro Nakatani. "High Frequency Time Modulation of the X-Ray Beam Diffracted from a LiNbO3 Crystal by Surface Acoustic Waves". In: *Japanese Journal of Applied Physics* 23.4A (1984), p. L193.

[10] A. Erko et al. *Modern Developments in X-Ray and Neutron Optics*. Springer, 2008.

[11] D.V. Roschupkin et al. "X-ray Bragg diffraction from langasite crystal modulated by surface acoustic wave". In: *Journal of Applied Physics* 94.10 (January 1995).

[12] D.V. Roschupkin et al. "X-ray Space Modulation by diffraction on a Ultrasonic Superlattice". In: *Nuclear Instruments and Methods in Physics Research* B72 (1992), pp. 471 –476.

[13] D.V. Roschupkin et al. "X-ray diffraction by standing sourface acoustic waves". In: *Nuclear Instruments and Methods in Physics Research B* 142 (1998), pp. 432–436.

[14] D. V. Roshchupkin, H. D. Roshchupkina, and D. V. Irzhak. "X-ray topography analysis of acoustic wave fields in the SAW-resonator structures". In: *IEEE Transactions on Ultrasonics, Ferroelectrics, and Frequency Control* 52.11 (2005), pp. 2081–2087. ISSN: 0885-3010. DOI: 10.1109/TUFFC.2005.1561678.

[15] R. Tucoulou et al. "X-ray Bragg diffraction of $LiNbO_3$ crystals excited by surface acustic waves". In: *Physical Review B* 64 (2001).

[16] I.A. Schelokov et al. "Dynamical theory for calculations of X-ray spectra from crystals modulated by surface acoustic waves". In: *Applied Cristallography* (2003).

[17] D.V. Roschupkin, E.D. Irzhak D.and Roshchupkina, and Buzanov O.A. "Investigation of Structural Perfection and Acoustic Properties of $La_3Ga_5SiO_14$ Crystals by High Resolution X-Ray Diffraction, Topography, and Microfluorescence Analysis". In: *Crystallography Reports* 49 (2004), pp. 80 –88.

[18] D.V. Roschupkin et al. "X-ray diffraction analysis of the surface acoustic wave propagation in langatate crystal". In: *Applied Physics A* 94 (2009), pp. 477–484.

[19] D.V. Roschupkin et al. "Advanced piezoelectric crystal $Ca_3TaGa_3Si_2O_{14}$: growth, crystal structure perfection, and acoustic properties". In: *Applied Physics A* (May 2013).

[20] D. Irzhak and D.V. Roschupkin. "X-ray diffraction on the X-cut of a Ca3TaGa3Si2O14 single crystal modulated by a surface acoustic wave". In: *Journal of Applied Physics* 115 (June 2014), pp. 614–623.

[21] D. Roshchupkin et al. "Piezoelectric Ca3NbGa3Si2O14 crystal: crystal growth, piezoelectric and acoustic properties". In: *Applied Physics A* 122.8 (2016), p. 753. ISSN: 1432-0630. DOI: 10.1007/s00339-016-0279-1. URL: https://doi.org/10.1007/s00339-016-0279-1.

[22] D. V. Roshchupkin, R. Tucoulou, and M. Brunel. "X-ray standing waves effects for a multilayer mirror modulated by surface acoustic waves". In: *Applied Physics Letters* 75.5 (1999), pp. 639–640. DOI: 10.1063/1.124466.

[23] J Dong, J Qi, and R Miao. "X-ray diffraction effect from surface acoustic waves traveling on a deposited multilayer". In: *Appl. Opt.* 49.11 (2010), pp. 2054–2058. DOI: 10.1364/AO.49.002054.

[24] D.V. Roshchupkin et al. "X-ray diffraction on a multilayer mirror modulated by surface acoustic waves". In: *Nuclear Instruments and Methods in Physics Research Section B: Beam Interactions with Materials and Atoms* 129.3 (1997), pp. 414 –418. DOI: http://dx.doi.org/10.1016/S0168-583X(97)00293-0.

[25] A.I. Erko et al. "X-ray Diffraction on a Multilayer Structure Modulated by Surface Acoustic Waves". In: *Nuclear Instruments and Methods in Physics Research* A282 (1989), pp. 634 –637.

[26] I-Tseng Tang et al. "Investigation of piezoelectric ZnO film deposited on diamond like carbon coated onto Si substrate under different sputtering conditions". In: *Journal of Crystal Growth* 252.1 (2003), pp. 190 –198. ISSN: 0022-0248. DOI: https://doi.org/10.1016/S0022-0248(02)02496-X. URL: http://www.sciencedirect.com/science/article/pii/S002202480202496X.

[27] R. Tucoulou et al. "X-ray diffraction from perfect silicon crystals distorted by surface acoustic waves". In: *Applied Cristallography* 33 (April 2000), pp. 1019–1022.

[28] S. Zhgoon et al. "Surface acoustic waves in diamond-like carbon films on LiNbO3". In: *Diamond and Related Materials* 9.8 (2000), pp. 1430 –1434. ISSN: 0925-9635. DOI: https://doi.org/10.1016/S0925-9635(00)00262-4. URL: http://www.sciencedirect.com/science/article/pii/S0925963500002624.

[29] Z. Insepov et al. "Surface acoustic wave amplification by direct current-voltage supplied to graphene film". In: *Applied Physics Letters* 106.2 (2015), p. 023505. DOI: 10.1063/1.4906033.

[30] Dmitry Roshchupkin et al. "Surface acoustic wave propagation in graphene film". In: *Journal of Applied Physics* 118.10 (2015), p. 104901. DOI: 10.1063/1.4930050.

[31] V.I Punegov, Y.I. Nesterets, and D. Roshchupkin. "Coherent and diffuse X-ray scattering in crystals modulated by a surface acoustic wave". In: *Applied Cristallography* 43 (2010), pp. 520 –530.

[32] I. A. Schelokov et al. "Dynamical theory for calculations of X-ray spectra from crystals modulated by surface acoustic waves". In: *Applied Cristallography* 37.10 (2004), pp. 52–61.

[33] D. Roshchupkin et al. "Diffraction of a focused x-ray beam from $La_3Ga_5SiO_{14}$ crystal modulated by surface acoustic waves". In: *Journal of Applied Physics* 110 (2011), p. 124902.

[34] J.F. Nye. *Physical Properties of Crystal, Their representation by tensors and Matrices*. USA: Oxford university Press, 1957.

[35] C. Kittel. *Introduction to Solid State Physics*. eight. USA: Wiley, 2005.

[36] T. Ikeda. *Fundamentals of Piezoelectricity*. New York, USA: Oxford university Press, 1996.

[37] H. F. Tiersten. "Thickness Vibrations of Piezoelectric Plates". In: *The Journal of the Acoustical Society of America* 35.1 (1963), pp. 53–58. DOI: 10.1121/1.1918413.

[38] H Goldstein, C. P. Poole, and J. L. Safko. *Classical Mechanics, 3rd edition*. pearson, 2002.

[39] A. J. Slobodnik. "Surface acoustic waves and SAW materials". In: *Proceedings of the IEEE* 64.5 (1976), pp. 581–595. ISSN: 0018-9219. DOI: 10.1109/PROC.1976.10180.

[40] W. R. Smith, H. M. Gerard, and W. R. Jones. "Analysis and Design of Dispersive Interdigital Surface-Wave Transducers". In: *IEEE Transactions on Microwave Theory and Techniques* 20.7 (1972), pp. 458–471. ISSN: 0018-9480. DOI: 10.1109/TMTT.1972.1127786.

[41] R. F. Milsom, M. Redwood, and N. H. C. Reilly. *Surface Wave Filters*. New York: Wiley, 1977.

[42] G. Tobolka. "Mixed Matrix Representation of SAW Transducers". In: *IEEE Transactions on Sonics and Ultrasonics* 26.6 (1979), pp. 426–427. ISSN: 0018-9537. DOI: 10.1109/T-SU.1979.31128.

[43] S. Datta and B. J. Hunsinger. "Element Factor for Periodic Transducers". In: *IEEE Transactions on Sonics and Ultrasonics* 27.1 (1980), pp. 42–44. ISSN: 0018-9537. DOI: 10.1109/T-SU.1980.31142.

[44] A. Authier. *Dynamical Theory of X-ray Diffraction*. London: Oxford university Press, 2001.

[45] S. Takagi. In: *Acta Crystallography* 15 (1962), p. 1311.

[46] S. Takagi. In: *Journal of Phys. Soc. Jpn.* 26 (1969), p. 1239.

[47] D. Taupin. In: *Bull. Soc. Fr. Mineral. Cristallogr.* 87 (1964), p. 469.

[48] N. Kato. In: *Jour. Phys. Soc. Jpn* 18 (1963), pp. 1785 –1791.

[49] N. Kato. In: *Jour. Phys. Soc. Jpn* 19 (1964), pp. 67 –77.

[50] R. Tucoulou et al. "Investigation of surface acoustic wave fields in silicon crystals by x-ray diffraction: A dynamical theory approach". In: *Journal of Applied Physics* 97 (2005).

[51] Y. Eperlboin, V. Mocella, and A. Soyer. In: *Philos. Trans. R. Soc. London* 357 (1999), p. 2739.

[52] M. G. Moharam et al. "Formulation for stable and efficient implementation of the rigorous coupled-wave analysis of binary gratings". In: *J. Opt. Soc. Am. A* 12.5 (1995), pp. 1068–1076. DOI: 10.1364/JOSAA.12.001068. URL: http://josaa.osa.org/abstract.cfm?URI=josaa-12-5-1068.

[53] O. L. Balysheva. "Materials choice criteria for surface acoustic wave sensors". In: *Automation and Remote Control* 77.7 (2016), pp. 1286–1293. ISSN: 1608-3032. DOI: 10.1134/S0005117916070158. URL: https://doi.org/10.1134/S0005117916070158.

[54] R. Fachberger et al. "Applicability of LiNbO/sub 3/, langasite and GaPO/sub 4/ in high temperature SAW sensors operating at radio frequencies". In: *IEEE Transactions on Ultrasonics, Ferroelectrics, and Frequency Control* 51.11 (2004), pp. 1427–1431. ISSN: 0885-3010. DOI: 10.1109/TUFFC.2004.1367482.

[55] M Reinhardt et al. "Optimized spatial overlap in optical pump-X-ray probe experiments with high repetition rate using laser-induced surface distortions". In: *Journal of Synchrotron Radiation* (2016), pp. 474–479.

[56] M.D. Abramoff, P.J. Magalhaes, and S.J. Ram. "Image Processing with ImageJ". In: *Biophotonics International* (2004), pp. 36–42.

[57] I. Ziza. "The At-Wavelength Metrology Facility at BESSY-II". In: *Journal of large-scale research facilities* A50.2 (2016). DOI: http://dx.doi.org/10.17815/jlsrf-2-72.

[58] K. J. S. Sawhney et al. "A Test Beamline on Diamond Light Source". In: *AIP Conference Proceedings* 1234 (2010), pp. 397 –390.

[59] I. Zizak. "mySpot: a versatile microfocussing station for scanning methods at BESSY II". In: *Journal of large-scale research facilities* A102.2 (2016). DOI: http://dx.doi.org/10.17815/jlsrf-2-113.

[60] Antoine Rousse, Christian Rischel, and Jean-Claude Gauthier. "Femtosecond x-ray crystallography". In: *Rev. Mod. Phys.* 73 (1 2001), pp. 17–31. DOI: 10.1103/RevModPhys.73.17. URL: https://link.aps.org/doi/10.1103/RevModPhys.73.17.

[61] Christian Bressler and Majed Chergui. "Molecular Structural Dynamics Probed by Ultrafast X-Ray Absorption Spectroscopy". In: *Annual Review of Physical Chemistry* 61.1 (2010), pp. 263–282. DOI: 10.1146/annurev.physchem.012809.103353.

[62] Helmholtz Zentrum Berlin. *Green light for upgrading BESSY II into a variable-pulse-length storage ring (BESSY-VSR)*. 2017. URL: https://www.helmholtz-berlin.de/pubbin/news_seite?nid=14610&sprache=en (visited on 12/08/2017).

[63] Helmholtz Zentrum Berlin. *Machine Status*. 2016. URL: https://www.helmholtz-berlin.de/quellen/bessy/betrieb-beschleuniger/betriebsmodi_en.html (visited on 08/01/2016).

[64] G. Wüstefeld. EPAC06, IPAC11.

[65] A. McPherson, W. Lee, and D. M. Mills. "A synchronized rotating crystal x-ray beam chopper". In: *Review of Scientific Instruments* 73 (2002), p. 2852.

[66] M. Cammarata et al. "Chopper system for time resolved experiments with synchrotron radiation". In: *Review of Scientific Instruments* 80 (2009), p. 015101.

[67] S.L.G. Husheer et al. "A prototype chopper for synchrotron time-resolved crystallographic measurements". In: *Review of Scientific Instruments* 81 (2010), p. 043905.

[68] Daniel F. Förster et al. "Phase-locked MHz pulse selector for x-ray sources". In: *Opt. Lett.* 40.10 (2015), pp. 2265–2268. DOI: 10.1364/OL.40.002265. URL: http://ol.osa.org/abstract.cfm?URI=ol-40-10-2265.

[69] A. Meents et al. "A fast X-ray chopper for single-bunch extraction at synchrotron sources". In: *Journal of applied Crystallography* 48 (2009), pp. 901–905.

[70] S. Plogmaker et al. "Versatile high-repetition-rate phase-locked chopper system for fast timing experiments in the vacuum ultraviolet and x-ray spectral region". In: *Review of Scientific Instruments* 83 (2012), p. 013115.

[71] A. D. LeGrand, W. Schildkamp, and B. Blank. "An ultrafast mechanical shutter for X-rays". In: *Nuclear Instruments and Methods in Physics* 275 (2002), pp. 442–446.

[72] A. McPherson et al. "A new high-speed beam chopper for time-resolved X-ray studies". In: *Journal of synchrotron radiation* 7 (1999), pp. 1–4.

[73] M. Gembicky et al. "A fast mechanical shutter for submicrosecond time-resolved synchrotron experiments". In: *Journal of synchrotron radiation* 12 (2005), pp. 665–669.

[74] M. Gembicky and P. Coppens. "On the design of ultrafast shutters for time-resolved synchrotron experiments". In: *Journal of synchrotron radiation* 14 (2007), pp. 133–137.

[75] K. Ito et al. "Application of a simple asynchronous mechanical light chopper to multielectron coincidence spectroscopy". In: *Review of Scientific Instruments* 80 (2009), p. 123101.

[76] R. Tucoulou et al. "High frequency electro-acoustic chopper for synchrotron radiation". In: *Nuclear instruments and methods in Physics Research B* 132 (1997), pp. 207–213.

[77] S. Vadilonga et al. "Observation of sagittal X-ray diffraction by surface acoustic waves in Bragg geometry". In: *J. Appl. Cryst.* 50 (2017). DOI: https://doi.org/10.1107/S1600576717002977.

[78] Simone Vadilonga et al. "Pulse picker for synchrotron radiation driven by a surface acoustic wave". In: *Opt. Lett.* 42.10 (2017), pp. 1915–1918. DOI: 10.1364/OL.42.001915. URL: http://ol.osa.org/abstract.cfm?URI=ol-42-10-1915.

[79] David Fluckiger. *GSolver Version 5.2 Users Guide*. 2012. URL: http://www.gsolver.com/UserManual.pdf (visited on 12/12/2017).

Acknowledgements

First and foremost, I thank Prof. Dr. Alexei Erko, for accepting me into the *Institute for Nanometre Optics and Technology* at *Helmholtz Zentrum Berlin* at the beginning of my Master at *Freie Universität* in the faraway October 2012, and for giving me the opportunity of writing my PhD thesis under his supervision. Aligning the diffractometer together in the X-ray laboratory is one of my most treasured memories.

I thank Prof. Dr. Kuch for accepting to be my second supervisor.

I have been working everyday with Dr. Ivo Zizak. I thank him for his constant support, his assistance during these years and valuable discussions. This last five years passed really fast now that I look back at it. I learned from you much more than physics. I am grateful for everything, from reciprocal space to Raspberry Pi.

I thank Ingo Packe, I had so much fun taking apart and mounting back the diffractometer, building sample holders and repairing motors with you.

I thank Ivo Rudolph and Dr. Alexander Firsov for their support and guidance in the cleanroom. I had a good time and I learned a lot.

I thank Dr. Sertsu for his support during the experiment at DLS and at the Optics beamline: long days, long nights, horrible food, but we survived.

I thank Dr. Andrei Sokolov, for his support during the beamtimes at the Optics beamline. It was not easy but at the end we got real diffraction peaks.

I thank Dr. Siewert, Dr. Baumgartel, Dr. Braig and Dr. Viefhaus for the valuable discussions and the good time spent together.

I thank my office mate and colleague Jürgen Probst for all the discussion about our future (that in a while will be our present).

I especially thank Dr. Dmitry V. Roschupkin from the *Institution of Russian Academy of Sciences Institute of Microelectronics Technology and High-Purity Materials RAS* for providing some samples used in this thesis and for his support during all the phases of the project. I also thank his colleague Dr. E. Emelin for showing me how to produce a SAW device.

I thank the joint group of *Ultrafast Dynamics in Condensed Matter* held by Prof. Dr. Matias Bargheer at *Potsdam Universität* and *Helmholtz Zentrum Berlin* for the assistance and instrumentation at XPP-KMC-3 beamline at BESSY II, especially Dr. W. Leitenberger and Dr. P. Gaal.

I thank the staff of the B16 beamline at the Diamond Light Source, Dr. Sawnhey, Dr. Dolbnya and Mr. Malandain for their support during the beamtimes.

Voglio ringraziare i miei genitori, per avermi insegnato a pensare con la mia testa, e avermi incoraggiato a fare quello che mi piace. Per supportato e aiutato quando ne ho avuto bisogno. Per avermi lasciato libero di scegliere, di sbagliare, di riprovare. Grazie per aver sempre avuto fiducia in me, per essere stati la mia base sicura.

I thank Núria. You make me happy and everything is so easy with you. Your approach to life is so simple and resolute, and I draw inspiration from you everyday. Gracies per tot, gràcies pels anys que hem passat junts, gràcies per estar sempre a prop meu.

Ludo, Albi e Momo: i week end con voi sono stati delle iniezioni di felicitá concentrata, il nostro continuo scriverci mi ha sempre aiutato a vedere le cose dalla giusta prospettiva. Grazie per esserci sempre stati.

Non avrei avuto l'energia per scrivere la tesi se non fossi andato in Kalimantan con Ali, Albi e Núria. Grazie per quel viaggio meraviglioso, sono felice di averlo fatto con voi. Al prossimo giro pinguini.

Grazie Helena e Jo, il tempo passato con voi prima dell'inizio del dottorato mi ha aiutato a mettere in ordine le idee e a partire carico! Obrigado!

Matteo: grazie per tutti gli arrosticini e le carbonare. Mi han dato piú energia di quanto ne avessi bisogno. Grazie per aver ospitato Núria e me in Abruzzo e per averci fatto da guida. Ti auguro tutto il bene possibile.

Fra, ex coinquilino burrascoso. Hai un cuore enorme, mi hai sopportato per due anni e hai sempre avuto un sorriso nelle giornate difficili. Grazie per ricordarmi ogni volta che ci vediamo che godersi la vita é una delle cose che rendono bello vivere.

I thank Monika and Bruno for their support. The lunch breaks would not have been the same without you guys. Complaining about the weather, the food and work made everything easier.

Voglio ringraziare la Prof. Meda. É stata la prima persona a farmi apprezzare la matematica. Averne di professori cosí innamorati del proprio lavoro da riuscire a trasmetterlo a un ragazzino delle medie! Se non l'avessi incontrata probabilmente non sarei arrivato dove sono. Grazie.

Ringrazio anche i professori della triennale. Dopo aver studiato con voi, mi sono convinto ad andare via. In Germania ho scoperto che c'é un mondo fatto persone che amano il proprio lavoro e i loro studenti.

Selbstständigkeitserklärung

Hiermit versichere ich, dass ich die vorliegende Dissertation mit dem Titel "Scattering of an X-Ray beam on a Surface Acoustic Wave" ohne fremde Hilfe angefertigt und keine anderen als die angegebenen Quellen und Hilfsmittel benutzt habe. Alle Teile, die wörtlich oder sinngemäß einer Veröffentlichung entstammen, sind als solche kenntlich gemacht. Diese Dissertation wurde noch nicht veröffentlicht und keiner anderen Fakultät oder Universität zur Prüfung vorgelegt.

Berlin, July 26, 2018:

(Simone Vadilonga):